Alma Mater Studiorum · Università di Bologna

Scuola di Scienze
Dipartimento di Fisica e Astronomia
Corso di Laurea Magistrale in Fisica

NETWORK APPROACHES FOR THE ANALYSIS OF RESTING STATE FMRI DATA

Relatore:
Prof. Daniel Remondini

Correlatore:
Prof. Daniele Marinazzo

Presentata da:
Claudio Corte Coi

Anno Accademico 2015/2016

Sommario

Negli ultimi anni la teoria dei network è stata applicata agli ambiti più diversi, mostrando proprietà caratterizzanti tutti i network reali. In questo lavoro abbiamo applicato gli strumenti della teoria dei network a dati cerebrali ottenuti tramite MRI funzionale "resting", provenienti da due esperimenti. I dati di fMRI sono particolarmente adatti ad essere studiati tramite reti complesse, poiché in un esperimento si ottengono tipicamente più di 10^5 serie temporali per ogni individuo, da più di 100 valori ciascuna.

I dati cerebrali negli umani sono molto variabili e ogni operazione di acquisizione dati, così come ogni passo della costruzione del network, richiede particolare attenzione. Per ottenere un network dai dati grezzi, ogni passo nel preprocessamento è stato effettuato tramite software appositi, e anche con nuovi metodi da noi implementati.

Il primo set di dati analizzati è stato usato come riferimento per la caratterizzazione delle proprietà del network, in particolare delle misure di centralità, dal momento che pochi studi a riguardo sono stati condotti finora. Alcune delle misure usate indicano valori di centralità significativi, quando confrontati con un modello nullo. Questo comportamento è stato investigato anche a istanti di tempo diversi, usando un approccio *sliding window*, applicando un test statistico basato su un modello nullo più complesso.

Il secondo set di dati analizzato riguarda individui in quattro diversi stati di riposo, da un livello di completa coscienza a uno di profonda incoscienza. È stato quindi investigato il potere che queste misure di centralità hanno nel discriminare tra diversi stati, risultando essere dei potenziali bio-marcatori di stati di coscienza. E' stato riscontrato inoltre che non tutte le misure hanno lo stesso potere discriminante. Secondo i lavori a noi noti, questo è il primo studio che caratterizza differenze tra stati di coscienza nel cervello di individui sani per mezzo della teoria dei network.

Abstract

Network theory has been recently applied to the most diverse fields, showing features which characterise real networks. In this work we applied the tools of network theory to brain resting-state functional MRI data obtained by two experiments. Functional MRI data naturally fall into the domain of complex networks, provided that a fMRI experiment typically encompasses the calculation of the time series of 10^5 voxels for each individual, leading to a potentially huge network.

Great effort was put into every data acquisition operation, as well as network construction step, since human brain data are much variable. In order to obtain a coarse-grained network from the raw data, each processing step had to be performed with specific software, and with new self-implemented methods.

The first analysed dataset has been used as a reference for characterising network properties, in particular centrality measures, since only a few studies have been carried out thus far. Some of these measures provided statistically significant centrality values, compared to a null model. This behaviour was investigated also at different points in time, using a *sliding window* approach, evaluated through a more complex null model.

The second analysed dataset contains individuals in four different states, ranging from full consciousness to deep unconsciousness. It has been used to investigate the power of these centrality measures as tools to discriminate between different consciousness states, turning out to be potential consciousness bio-markers. We show that not all the measures have the same discriminant power. To our knowledge this is the first study to characterise differences among conscious and unconscious states in healthy brains using network theory.

Contents

Introduction

The human brain is indeed a complex system of interacting elements. As a means to study its functioning, functional magnetic resonance imaging (fMRI) has become more and more popular, since it is a non-invasive procedure and it provides a good balance between temporal and spatial resolution. It is controversial, in that the signal it gives is not a direct indication of neural activity, rather it is a response of the increased request of oxygen in spread out brain regions. The signal it measures is known as blood oxygen level dependent (BOLD) signal.

fMRI has mostly been utilised to mark regions associated with certain functions. A control image is subtracted to a task image to identify differences between healthy and injured brains, and to highlight the areas related to the task being performed. fMRI has become even more popular after the discovery, in the mid '90s, of regular signal patterns in absence of any task, the so called *resting state*.

Many theories suggest possible tasks of the brain at rest. A sceptical view is to think it is just due to experimental noise, such as heart-beat, respiration, and so forth. Many evidences, however, suggest this is not the case, and many preprocessing steps have to be carried out in order to rule out these contributions. More optimistic and fascinating theories involve processing of previously acquired information, memory consolidation and preparation to a future task. A definitive answer, however, is far from being reached, and a lot of work has to be done even to understand much simpler processes.

Studying the resting state is impossible with the traditional subtraction technique, therefore new methods have been implemented. Network theory, a set of tools lying across the fields of applied maths, statistical physics and sociology, is particularly suitable in studying any complex system whose constituents are interacting in non-trivial ways. Network theory can be applied to study systems whose elements, or *nodes* interact with one

another through relations modelled by network *edges*. It has rapidly spread along with the development of technology and the need to analyse high-throughput data, as in the case of brain imaging, where for every time point, a volume contains more than 10^5 data.

In this thesis we characterised network properties, in particular the concept of *centrality*, which represents the importance of each node in a network; in this case it is a measure of the importance of a region in the brain. Using a publicly available dataset, we studied the behaviour of two well known and already utilised measures, eigenvector centrality and betweenness centrality, as well as a new class of centrality measures, the k-spectral centralities. Moreover we utilised another data set encompassing different states of consciousness and we used centrality values as features to discriminate between them. Studies have already been made which characterise differences in brain structures among different states, especially in injured brain. However, to our knowledge, the present study utilises a unique design, in that it is the first to use network measures, and in particular to use network centralities as features to discriminate between a conscious and an unconscious state in healthy brains.

This work is structured as follows.

- **Chapter 1:** the introduction on brain constituents, how the brain is organised and the techniques utilised to study it, with particular attention to fMRI is discussed. Moreover the preprocessing steps needed in a fMRI analysis are explained. The state of the art on resting state studies is also presented.

- **Chapter 2:** the basics of network theory is outlined, with particular focus on the centrality measures and real networks structures. Moreover the studies on brain using networks as well as the processing step which need to be taken in a brain network analyses are discussed.

- **Chapter 3:** first, the two data sets are presented, along with the preprocessing steps we performed. Second, we outline the network construction procedures and the issues we encountered. Third, all the approaches to network measures taken, the algorithms and the statistical tests are explained.

- **Chapter 4:** we present the results of our analyses. First of all we show the characterisation of the networks, with the similarities and differences between our work

and previous studies. Then, we show how our methods may constitute useful tools for discriminating among different consciousness states, becoming potential consciousness *bio-markers*.

Chapter 1

The resting state

The brain *resting state* can be defined as a cognitive state in which a subject is quietly awake and alert but does not engage in any specific cognitive or behavioural task [10]. The studies on resting state were triggered after then a PhD student at the Medical College of Wisconsin in Milwaukee, Bharat Biswal, was trying to improve functional magnetic resonance imaging (fMRI) images by identifying background signals from fMRI scans. Indeed at the time the assumption was that all that background activity was just noise. However, while looking at scans taken when people were resting in the scanner, he saw regular, low-frequency fluctuations in the brain. As a result he suggested that neuronal activity was taking place even during such a resting state. Since it had been viewed as *noise* in task-response studies, this spontaneous component of the fMRI signal was until then usually minimised through averaging. The presence of neural activity at rest should not be surprising, if the amount of energy devoted to it is any indication. In fact, depending on the approach used, it is estimated that 60% to 80% of the brain's enormous energy budget is used to support communication among neurons, functional activity by definition [40]. On the contrary, the energy associated with momentary demands of the environment does not overtake 1.0% of the total energy budget. This cost-based analysis suggests that intrinsic activity may be at least as important as evoked activity in understanding overall brain functioning. Among the regions highlighted during resting state, great importance is given to the *default-mode network*, a set of brain regions that are consistently deactivated during the performance of diverse cognitive tasks [10].

This introductory chapter outlines the neuroscientific framework of the study. While a too detailed analysis on the biology of brain processes and fMRI is beyond the scope of this work, some background knowledge about the mode of brain functioning and the techniques used to analyse it, with the issues that they carry, is certainly helpful for understanding the presented analyses.

First of all this chapter introduces the current knowledge on how brain works, its constituent and how it is investigated (section 1.1). Particular attention will be placed on its network structure, and on the concept of *connectivity*.

Then the focus will shift on resting state and an overview of the related benchmark studies is provided (section 1.2).

In section 1.3, one of the most commonly used techniques to study brain functioning is explained, as well as the physical principles on which it lies. Moreover the blood oxygen level dependent (BOLD) signal will be described, with the issues which it makes arise. The last paragraph of this section analyses the common pre-processing steps which need to be performed after an fMRI acquisition.

1.1 Brain fundamentals

The human brain accounts for only the 2% of the body total mass but it takes up the 20% of the body's energy, most of which is used to support spontaneous neural activity. The fundamental neural unit is the *neuron*, whose diameter can vary between 4 and 100 μm. About a hundred billions of neurons constitute our brain and they transmit the signals to one another through *synapses* - either chemical or electrical - which represent neuronal connections. Each neuron can have up to 10^5 inward connections and, taking into account that about 100 billion neurons are present in the human brain, they are organised into a huge and complex network of connections - which could theoretically reach 10^{16} [1] - known as *connectome*. This complex structure makes the brain particularly apt to be studied through the tools of network theory, (chapter 2).

A neuron is made up of a cell body - its "computational unit" - and by fibres connecting them, dendrites and axons, which are the receive and send the signals, respectively. Axons

[1] the current estimate of the number of connections is 10^{14}

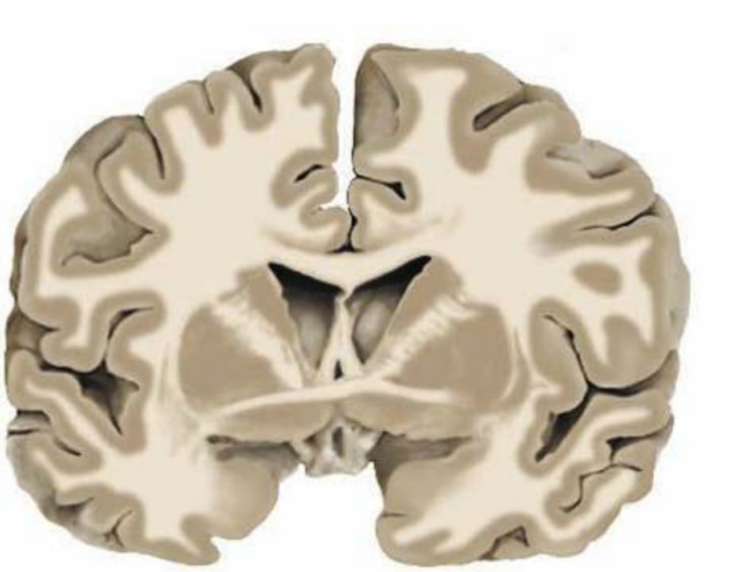

Figure 1.1: A coronal section of the brain where the difference between white matter (light gray) and gray matter (dark gray) is visible. The black or darker gray areas are filled with cerebrospinal fluid and the two triangle-shaped areas in the middle are the ventricles, where the cerebrospinal fluid is produced [39].

can reach lengths of one metre and due to the myelin sheath covering them are often referred to as *white matter*, opposed to *gray matter*, constituted basically by cell bodies and unmyelinated axons. Gray matter is usually found within the cortex, the part of brain close to the scalp and in some subcortical regions called nuclei, whereas white matter comprises all the axonal fibres connecting areas from the left hemisphere to the ones in the right hemisphere, and vice versa as well as connections within the same hemisphere. These cells lie in the so called cerebrospinal fluid. It is important to know the difference between these components since in functional studies we are only interested in signal coming from gray matter, whereas in tractography we are mainly concerned with the axon fibres. The location of gray and white matter within the brain is shown in figure 1.1.

Two different and complementary properties characterise the connectome: *segregation* and *integration*. Segregation refers to the property of some functions to be localised in certain brain areas, whereas integration involves the computation the brain performs in

order to put together and elaborate information coming from different areas. How these two properties arise due to the intrinsic structure of brain is an investigated matter.

At the beginning of nineteenth century, it was thought that brain was the organ of mind and that it was composed of separate areas, each being the organ of a specific behaviour; this pseudomedicine is known as phrenology, and it was the fundamental of many psychological and psychiatric theories of the time. This also lead to many cruel surgical interventions to remove brain areas in order to correct for some behaviours which were considered wrong. These *lobotomies* obviously resulted in catastrophic damages for individuals undergoing them, showing impairment in some behaviour. Although phrenology relied on some true bases, it was certainly representative of a very little part of the processes going on in the brain. Scientists started to understand that brain does not have a purely localised structure, rather all the different areas interact in order to perform more complex functions. Indeed it holds true that simpler functions refer to specific areas within the brain. Thus we can talk about more localised structures dedicated to simpler functions, as the sensory cortices (visual cortex, auditory cortex, somatosensory cortex) and the motor cortex. Furthermore each different patch of the somatosensory cortex corresponds to a different body parts, the most sensible, such as fingers, being overrepresented in size compared to other components, such as back, chest and so forth. However association areas are responsible for performing more complex operations or for emotions. How this view is nowadays influenced by phrenology is still a debated matter.

Nevertheless, the most common neuroscientific way of thinking about brain mechanisms is in term of *connections* or interactions between different specialised areas. With this viewpoint, then, an area is specialised to a given function rather than to another because neurons in that area are connected, cooperate and activate together. However connections are present among very different parts: an example is carried by the high number of axon fibres connected cortical neurons among the two hemispheres. Nevertheless it has to be noted that brain connections are not static and determined once and for all. Synapses can be formed and deleted in various ways and these processes are thought to be the underlying neurobiological bases from which the concept of memory arises .

We point out that the brain is a complex system characterised by different level of complexity. Therefore, opposed to the nanoscale or microscale, used by neurobiologists to study the way individual neurons interact, another approach is to study brain at the

mesoscale or macroscale, through the interactions among bigger areas comprising groups of several neurons. Studying brain as a network of connections has been aided by the development of *complex network theory* (chapter 2).

1.1.1 Brain connectivity

There are different ways of studying connections in the brain, each of which reflects different nature of connections: *structural*, *functional* and *effective* connectivity. The first, as the name says, reflects the anatomical links that are present among brain regions, mainly represented by axon fibres. The second represents co-activation patterns, that is it associates regions whose signals are related, independently of physical links; it is often measured through correlation or spectral coherence. The third, inspects also the *causality* of this relation, with methods such as perturbation of the system and the study of its time series through the use of Granger Causality and transfer entropy [46, 47]. The interaction between these types of connectivity, and in particular if and how the structure gives rise to function in neuroscience are among the current neuroscience challenges [46, 16].

Athough FC has been always seen as static, lately evidences indicated that they are dynamic [27, 22, 48], even though this is a debated matter. Many studies argue that the simple variation of correlation among time-series is not an indication of dynamical functional connectivity, because changes in correlation values can occur also among to random noise signals. Accordingly, adequate statistical tests have to be employed in order to assess the nature of these temporal variations [23, 24, 29].

The use of correlation itself as a means to infer functional connectivity has sometimes been criticised, however problems with this measure arise only when this is not tested with null models [55]. Recent approaches toward the studying of dynamical connectivity have relied mainly on the so called *sliding window* method [30, 11], which will be explained in chapter 3. A pitfall of this method is the confounding contribution of non-neurogenic signals such as motion, instrumental drift, and thermal noise, which is difficult to distinguish from the “true” signal, especially when using short time windows. As a result statistical tests and null models have to be employed, in order to rule out the hypothesis of spurious dynamics.

1.1.2 How to investigate the brain

There are different methods to investigate the structure as well as the function of the brain. As for brain function, the techniques mainly fall into two distinct classes: electro-physiological recording and functional imaging. Electro-physiological methods directly detect neural activity. The most common techniques are electroencephalography (EEG), electrocorticography or internal EEG (ECoG, or iEEG), magneto-encephalography (MEG) and multielectroarray recording (MEA).

- EEG is a non-invasive technique, because the electrodes are placed along the scalp. While having a high temporal resolution, it has really poor spatial resolution. It is mainly used to detect overall increase in brain activity such in epilepsy, or in behavioural studies.

- When EEG is performed with intracranial electrodes it is called electrocorticography (ECoG), or intracranial electroencephalography (iEEG). Here electrodes are placed directly on the exposed surface of the brain. Since it involves a craniotomy (a surgical incision into the skull) to implant the electrode grid, ECoG is an invasive procedure and it is not applied on healthy brains, thus it is used when surgery is required for other purposes.

- Magnetoencephalography (MEG) is the analogous of EEG which detects magnetic fields produced by electrical currents occurring naturally in the brain, rather that electric signals. Arrays of superconducting devices are used as magnetometer. MEG, as EEG, applies on basic research into perceptual and cognitive brain processes, localising regions affected by pathology before surgical removal, and determining the function of various parts of the brain.

- Multielectrode arrays (MEAs) or microelectrode arrays are devices containing multiple plates through which neural signals are obtained or delivered. These plates serve as neural interfaces that connect neurons to electronic circuitry. MEAs can be implantable MEAs or non-implantable MEAs, used in vivo or in vitro, respectively.

Imaging techniques on the other hand are mainly PET (Positron Emission Tomography) and fMRI (functional Magnetic Resonance Imaging).

- PET is a nuclear medicine technique used to observe metabolic processes in the body. After the injection of a (β^+) radionuclide tracer, the system detects the pairs of gamma emitted by the positrons. The tracer is introduced in the body through a biologically active molecule, for example Flurodeoxyglucose (18F) (FDG). Fluorodeoxyglucose is uptaken by the brain when needed and thus in these areas pairs of gamma rays are produced. This is useful in exploring the presence of cancer metastasis. The drawback of this technique is that, even though not directly invasive, the injection of a radioisotope is harmful for the organism.

- fMRI is a non-invasive technique which does not directly measure the activity, but relies on the oxygen consumption in areas where energy is required, measuring the Blood Oxygen Level Dependent (BOLD) signal. This technique is the basis of this thesis, therefore it will be further explained later (section 1.3).

A comparison of this measure makes fMRI probably the most used tool in many applications. It has a much better spatial resolution than electrophiosiology recordings (about 3 mm) which goes to the detriment of temporal resolution (about 2 seconds, whereas EEG can reach 0.01 seconds). Moreover fMRI detects well signal coming from inner areas, whereas EEG detects better superficial signals, given that electrods are placed on the scalp. Studies utilising PET and EEG recordings are consistent with data obtained from fMRI and thus provide a proof of the validity of fMRI as a technique to study brain networks.

When studying the functioning of the brain, one wants to know also to what brain area a signal is related, not just its abstract spatial location. As a result, structural imaging of the brain have to be taken and overlapped to functional ones. Structural MRI principles are almost the same of fMRI and will be better inspected later (section 1.3) . The fundamental difference is that for structural images the water content of different tissues is exploited, instead of the properties of oxygen . A variant of MRI, which is specific in studying fibre tracts is DTI (Diffusion Tensor Imaging). It relies on the alignment of the magnetic fields of water molecules, which is basically in the fibre direction. It is a special case of DWI (Diffusion Weighted Image), which is based on the directions in which the water is diffused. Of course when the diffusion is constrained it reveals important information about the structure. Some measures used to quantify the fibre tracts with DTI are fractional

anisotropy (FA), mean diffusivity (MD), fibre count and probabilistic tractography.

1.2 Resting state studies

Usual fMRI experiments involve the comparison of two images: the images acquired under task, and a control image, that is an image acquired when the task is not performed. The neural activation is then detected subtracting the control image to the task image. As previously mentioned when Biswal was trying to reduce the baseline noise of a fMRI task experiment, he saw coherent patterns of activity on the baseline [7], as reported in figure 1.2. This signal expressed mainly low-frequency components, ranging from 0.01 to 0.1 Hz approximately. In his experiment a time course of a seed region-of-interest(ROI) in the left motor cortex was correlated with the time-course of all other brain voxels. The resulting map demonstrated functional connectivity between the left and right motor cortex even in the absence of a task. After this discovery, other pattern of activities were found, leading to the discovery of many resting state networks (RSNs). Common RSNs found by subsequent studies are visible in figure 1.3. Interestingly researchers began noticing that some areas decrease their activity in task conditions, compared to control conditions. This means that such areas are to some extent more active at rest than they are during task. These regions proved to be consistent across subjects. The idea arose that they constitute a *Default Mode Network* (DMN), whose function is still not clear. This network has been highlighted by many resting state studies (figure 1.3).

In order to identify such networks at the beginning the same technique as Biswal's was used, namely only a seed region was selected, and correlation computed. In following studies, however, other techniques to detect and study resting states were used; one is independent component analysis (ICA) [6, 13]. ICA decomposes the 4-dimensional BOLD signal, that is the signals of the 4-D brain volume repeated over time, into a set of spatially distinct maps and their associated time-courses. Among these independent components are several readily identified functional brain networks, but also artefacts related to movement and physiological noise [14]. This is due to a general limitation of resting-state fMRI, that is it is difficult to separate physiological noise, induced by the cardiac pulse and respiration, from the BOLD signal. Even if in principle ICA does separate this physiological noise, a little component might still be present. This drawback lead a few re-

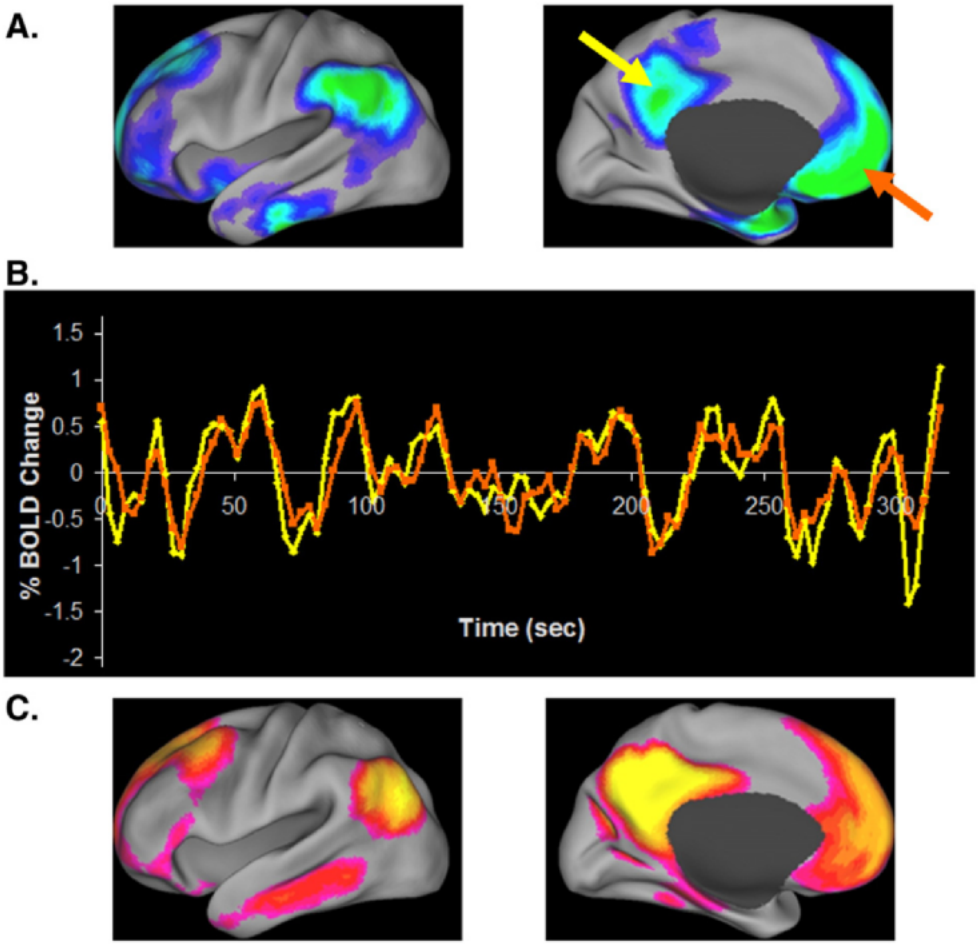

Figure 1.2: Resting state signal of two regions belonging to the so called Default Mode Network [40]. In (A) the regions which show a decrease in activity during task experiment are highlighted. The signals of two different regions, indicated by the arrows, show high consistency (B). Using these fluctuations to study the network, reveals a level of functional organisation which parallels the one showed in task studies (C).

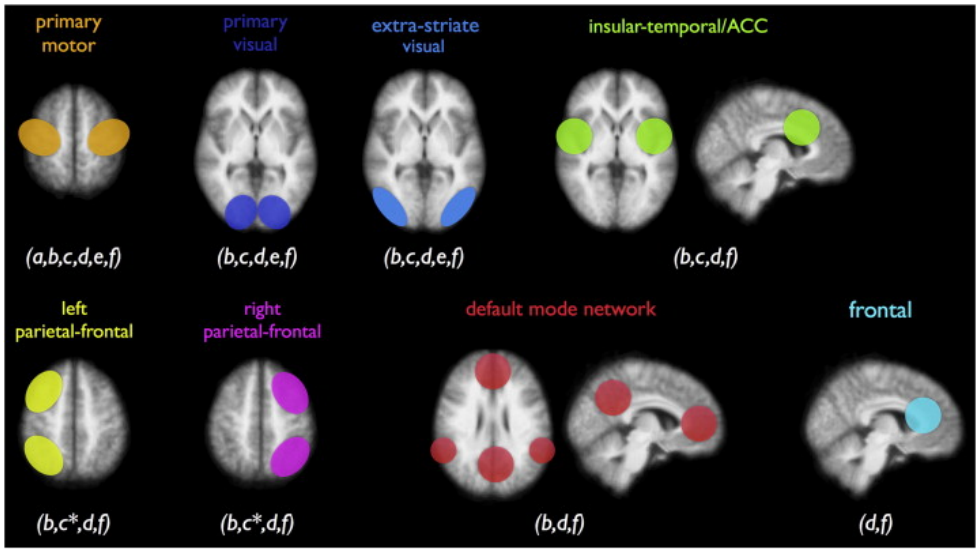

Figure 1.3: Resting state networks commonly identified in the literature as summarised by Van Den Heuvel et colleagues [52]. Letters refer to the studies which found the corresponding resting state: (a) [7], (b) [6], (c) [15], (d) [13], (e) [42], and (f) [53].

searchers to claim that the resting state signals are just a result of this physiological noise. There are many indications, however, that this is not the case: the most convincing is that RSNs resemble areas already known to be specific to a given task.

Another way to inspect the RSNs is represented by clustering approaches. A benchmark study in the organisation of cerebral cortex in resting state networks, employing a clustering approach, is the one made by Yeo et al. in 2011 [54]. In this study they considered 1000 subjects to provide a reference map for the organisation of human cerebral cortex in functional connectivity and to better investigate a few specific networks. As for the maps they used a clustering based approach and found 7 RSNs, which had a good overlap to the ones obtained in the literature. This is one of the furthest proofs of the existence of RSNs. The map resulted from their study is visible in figure 1.4, and the label corresponding to the RSNs are visible in table 1.1. Most of the networks are in accordance with previously found networks, as seen in figure 1.3, nevertheless the Yeo's study extended some networks. As should be clear from the definition of resting state and functional connectivity, we point out that the two concepts are deeply entangled. Resting state studies

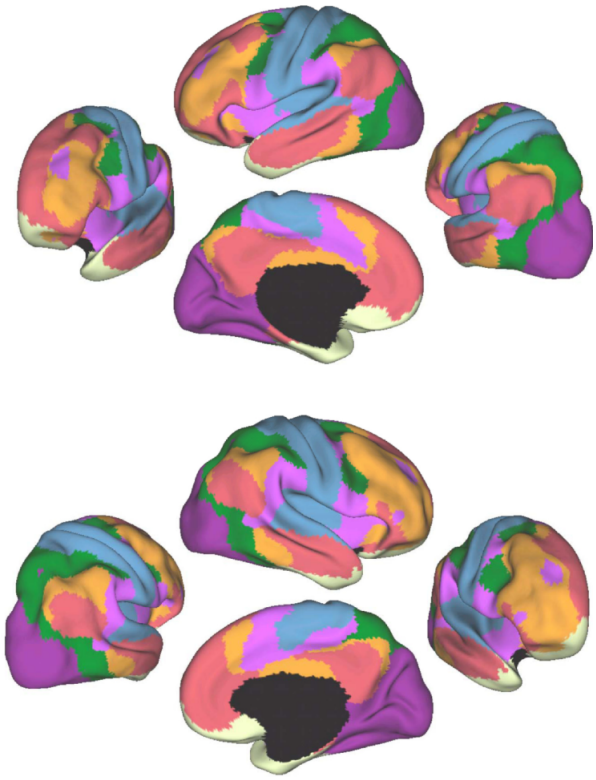

Figure 1.4: Resting State Networks as identified by the Yeo benchmark study [54]. A first evidence is that such networks embed also areas which are not connected. Another feature is that motor and sensory areas are distinct from association cortices; the latter converged and extended on networks previously described in the resting state literature, including the dorsal attention, ventral attention, frontoparietal control and default network (figure 1.3).

color	RSN
purple	visual
blue	somatomotor
green	ventral attention
violet	dorsal attention
cream	limbic
orange	frontoparietal
red	default

Table 1.1: Label of the resting state networks of figure 1.4.

mainly studies functional connectivity, which, in turn, is organised in a way that gives rise to the resting state networks. Related to these concepts, also network theory (Chapter 2), plays a pivotal role in the study of resting states.

1.3 The fMRI technique

fMRI, as told is the most used non-invasive technique to study the brain functioning. It is an indirect measure of brain activity since it relies on the Blood Oxygen Level Dependent (BOLD) signal. The resulting image is a collection of 3-D volumes, one for each sampled time point. The time intercurring between each scan is called repetition time (TR), which is typically 2 or 3 seconds, even though with the *echo-planar* imaging, a scan is performed in a few hundreds of milliseconds.. Each volume is divided into *voxels*, a set of "cubes" (more precisely they are rectangular prisms) which can be considered the 3-D version of pixels. Voxels are the result of the digitalisation of the acquired image and their dimensions determine the resolution of the image. Even though one can think that smaller voxels increase the resolution, actually this is not the case, given that a lower limit in resolution is intrinsically present due to the nature of the BOLD signal. Voxels' size is typically (3x3x3.5) mm, and a human brain can have about 32-34 slices containing a 64x64 array of voxels [5]. If we use these parameter, each volume will contain 135168 voxels. Considering that a typical scanning session is 20-30 minutes, more than 100 time

points can be acquired, resulting in an order of magnitude of 10^7 values, which is indeed a huge number.

Physical principles of fMRI rely on the magnetic property of materials, in particular materials whose constituent nuclei have non-zero spin. Since spin has a magnetic moment associated with it, when these nuclei are placed in a magnetic field $\vec{B_0}$, they align themselves with the magnetic field, distributing in the possible energy levels according to the Boltzmann distribution. As a result a total magnetisation vector $\vec{M}$ is built up, which is again aligned with the total magnetic field. When the nuclei placed in such magnetic field are also subjected to a time-varying (radio-frequency) electromagnetic pulse $\vec{B_1}(t)$, perpendicular to $\vec{B_0}$, the magnetisation varies. MR images are related to how the system goes back to the equilibrium state. There are two characteristic times which guide this relaxation, usually called T_1 and T_2. The first refers to the spin-lattice relaxation when recovering M_z, namely how fast the magnetic moments realign with $\vec{B_0}$, the second refers to spin-spin interaction and depends on the different chemical neighbourhood in which the nuclei are placed. A universal feature is that $T_2 < T_1$. The two equations representing the evolution of the magnetisation along time are called Bloch equations and lead to

$$M_z(t) = M_z(0)e^{-t/T_1} + M_0(1 - e^{-t/T_1}) \tag{1.1}$$

and to

$$M_z(t) = M_{xy}(0)e^{-t/T_2} \tag{1.2}$$

for the components which are parallel and perpendicular to $\vec{B_0}$, respectively. Since the decay of the signal following a single radio-frequency pulse is usually too fast and depends mainly on field inhomogeneities, sequences of impulses are used. Combining (1.1) and (1.2), after some manipulations one gets the following equation for a particular sequence, known as spin-echo, with so called the spin-warp method:

$$M_{xy}(T_R, T_E) = M_0[1 - e^{-T_R/T_1}(2e^{T_E/2T_1} - 1)]e^{-T_E/T_2} \tag{1.3}$$

Here T_R and T_E are two different parameters used in the sequence. In particular TR is the aforementioned repetition time, whereas TE is called *echo time*. From (1.3) one can see that modifying the parameters T_E and T_R, one can weight the image in T_1 ot T_2. This

means that if different tissues or areas have different decay times, these parameters are chosen in a way that the signal from one tissue or area has completely decayed, while the other is still present.

Structural images are T1-weighted: white matter (more fatty) has a signal decreasing faster than grey matter, in that its relaxation time is smaller. For functional images a T_2 weighting is often employed.

1.3.1 The BOLD signal

The BOLD signal, as the name says, is a measure of the amount of the oxygen contained in blood flowing in neural regions. In order to work the brain needs energy, in the form of Adenine TriPhosphate (ATP), which, in turn, is produced through a chemical reaction involving glucose and oxygen. As neither glucose nor oxygen are stored in the brain, they need to be carried to the brain by blood. Oxygen is transported by haemoglobin, in a chemical form which is known as oxy-haemoglobin, in contrast to deoxy-haemoglobin, the form haemoglobin assumes when it releases the additional oxygen. These two molecular forms differ in their magnetic properties: oxy-haemoglobin is paramagnetic, whereas deoxy-haemoglobin is diamagnetic. When energy is required in a particular area the amount of incoming oxygen (oxyhaemoglobin) is much higher than the oxygen being consumed to form ATP. As a result these areas show an increase in signal intensity.

Oxy-haemoglobin and deoxy-haemoglobin have different T_2, the first being diamagnetic while the second being paramagnetic. This results in a low field inhomogeneity and slow spin dephasing for oxy-haemoglobin, instead this leads to a higher field inhomogeneity and a faster spin dephasing for deoxy-haemoglobin. Accordingly oxy-haemoglobin has a higher T_2 than deoxy-haemoglobin. Choosing suitable parameter allows to measure only the signal from oxygenated areas, with enhanced contrast. It has to be pointed out, however, that the oxygen influx is leading to the BOLD signal is not a consequence of neural activity, rather they are parallel processes. In fact Glutamate-generated calcium influx releases many vasodilators. Blood flow is related more to local field potentials than individual neurons spiking [31], therefore it is increased over an area larger than the one with neuronal activity. Global blood flow changes also associated with dopamine, noradrenaline and serotonin, therefore not related to energy consumption. As a result some

controversies remain and the way it is related to neural activity has still to be investigated and can lead to improvements in the fMRI technique. Nevertheless attempts to model the BOLD signal are made, since the goal of fMRI is to learn something about the underlying neural processes.

Most fMRI applications do not need to make assumptions on the signal at a cell-detailed level. Instead neural activation is treated as a rather abstract unobservable variable, which is assumed to increase along with neural activity. In order to make inferences about this activity, a precise relation between the BOLD signal and neural activity has to be made. The link between the the BOLD signal and the true neural signal lies in the haemodynamic response function (HRF). Mathematically the BOLD signal is a convolution between the actual neural signal and the HRF, which accounts for how the system responds to the stimulus.

$$B(t) = N(t) * h(t) = \int_0^t N(\tau)h(t-\tau)d\tau \tag{1.4}$$

This is true when we assume that the system response is linear and time invariant. In fact, a neural signal can be written as

$$N(t) = \int_{t=0}^{\infty} \delta(t-\tau)n_\tau d\tau \tag{1.5}$$

Given that the BOLD function is a function of neural activity, $B(t) = f(N(t))$, linearity implies that

$$f\left(\int_{\tau=0}^{\infty} \delta(t-\tau)n_\tau d\tau\right) = \int_{\tau=0}^{\infty} f[\delta(t-\tau)]n_\tau d\tau \tag{1.6}$$

This in turn proves 1.4. Although many evidences indicate that BOLD signal is non-linear, the departures from linearity are often small and linearity assumptions are quite valid in many applications.

The HRF depends on how the oxygen is consumed when energy is requested by neurons, and it is thus quite a complex function to model. Even though equation 1.4 holds true, the issues derive from $N(t)$ and $h(t)$ being both unknown. As a result a method is needed to estimate the HRF, in order to be able to calculate the neural signal. Several methods have been implemented but all of them carry some pitfalls. The ways which have

been tried so far rely mostly on (i) recording the response to a given neural input , (ii) deconvolving equation 1.4 assuming a model for N(t), and (iii) trying to"guess" the function and adjust it with some parameter fitting. Whatever model is employed, one main feature about the HRF is always present, and important on the consequence it induces on the BOLD signal $B(t)$. $h(t)$ has a low response, due to oxygen being quite slow (10 seconds) to reach its maximum value after neural *activation*. As a consequence if there are impulses which are close to one another, the BOLD response does not have time to decrease, because of the convolution with the HRF. In conclusion we can say that BOLD always smooths the underlying neural signal.

1.3.2 Data preprocessing

The preprocessing of fMRI includes all the transformations which are needed to prepare the data for the subsequent - whether task or resting - analyses. Preprocessing steps typically are the same for all experiments so they do not depend on the specific hypotheses made for a particular experiment. The aim of data preprocessing is to reduce the statistical noise, in order to better extract the true signal. If this holds true for task-based studies, where the peak usually does not exceed a few percentage of the baseline value, it becomes particularly important in resting state analysis, given that there is no peak in the time series compared to the average value of the entire series. The maximum variation from the average often does not even overcome 1% as visible in figure 1.2.) Here, an overview of the most utilised preprocessing steps is outlined.

- Slice-timing correction: All fMRI data are collected in slices, which in turn contain arrays of voxels. The TR is the time which spans the onsets of consecutive whole brain scans, that is the time we need to collect data from all the brain voxels at a given point in time. This makes arise some problems, i.e. not all the brain voxels in a given TR are acquired simultaneously: a TR time is needed to take all the slices between the first and the last. The bias is dependent on the order in which slices are taken. The most common approach to deal with this issue is a form of temporal interpolation, which can be linear, spline, or sinc. Linear interpolation is good when data do not vary much rapidly from one time acquisition to the other. This approach simply consists of estimating a continuous BOLD function from the

discrete sampling; when using a linear function, a simple line is estimated between two points, and the value at the point of interest is taken.

- Head motion correction: It is probably the most important preprocessing step. During task studies, for example, a movement of 5 mm can increase activation values by a factor of 5, and it can completely mix up signal from different voxels in resting state studies. All the corrections have the assumption that during movements brain does not change size or shape, as a result the only change is due to rigid body movement. Indeed, the movement can be characterised by six parameters, 3 translational and 3 rotational, as described by classical mechanics. Voxels are defined by their position within the scanner, rather than by position within the subject's brain. To correct for this a rigid body registration is performed, which consists of taking (usually) the first TR as the standard and then performing rigid body movements on the second TR, until the activation signal is as close as possible to the reference one. This assumes that the signal does not vary much in time. Of course if the signal did not vary at all the whole study would be meaningless; fortunately, however, different areas have different absolute intensities, which ensures this approach is feasible.

- Coregistration: functional data have to be mapped onto structural data in order to assess where in the brain the signal is coming from. These is not straightforward due to the two images being taken with different spatial resolutions. Given that functional images have to be taken within a few seconds, as a consequence of a speed-accuracy trade-off, they have quite a poor spatial resolution. Structural images, on the other hand, can take even 10 minutes in order to be formed, to provide a precise mapping of every region. This results in different voxel sizes: a typical fMRI voxel is (3x3x3.5) mm, whereas sMRI can have voxels with sizes down to (0.86x0.86x0.89) mm. After coregistration, however, structural resolution can be employed to improve functional resolution. Another problem arises from the different parameters used in the acquisition of the two types of images. These two reason make impossible to use the same approach as in head movement corrections, because a reliable objective function to minimise cannot be found. Early methods aimed at identifying key landmarks in the two different images and then trying to align them, but this is reliable just if it is done by hand, and require excellent neuroanatomical abilities.

Thus the use methods different from landmark identification is needed. One of the common procedure relies on the minimisation of mutual information between histograms of the images, i.e. finding the rigid body movement that minimises this quantity.

- Normalisation: each individual has a different brain, with different global size and different local regions sizes, too. This leads to many problems when one wants to see if a signal observe in one region is observed in the same region in another patient. Moreover when performing group analyses, brains have to be overlapped, in order to increase the signal to noise ratio and the statistical significance of the analysis. However, if we overlap two regions which have nothing to do with one another, the signal is quite likely to average out. Therefore warping the subject's structural image to a standard brain atlas is needed.The most common reference system is the MNI space, developed by the Montreal Neurological Institute [17], from 305 different individuals, which took over the Talaraich atlas [49] in many applications, since this latter just relied on a dissected brain of a 60-year-old French woman. Whatever atlas is used, the problem is more complicated than for head motion correction or coregistration, since this does not simply involve a rigid body movement, but linear transformations to correct for differences in size and non-linear transformation to correct for differences in shape.

- Segmentation: sometimes when the process of normalisation is indirect, one has to divide the brain areas into white matter, gray matter and cerebrospinal fluid, depending to the application one wants to use. However, depending on the software used, this process may be embedded in the normalisation step.

- Data smoothing: intensity values from individual voxel have an embedded component of noise. In order to reduce this noise spatial smoothing is needed; basically the intensity value of a voxel is replaced with a weighted average of the values of neighbouring voxels, through the convolution between the voxels and a function of the neighbourhood known as *kernel*. Indeed close voxels contribute much more than distant voxels. There is no fixed size for the definition of neighbourhood, but usually a kernel with a radius of 1 to 3 voxels is utilised. Other that increasing SNR

this procedure is useful since , as explained by the central limit theorem, it makes the distribution of intensities more normal and facilitates the multiple comparison analysis in task studies.

- Temporal filtering: it is applied to remove the effect of particular frequencies. Usually high frequencies do not give problems, since, according to Nyquist-Shannon theorem, with a TR of 2 seconds, the maximum frequency which is present is 0.25 Hz.The application of a bandpass filter is required. In task studies the goal is to reduce the effects of slow fluctuations, therefore a high pass filter is applied. The rule of thumb in resting state analysis, instead, is to keep the frequencies ranging from 0.01 Hz to approximately 0.1 Hz.

All these preprocessing steps, as well as many other data processing operations can be performed with several software. The most famous are SPM [4] or FSL [25], which are both open source. The two software allow to perform the most common preprocessing operations, as well as many post processing operations, either from the command line or from GUIs. The most common fMRI file formats are the *DICOM*, and *analyze*, *NIfTI*, which differ mainly in the header file being embedded in the data file or in two separate file, and in the way the MR coordinates are read. SPM and FSL allow to deal with all the types of files and the default in the newer versions is NIfTI.

Chapter 2

Network theory

Network theory is the study of networks, structures analysing the relation between entities which can be of the most different types. The solution to problem of Königsberg bridge, stated by Euler in 1735 is considered the first proof of the theory of networks [36]. In the twentieth century, then, network theory has developed into a substantive body of knowledge. The first application is found in social sciences, in the 1970s. Typical network studies in sociology involve the circulation of questionnaires, asking respondents to detail their interactions with others. More in general it was used as a means for explaining and modelling the relations among social entities. In the last twenty years, however, it has spread onto many other fields, such as informatics (the World Wide Web), economics, biology, neuroscience and climatology, yielding *Complex Network Theory*. In many fields it is employed to study the interactions among elements in big datasets, especially when a full knowledge of the processes triggered by the undergoing interactions is lacking. Here we mention just a few examples which show why networks are suitable to be utilised. In biology the cell is best described as a complex network of chemicals interacting through chemical reactions and the same can be said about metabolites, genes and proteins. In informatics the Internet is a complex network of routers and computers whose links can be physical or wireless and the World Wide Web is an enormous virtual network of Web pages connected by hyperlinks [1].

This chapter deals with the mathematical tools of graph theory, on whose basis the whole theory is built (section 2.1). Concepts such as the *adjacency matrix*, the *laplacian*

matrix, weighted and directed networks are introduced. Moreover theoretical network types such as the *Erdos-Renyi* network, which is often used as a null model, are presented.

In section 2.2, some fundamental properties of real networks are explained, introducing a first distinction between global properties, and properties of single vertices.

Among the properties, the focus is placed on the concept of *centrality*, which deserves a separate section (sec. 2.3), since it is the core of this work. In particular the three different types of centrality measures used in the following analyses (Eigenvector, Betweenness, and Spectral) are discussed.

Section 2.4 explores the common features and structures of real networks, as *small world* and *scale free*, as well as cluster and modular behaviours and the concept of graph *partition*. The most common ways of assessing the goodness of a partition are also presented and the tool of multilayer networks and in particular *multiplex networks*, a possible future direction for this work, is outlined.

Eventually the state of the art concerning networks in brain studies is discussed, along with the most popular utilised approaches and the results obtained thus far, with particular attention to resting state analyses and the studies on centrality measures for the identification of possible hub nodes.

2.1 Graphs

Networks are entities composed of different actors, which can be of any type, and ties between actors. They are studied in the mathematical area known as graph theory. In such context actors are called *nodes* or *vertices*, whereas ties take the name of *edges* or *links*. A graph is then formally a structure $G(V, L)$ composed of a non-empty finite set of nodes V connected by a set of links L. Some preliminary concepts, which are the basics of network structures, need to be introduced.

- Networks can be *unweighted*, if links have all the same strength, and *weighted*, where links can take on different values. Usually a weight lies within the interval $[0, 1]$ which can be the strength of a two nodes connection or on the contrary, the proximity (distance) between the two nodes.

- Graphs can also be *directed*, when the link between node i and node j is different

from the link between node j and i (e.g. a road which can be travelled only in one way), or undirected, when the two relations are equal. In the latter case the adjacency matrix (sec. 2.1.1) is symmetrical ($A_{ij} = A_{ji}$), whereas in the former it is not.

- A network can be *connected* or *disconnected*, the last case occurring when at least two sub-networks can be found, whose elements have no connections *between* the two sub-networks, but only *within* them. In this case the adjacency matrix can always be written as a block diagonal matrix. A network is *fully connected* or complete, when every node is connected to every other node. Indeed, complete networks are meaningful only if links are weighted.

2.1.1 Network matrix representations

A graph is usually mathematically represented through an *adjacency matrix* A, whose rows or columns indices are the network nodes and whose entries are the links between all pair of nodes. Indeed, any given entry A_{ij} represents the link between node i and node j. Formally

$$A_{ij} = \begin{cases} 1 & \text{if there is a link between i and j,} \\ 0 & \text{otherwise} \end{cases} \tag{2.1}$$

In the case of weighted network, the value 1 is substituted by the weight of the link.

Another representation, even though not as widely utilised as the previous, is the *incidence matrix* I. It consists of n rows and m columns, where n and m are the number of vertices and edges, respectively. $I_{ij} = 1$ if edge j is a link between node i and another node, $I_{ij} = 0$ if edge j does not connect node i to any other node.

Particularly useful in this work, for it is the basis on which spectral centrality lies (sec. 2.3), is the *laplacian matrix* L. It is defined as follows.

$$L = D - A \tag{2.2}$$

where D is a diagonal matrix defined as the sum of each node's weights

$$D_{ij} = \begin{cases} \sum_{j=1}^{n} A_{ij} & \text{if} \quad i = j, \\ 0 & \text{if} \quad i \neq j \end{cases} \tag{2.3}$$

Ruling out the presence of self loops (i.e. any self-connected node), then the adjacency matrix has a 0-valued diagonal and the laplacian becomes

$$L_{ij} = \begin{cases} \sum_{j=1}^{n} A_{ij} & \text{if} \quad i = j, \\ -A_{ij} & \text{if} \quad i \neq j \end{cases} \tag{2.4}$$

From the definition it is clear that the sum of each row and each column is zero. Other important properties of the laplacian come from its eigenvalues and eigenvectors, as will be explained in section 2.2.1. Sometimes the normalised version of the laplacian is used, namely

$$L_{norm} = D^{-1/2} L D^{-1/2} \tag{2.5}$$

even though less common.

2.1.2 Theoretical graph structures

Beside the common properties and representations that all networks share, they can have quite different structures. Among the simplest structures we can find lattices and random networks.

- A *lattice* is the most regular type of network. Each node has a given number of links k, that is the number of connections (degree) with the nearest neighbours is fixed. In the 1-D case it is simply a chain with a circular adjacency matrix, that is a matrix whose only non-zero values are in the second diagonals. Lattice networks are useful as toy models to test other network measures. They are also interesting for their spectral properties (sec. 2.2.1).

- A *random network*, whose most famous type is the Erdos-Renyi network, on the other side, shows no regularity in nodes connections. There are different ways of

building random networks, depending on the type of ensemble one chooses: the ensemble can be microcanonical, canonical, gran-canonical in analogy with statistical physics.

These simple structures, especially random networks, are often used as *null models* to test real network properties. Many complex networks, in fact, such as the World Wide Web, were first modelled as random networks, however they soon showed much different and more complex properties; their structures often lie in between these two extremes. Random networks are therefore an useful term of comparison to assess the behaviour of real data.

2.2 Network basic measures

Networks can be characterised by a vast set of features. First of all one can distinguish between *local* and *global* features. Local features encompass properties of single nodes and their nearest neighbours, whereas global features are characteristic of a network as a whole. Among the first measures one can find centrality (the importance of a node), degree or connectivity of single nodes, closeness and more in general any parameter which can be related to single nodes. Centrality constitutes one of the most studied properties in this work, thus it deserves a separate section (sec. 2.3). Among global properties some examples are number of nodes or links, spectral properties (eigenvalues, eigenvectors), diameter, clustering coefficient, modules, assortativity.

Here we will briefly introduce these measures.

- *Degree* is defined as the number of connections or links that one node has, regardless the weight (where present).

- The version of degree for weighted network is *strength*, which is defined as the sum of weighted links. Referring to the adjacency matrix strength of a node i is written as

$$s_i = \sum_{j \neq i} A_{ij} \tag{2.6}$$

- A useful measure related to degree is *degree distribution*, that is the count of how many nodes have a given degree. The degree distribution often characterises a network.

- The *shortest path* between two nodes is the minimum distance - measured by number of links - which is needed to travel between each other.

- *Diameter* is the shortest path that can be found among the two furthest nodes in a network; as a result it is a global measure of how network elements are topologically close to one another. However it is not always a good representation because it is to sensitive to outliers.

- A stabler measure in this sense is *average path length*, which represents the average number of steps along the shortest paths for all possible pairs of nodes. This is defined as

$$l_G = \frac{1}{n(n-1)} \sum_{i \neq j} d(i,j) \tag{2.7}$$

  where n is the number of nodes, and $d(i,j)$ represents the shortest path between nodes i and j.

- A measure of nodes similarity is given by a network's *assortativity*, which represents the preference for a network nodes to connect to nodes which are similar in some ways; one type similarity can be sharing the same links, which leads to the concept of clustering coefficient.

- *Clustering coefficient* is a measure of how nodes tend to cluster together, that is how many nearest neighbours of a node i show also connections among them. Alternatively it represents the number of triangles (i.e. three nodes all connected to one another) in a given structure. Mathematically clustering coefficient is written as

$$c_i = \frac{e_i}{max(e_i)} = \frac{2e_i}{k_i(k_i-1)} \tag{2.8}$$

  where k_i is the number of nearest neighbours of i, and e_i the total number of connections among nearest neighbours. More clustering properties are inspected in section 2.4.

2.2.1 Spectral properties

A graph can be characterised in term of the eigenvalues and eigenvectors of its matrices. The *spectrum* of a graph, that is the set of its eigenvalues can provide many interesting insights about the network structure. However, the correspondence between a given network and its spectrum is not univocal. In fact different graphs can have identical spectra. Spectral analyses are interesting since they can reveal information on other graph properties. They are related to shortest paths length, diameter, number of edges, and many more.

For example the k-th power of A_{ij}, defined by the matrix product between A and itself, gives the length of the shortest path between i and j. The trace of A, which is the sum of its eigenvalues, gives the number (for an unweighted graph) of closed paths in the graph. Moreover the trace of a power of A gives information on the distribution of its eigenvalues, or *moments*.

If no self-loops are present the mean of the eigenvalue distributions is 0, but some higher order moments might be non-zero. The highest eigenvalue is a superior limit on the degree, whereas the number of distinct eigenvalues limits the diameter. Many other properties can be found and for each network particular properties can be inferred. An example is represented by a lattice network, with the eigenvalue equation

$$\sum_j A_{ij} x_j = k x_i \tag{2.9}$$

Here the eigenvalue k represents the degree and the eigenvector is $x_i = (1, 1, ...1)$.

The most interesting features for this work, however, is general and comes from the first eigenvalue, as it is closely related to the concept of *eigenvector centrality*, which will be discussed more in depth in section 2.3). Let us just note that for matrices with non-negative entries the highest eigenvalue exists and is unique. This is an extension of Perron-Froebenius theorem, which was first stated only for positive entries.

Also the laplacian matrix, defined in eq. 2.2 has a lot of important spectral properties. One important feature is that its 0 eigenvalues multiplicity gives the number of connected components, or blocks, of the network. Its structure assures that all the other eigenvalues

are positive, in fact from the eigenvalue equation we can write

$$\lambda_i = x^T L x = \sum_j A_{ij}(x_i - x_j)^2 \tag{2.10}$$

always yielding non-negative λ_i. If the network is connected, only the first eigenvalue will be equal to zero, with eigenvector $\vec{x} = (1, 1, ..., 1)$. Moreover, the smaller the second eigenvalue (also known as *Fiedler number*), the better the division of the graph into two separate blocks; this represents the so called *ratio-cut* problem. The eigenvector entries of the Fiedler number fall into two different groups, one having positive values, the other having negative values, with sum equal to zero. This plays a pivotal role in the definition of spectral centrality, as it is related to the importance of a link or a node in the network, or more in general, a group of nodes or links. Centrality is assessed looking at the variation of λ_2, when removing the element or structure whose importance we want to test for (section 2.3).

2.3 Centrality measures

The centrality of a network node is a measure of the node's importance within the graph. Nevertheless each centrality measure encodes different information. A common feature across the different measures of centrality is that they provide the same answer when applied to a star-like network, namely a network in which one node is connected to all the other, which are not connected to one another. Indeed, the central node should assume the highest value of centrality [19].

Moreover, Borgatti argued that centrality measures can be characterised along two dimensions [8]. The first dimension tells how information flows between nodes. The flow can be a serial transfer, when information travels as a compact object, as it happens for package delivery; it can also be a serial duplication, as in the case of mitotic reproduction, or parallel duplication, as in the case of email viruses. The second dimension is related to the trajectory that information follows. When assuming a shortest path transfer this implies that information has a global knowledge of the topology of the network. Alternatively information can follow trails (repeated nodes allowed) or walks (both repeated nodes and

edges allowed).

We already mentioned two quite trivial measures of centrality in section 2.2, *degree* and *strength*. Even though these measures can give a hint in guessing nodes importance, when network structure becomes more complicated they lose significance. This is due to the fact that they are *local* measures, that is they depend only on the immediate surroundings of each node.

Closeness is a measure directly related to the concept of shortest path, and in particular to its average value. In fact it is defined as

$$Cl_i = \frac{n-1}{\sum_j P_{ij}} = \frac{1}{< P >} \tag{2.11}$$

where P_{ij} represents the shortest path between nodes i and j. Basically it indicates how close the other nodes are to node i. The closer the nodes, the more important the node under analysis. Unlike degree and strength, then, it is based on distance among nodes rather than weight of their connection. To be calculated, it depends on the whole network, therefore it is a global measure.

The following measures are the three types of centrality employed in this work. They are global, too, and, as a consequence, they can deal with more complex network structures better than simple measures.

2.3.1 Eigenvector centrality

Eigenvector centrality (EC) of node i is defined as the i-th entry of the eigenvector corresponding to the highest eigenvalue of the adjacency matrix. Eigenvector centrality favours nodes connected with nodes that are in turn central within the network; this makes it quite different from degree and strength centrality. Eigenvector centrality of each node is contained in the eigenvector entries (the i-th entry gives the centrality of the corresponding node). For the eigenvector to exist, the maximum eigenvalue must be unique, which is guaranteed by the non-negative entries of the matrix and its symmetry (Perron Froebenius theorem). Mathematically EC of the i-th node is defined as

$$x_i = \frac{1}{\lambda} \sum_j A_{ij} x_j \tag{2.12}$$

where A is the adjacency matrix and x is the eigenvector corresponding to its largest eigenvalue.

Many algorithms exist by means of which one can calculate this measure. The most famous is certainly the power iteration algorithm [20], which is an iterative method; it consists of applying the adjacency matrix to a random vector v_0, and then iteratively to the resulting vector v_i n times until a sufficient close estimate v_n of the first eigenvector is obtained.

2.3.2 Betweenness centrality

Among the three considered measures, betweenness centrality (BC) is the only one not being based on eigenvectors. It evaluates the number of shortest paths that pass through a node compared to the total number of shortest paths, and it is therefore particularly important when a node is the connecting point between two otherwise separate sub-networks. One can think of it as a measure of the amount of *traffic* flowing through a node. Mathematically it reads

$$BC_i = \sum_{m \neq i} \sum_{n \neq m,i} \frac{P_{mn}(i)}{P_{mn}} \tag{2.13}$$

where i is the node for which Betweenness Centrality is measured and P_{mn} is the number of shortest paths between node m and node n.

In order to compute the shortest paths one needs to use a specific algorithm, for example the Dijkstra algorithm. The algorithm must be able to take into account the weights of the edges in the network. Due to this algorithm, BC is computationally quite heavy and thus, when a high number of nodes is taken into account, other measures might be preferred.

Betweenness and eigenvector are different, especially when the graph has a bridge structure, that is a node connecting otherwise separate parts of the graph. In particular betweenness does not fail in recognising the node's importance, when this is a bridge point with few connections. Eigenvector centrality, on the contrary, might not assign a high value to a bridge point, unless it is in turn connected to important nodes.

2.3.3 Spectral centrality

The k-spectral centralities (k-SC) consist of a new set of centrality measures based on the laplacian matrix [37]. Here we will consider the 1-spectral centrality, that is the k-SC related to the first eigenvalue of the laplacian and the 2-spectral centrality. Either the normalised version of the laplacian or the non-normalised version can be used. Spectral centrality is mathematically written as

$$S_i^k = \sum_{j=1}^{n} A_{ij}[(\nu_i)_k - (\nu_j)_k]^2 \tag{2.14}$$

where S_i^k is the spectral centrality measure for node i and eigenvalue k ($k = 1$ corresponding to the Fiedler vector), associated to eigenvector $(\vec{\nu})_k$ of the laplacian matrix. As defined in (2.14), it evaluates how much the network structure changes after removing a node. The equation says that a node is as important as the weighted sum of its edges. The weight are represented by the eigenvector entries, which, as seen in section 2.2.1, fall into two groups, one having positive and one having negative values, summing to zero. Being a spectral decomposition the first component, again the one related to the Fiedler vector, is the most important. This does not imply, however, that some useful information which cannot be revealed by the first component cannot be revealed by higher components, as shown by Pauls and Remondini [37].

Spectral centrality can be defined also for single link removal, as well as for multiple nodes or links removals. Spectral centrality for a link removal is

$$s_{i,j}^k = [(\nu_i)_k - (\nu_j)_k]^2 \tag{2.15}$$

As a result a link with high centrality value, in accordance with the ratio-cut problem, connects two vertices which are far apart, measured by the Fiedler eigenvector.

Spectral centrality does not a priori determine if the nodes with highest values are the most central or the least central. In fact this usually depends on the number of entries which have positive or negative values in the Fiedler eigenvector: if only a few nodes have negative values, then a lot of nodes will be far from them and only a few nodes will be close, unequivocally increasing the value of centrality in 2.14. This issue is easily

overcome, however, if we have a rough prior knowledge of what the nodes which are supposed to be more important are, also comparing it with other measures.

Spectral is usually quite similar to other centrality measures for sparse networks whereas they differ for dense weighted networks.

2.4 Modelling real networks

As previously mentioned, real networks often show properties which cannot be found in simpler networks. Thus, in order to study real networks, *complex network theory* - opposed to the standard "simple" theory - has arisen. It combines graph theory with elements from statistical physics, resulting in a powerful and constantly expanding set of tools for the study of networks complexity.

Here some of the common networks structures are presented.

2.4.1 Small world and Scale free networks

Among the structures characterising real networks we can certainly find scale free networks.

- *Scale free* networks are graphs whose degrees distributions follow a power law, especially for large k:

$$P(k) = k^{-\gamma} \tag{2.16}$$

  where usually $2 < \gamma < 3$. Scale free structures can emerge as a consequence of *preferential attachment*. With preferential attachment nodes are progressively added to an existing network and links are introduced to the existing nodes. In this way the probability of being linked to a given node i is proportional to the number of existing links k_i that node has; this is the so called *rich gets richer* process. A measure related to this structure is the *rich club coefficient*, which tells how well connected nodes - that is nodes with many connections - are also connected to one another. More specifically it counts how many nodes which have degree at least k are connected to one another.

- *Small world* networks represent another category of real networks. They are connected networks where the mean geodesic distance between nodes increases sufficiently slowly as a function of the number of network nodes. Usually the growth follows a logarithmic function

$$l_G \propto log\,\mathrm{n} \tag{2.17}$$

where l_G is the average path length as defined in (2.7)and n the number of nodes. Any vertex can reach any other node with a small number or steps. Our real world in many societies has such small world features. In the context of a social network, this results in the phenomenon of strangers being linked by a short chain of acquaintances, typical of a small world network. The psychologist Stanley Milgram conducted an experiment on letters sent to trace chains of acquaintances. He showed that in the US any person could reach any other within an average of only six different steps, that is six degrees of separation [35]. The acquaintance small world structure is certainly more pronounced nowadays, with the spreading of social networks. Moreover this structure is present in many other real networks.

It has to be pointed out that these two features can coexist in the same network: often real networks show both properties. Random networks, instead, usually show neither of these two properties, therefore scale-free and small-world are marking tracts of real networks.

2.4.2 Clustering and community structures

Another characteristic feature of real networks is their tendency to cluster, that is to group into different subsets of nodes or *communities*. This is again due to the fact that their links are not just randomly placed, rather they emerge according to specific processes, as the preferential attachment previously described. It often happens that vertices which are connected are in turn tied to roughly the same nodes, that is they have a high clustering coefficient (section 2.2). As a consequence nodes in a cluster are tightly connected to one another, while being sparsely connected to nodes outside the cluster. Vertices belonging to the same cluster usually have the same function within the network, which is why studying these structures is important. Community structures have been found in all types of real

networks, from social networks to collaboration networks, from biological networks to brain networks and so forth.

Formally, in a graph G with n nodes a *cluster* or *community* is defined as a subset C composed of n_c nodes. The division of a given graph into clusters is called a *partition* if each node is univocally assigned to a cluster, whereas it takes the name of *cover* if a node is allowed to be assigned to more than one community.

The basic measure related to a cluster is its *internal density* $\delta(C)_{int}$ defined as

$$\delta(C)_{int} = \frac{\#\text{ edges within } C}{\#_{\max}\text{ of edges within } C} = \frac{m_C}{\frac{n_C(n_C-1)}{2}} \tag{2.18}$$

where m_c represents the actual number of edges connecting nodes in cluster C and $n_c(n_c-1)/2$ represents the maximum number of edges that a cluster can contain given the number of nodes it has. Similarly one can define the *external density* as

$$\delta(C)_{ext} = \frac{\#\text{ intercluster edges of } C}{\#_{\max}\text{ of edges outside } C} = \frac{m_{C-(G\setminus C)}}{n_C(n-n_C)} \tag{2.19}$$

where $m_{C-(G\setminus C)}$ is the number of edges between C and all the other nodes.

Clustering methods can be classified into local and global methods, depending on whether one analyses only one subgraph and its close neighbours or all the subsets are considered for the correct functioning of the whole network. In both situations, measures to assess the goodness of a cluster structure - or to group objects - can be divided into measures based on nodes similarity (or dissimilarity) and measures relying on the optimisation of some *quality function*. In the first case distance between intra-cluster vertices should be minimised, whereas distance among inter-cluster vertices should be maximised. A common example of distance is given by the Minkowski metric, but any kind of metric can be employed [18]. Also weight of edges (i.e. simply the entries of the adjacency matrix) can be used as a measure of distance between vertices. The optimisation of a quality function, on the other hand, consists of defining a given measure, the *quality function*, which is dependent on cluster variables such as 2.18.

An example of global function is *performance*, defined as

$$Per(P) = \frac{|\{(i,j) \in e;\ C_i = C_j\}| + |\{(i,j) \notin e;\ C_i \neq C_j\}|}{n(n-1)/2} \tag{2.20}$$

Basically, it counts the number of correctly interpreted pairs of vertices, that is two vertices (i, j) connected by an edge e, when belonging to the same community $C_i = C_j$, or two vertices not connected by an edge when belonging to different communities [18].

In this framework another common measure is *modularity*. This is defined as

$$Q = \frac{1}{2m} \sum_{ij} (A_{ij} - P_{ij}) \delta(C_i, C_j) \tag{2.21}$$

where A is the adjacency matrix, m is the total number of edges in the graph, P_{ij} represents the probability that node i and node j are connected, whose particular form is dependent on the way one builds the null model and δ is equal to 1 if i and j belong to the same community, whereas it is equal to 0 if they belong to different communities.

Even though only two measures are presented here, any measure which is a function of cluster variables can be considered. Moreover we point out that there is no best measure in general to define or evaluate clusters or partitions, rather different measures are likely to perform differently in different situations. Beside this, when evaluating if a partition or a cluster structure is actually present, the method is again computing a measure and then comparing it to the distribution of values it would have in a random network. How to build a random network to use as a null model is often a debated matter. The simplest way would be building a random network with the same number of nodes and the same density of links, which are randomly distributed across nodes (Bernoulli random graph). This model does not reflect properties of a real network, however. As a result the use of models which resemble more closely a real network structure is preferred. Such models can be obtained for example fixing the degree distribution of edges.

2.4.3 Multiplex networks

A drawback of simple mono-layer networks lies in their inability to account for different types of links. The best they can do is letting the differences collapse onto a link weight, in

the case of weighted networks, while nothing can be done in the case of unweighted networks. Many real situations are not suitable to be modelled this way, given that choosing only one type of relation, rather than another, can lead to quite different network structures, which may highlight results that would otherwise be hidden.As a consequence, the need to develop different models, in the form of *networks of networks* has arisen. These structures are called *multilayer networks* and allow different types of links to be considered in the same structure, without making them collapse onto a weighted edge, and can even account for different nodes.

Unlike classical networks, in fact, multilayer networks are not composed just by nodes and edges, but also by *layers*. Due to the presence of different layers, these networks can adequately represent different types of edges and nodes within the same structure. *Multiplex networks* form a subset of multilayer networks where nodes do not change between different layers; only different edge types are considered.

The layers of multiplex networks can be studied using different approaches: one consists of inspecting the links among the nodes belonging to one layer, while the other encompasses the comparison of links between the same nodes among different layers. With the formalism of multiplex the adjacency matrix A is characterised by three indices, and therefore its entries read

$$A_{ij}^{\alpha} \begin{cases} a_{ij}^{\alpha}, & \text{if there is a link between } i \text{ and } j \text{ in layer } \alpha \\ 0, & \text{otherwise} \end{cases} \tag{2.22}$$

where, again, i and j are node indices, whereas $\alpha = 1, ..., M$ is the index referring to the α-th layer, in a multiplex with M layers. As previously discussed, the multiplex structure is useful for identifying similarities and differences among different layers. In order to pursue this goal, the *multilink* vector between any two nodes i and j is introduced as

$$\vec{m} = (m_1, m_2, ..., m_M) \tag{2.23}$$

where each entry m_α is equal to 1 if there is a link between the two nodes in layer α, 0 otherwise. An example of multiplex, which clarifies the concept of multilink is shown in figure 2.1. Multilinks allow to rewrite the adjacency matrix in a more compact form,

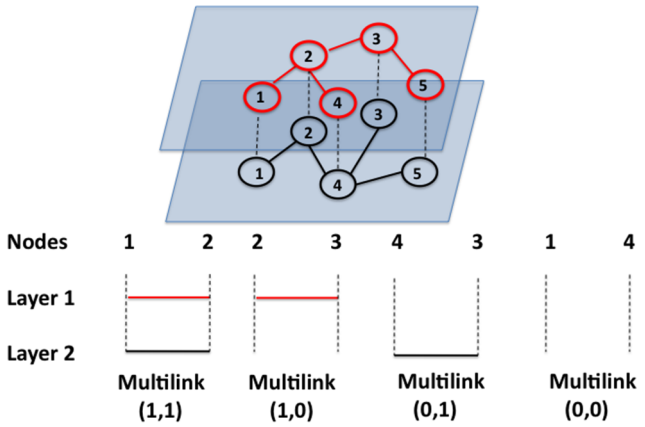

Figure 2.1: Example of multiplex with five vertices and two layers [34]. Black circles and lines represent vertices and edges of the first layer, respectively, whereas red ones represent nodes and links belonging to the second layer.

which is

$$A_{ij}^{\alpha} = \prod_{\alpha=1}^{M} [\Theta(a_{ij}^{\alpha}) m_{\alpha} + (1 - \Theta(a_{ij}^{\alpha}))(1 - m_{\alpha})] \tag{2.24}$$

where $\Theta(x) = 1$ if $x > 0$ and 0 otherwise,is the Heaviside function.

Even though multiplex networks have not been used in this work, this is one of the future directions which comes up naturally from the study, as will be explained later. (sec. 3.2).

2.5 Network theory in brain studies

As mentioned in section 1.2, graph theory can be a powerful tool in brain studies. After the first implementation in 2005 [42] in the last decade the use of network theory in brain studies has undergone a huge increase, this being due to a vast set of factors. First of all high-throughput brain data have been made available as a consequence of the development of techniques such as fMRI and technological progress in general. Second, graph theory quantifies brain networks with a set of easily computable - but at the same time neurobiologically meaningful - measures. Third, it maps both functional and structural connec-

tion onto the same space, allowing for their comparison [41]. This comparison is very useful because it appears to reveal connectivity abnormalities in injured brains and thus these methods might provide bio-markers for brain diseases. Brain connectivity datasets comprise networks of brain regions connected by anatomical tracts or by functional associations (section 1.2). These networks are therefore invariably complex and share a number of common features with networks from other biological and physical systems.

Even though graph theory can be implemented in task studies, it is more useful in resting state analysis. This is mainly due to the fact that task fMRI can be studied with the traditional image subtraction technique, but also studying the resting state may shed light on the functioning of the brain even during task activities, as well as on the global functional and structural organisation, as already pointed out in the previous chapter.

2.5.1 Construction of brain networks

A brain network requires different steps in order to be built up, which are summarised in figure 2.2. First, network nodes have to be defined. They can be electroencephalography electrodes, histological, MRI or diffusion tensor imaging data. In an MRI analysis a parcellation, that is the definition of network nodes, has to be defined. In the case of fMRI the parcellation can be either structure-based or function-based. This will be better explained in the next section.

After data acquisition, a measure of similarity among nodes has to be defined, for example correlation or spectral coherence for fMRI, number of fibre tracts in DTI and so forth. Subsequently the adjacency matrix can be computed, and a threshold can be applied to remove spurious edges. As for dynamical functional connectivity, a network is build for every time point or window which is considered, yielding as many networks as time windows. Of course each step affects the final result, and therefore particular attention should be paid during network construction.

When adopting a particular parcellation scheme, ideal features on the nature of nodes and links should be borne in mind. Indeed, nodes should represent regions with coherent patterns of connectivity, otherwise the node signal might be meaningless. Nodes should also cover the entire brain cortex (sometimes plus cerebellum and subcortical regions) and there should be no overlap, that is one patch of cortex has to be unequivocally assigned to

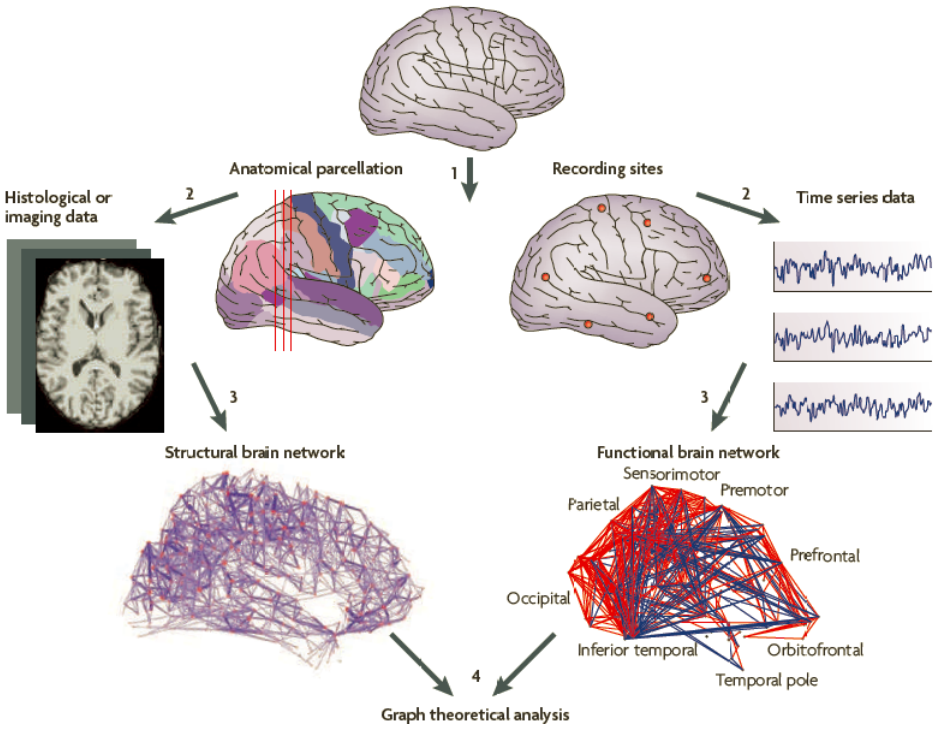

Figure 2.2: [10] Steps of brain network construction. 1) nodes definition subsequent to a parcellation scheme, 2) data acquisition (MRI, DTI, EEG, histology), 3) computation of an association measure to build network links, 4) graph analysis. A structural connectivity scheme and a functional connectivity one are represented on the left and on the right, respectively.

a node.

Also links have different natures. As for the case of previously described general network, links can be weighted, thus accounting for different strength of brain connection or binary. In many networks weights are often discarded, since binary networks are usually easier to deal with. In functional networks the binarization is always subsequent to thresholding, however the choice of a given threshold is quite subjective. We distinguish between two types of threshold: one is a weight threshold, discarding all the links below a given weight, while the other is frequency based, keeping a given percentile of the links e.g. the top 10%. It is important to note that, given that functional connectivity is independent of directionality, links are undirected. Directionality could in principle be inferred from changes in functional activity that follow localised perturbations; nevertheless this falls into the domain of effective connectivity.

A threshold can be chosen in order to maximise some objective function. For example one would like to keep the same link density as in the corresponding structural network, or minimise the difference with the same property in the corresponding brain network. In fact, differences in density between anatomical and functional networks make global comparisons between these networks less straightforward. Functional networks are likely to be denser than anatomical networks, as they will typically contain numerous connections between anatomically unconnected regions [41]. This becomes pronounced in larger, more highly resolved networks, since anatomical connectivity in such networks becomes increasingly sparse, while functional connectivity remains comparatively dense. Notably, comparisons between anatomical and functional modular structure remain meaningful despite differences in density. Beside density, other factors that may affect the comparison of structural and functional network topology include degree and weight distributions.

2.5.2 Parcellation

Parcellation is the process of dividing brain into a given number of regions. In fMRI experiments it consists of grouping voxels into these regions and averaging the time-courses to assign to each region only one time series. Two main classes of parcellations exist, anatomical and functional parcellations. The most common parcellation is the automatic anatomical labelling (AAL). It divides the cortex into 90 regions, and subcortical regions

and cerebellum provide 26 additional regions. to often a non trivial task. A positive feature of this parcellation is certainly that it clearly assigns to each node a region which is known in the literature, and with anatomically well defined borders. However, in fMRI studies anatomical parcellations carry potentially severe pitfalls. As Shen and colleagues pointed out "A potential pitfall in using such atlases is that the mean time-course of a node may not represent any of the constituent timecourses if different functional areas are included within a single node", and this results in a loss of information, which is quite intuitive [45]. Another drawback of this anatomical parcellation is that the node sizes are very different from one another. For example in principle a node may be built grouping 100 voxels, while another with 5000. This affects network's stability.

In order to overcome this inconvenience Shen et al. developed another type of parcellation. They divided the brain based on functional resting state analysis over 79 healthy individuals. This approach assures that we do not average regions with different timecourses. They performed a multigraph K-way clustering with different numbers of maximum clusters K. On one side it is desirable to increase the number of clusters in order to have a network with a high number of nodes. On the other side, increasing the number of clusters results in a loss of consistency among patients, i.e. we do not find the same regions in different patients, and the parcellation is therefore not general and not applicable to other individuals. $K = 300$ proved to be a good balance: after "cleaning" of some regions, they obtained a 268 atlas and a 278 atlas. Another positive feature of this parcellation, compared to the AAL is the homogeneity of its regions: they all have almost the same size.

2.5.3 The state of the art in centrality studies

Among the features brain network show, there are small world and scale free structures (sec. 2.4). This is clearly visible exploring brain degree distribution - often long tailed - and average path length. Brain networks also showed highly clustered structures, corresponding to the resting state networks described in section 1.2.

As for centrality, many most studies indicate the presence of hubs. Hubs are regions which are considered to have a considerably higher importance than others. We can distinguish between *provincial* hubs, which show many connections within a given cluster

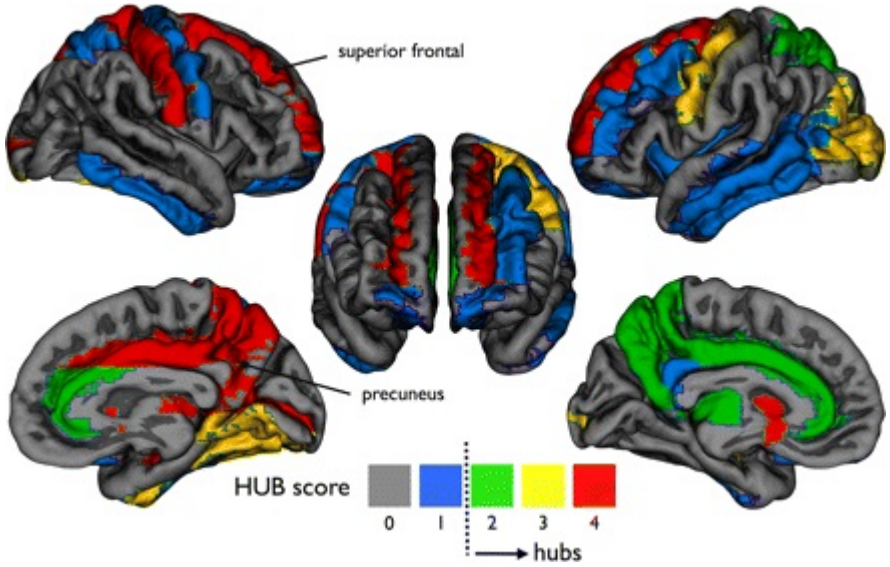

Figure 2.3: Hubs as identified by Van Den Heuvel et colleagues [51], according to top 20% strength and betweenness and bottom 20% clustering coefficient and average path length. A score of four indicates that the corresponding region possesses all the four features. The highlighted resting state hubs are left and right caudate, left and right superior frontal gyrus, right middle cingulate gyrus, right precuneus, left and right putamen, left thalamus.

and *connector* hubs, connecting otherwise separate parts, and therefore playing a pivotal role in functional integration. This suggests a hierarchical organisation of brain networks. Features characterising hubs nodes are high degree, apex ratio[1], betweenness, and low clustering coefficient and average path length; hubs as defined by these parameters are reported in figure 2.3. It may seem strange that nodes with high degree or strength are not candidates to be connector hubs. Until a few years ago high degree and strength values were considered a good indication of connector hubs. However it has been shown that this is not the case, due to a bias coming from the definition of functional connectivity. In fact functional connections are based on correlation, and as a result nodes which are only indireclty related are connected by a link. Consequently the brain is highly clustered and nodes have a degree which is proportional to the size of the cluster. Indeed, nodes belonging to a larger cluster have a higher degree, and the claim is that previous studies on brain hubs just identified large portions of brain, rather than true hubs [38]. Betweenness and Spectral on the other hand are supposed to be more appropriate in finding connector hubs.

Each centrality measure implies different hypotheses on the dynamic flow of information in the brain. For instance if we assume that information flows through shortest paths, betweenness should be a good hubs indicator. A parallel duplication and a parallel transfer - where information is transferred to multiple targets simultaneously - have been proposed as models for information communication among neurons [50]. Again, we point out that each model has different implications on the best centrality measure to implement. Nevertheless, all hypotheses are quite subjective and usually a consensus approach for hubs detection is used, which combines the results coming from different measures. Moreover, to assess whether hubs are present or not it is common to preliminary analyse the distribution of centrality measures, in order to see if some nodes present unusually high values. Among measures for detecting differences between conditions eigenvector has proved to be efficient in discriminating between hungry and sated individuals [32]. Furthermore new measures are being developed to characterise network hubs. This is the case of leverage centrality [26], which proved to yield different results in terms of hubs detection, with more differences when compared to random networks, although nothing is said about the measure's ability to characterise differences among brain states.

[1] motifs where a node connects to nodes which are not connected

Certainly, the state of the art on these measures is still at the beginning, and a lot has to be done in order to have a comprehension of the importance of many measures. Consensus of the best threshold to use for links characterisation is needed, which can dramatically vary the scenarios depicted thus far. Moreover many comparison studies can be performed in order to shed light on the potential of centrality measures to reveal differences among healthy and injured brains, for which a few network studies have been made. Another area of applicability is in studies on different brain states such as consciousness versus unconsciousness, for which graph theory has not yet been implemented.

Chapter 3

Methods of data Analysis

In this chapter the methods we applied to analyse our data are explained. Once more we remark that in many cases there are no general prescriptions to follow, in fact the methodologies used thus far in the literature are still debated, and always new approaches are being developed. For a few analyses we also implemented approaches which, to our knowledge, were never used in this field before.

Initially we describe the two datasets and how they are obtained. While the second data set consists of already preprocessed data, the first contains raw data to be preprocessed. The utilised preprocessing procedure is reported in section 3.1.

Afterwards the steps which led to the final networks are discussed (section 3.2). In this context particular focus is placed on the used parcellation scheme. The thresholding of the network links is also analysed, with the motivation that led to such choice, as well as other manipulations made on the correlations values in order to obtain link weights. Then we explain how a series-wise approach and a sliding window approach have been implemented to build the network, and the differences between them. The series-wise approach basically computes correlation along the whole window series, whereas the sliding window approach considers correlations for restricted time windows, accounting for the *dynamics* of the network.

In section 3.3 we explain how the different centrality measures have been characterised. First we computed the centrality measures and we averaged them over the 16 individuals. Second, we implemented a null model, consisting of adding a different ran-

dom offset to the time series of each region. Moreover another null model, which tests for the non-stationarity of the time series, in order to inspect the presence of dynamical (non-stationary) correlations, is utilised. Eventually we explain the false discovery rate, which is the correction for multiple comparison we implemented for all the null models.

A summary of the operations we performed, which can give a better idea of the characterisation of networks in the first data set is reported in figure 3.1.

In section 3.4 we outline the methods we used in the second dataset to discriminate between different states of consciousness. Basically we used the centrality measure of each region as discriminating features, while patients are the observables. We describe the applied discriminant analysis and feature extraction and selection procedures, such as principal component analysis.

3.1 The data sets

In this work we analysed two different data sets. The first is freely available on the OpenfMRI website, which is a project dedicated to the free and open sharing of raw magnetic resonance imaging (MRI) dataset. It is a repository of human brain imaging data collected using MRI and EEG techniques, starting from 2010. One of the aim is the savings which can derive from taking already available data, rather than collecting new ones. Since the beginning of the project data from about 1800 individuals have been uploaded across all the data sets. The data analysed here are part of the Consortium for Neuropsychiatric Phenomics (CNP). The CNP is a large study funded by the (US) National Institute of Environmental Health Sciences Roadmap Initiative that aims to facilitate discovery of the genetic and environmental bases of variation in psychological and neural system phenotypes, to elucidate the mechanisms that link the human genome to complex psychological syndromes, and to foster breakthroughs in the development of novel treatments for neuropsychiatric disorders. However we took only a subset of healthy subjects; in particular among the 290 subjects only 16 were chosen, in order not to increase the computational cost of analyses that are already computationally expensive and time demanding. This dataset was chosen due to its availability, which ensures that many studies are performed on it, making it a reliable source.

The participants, aged 21-50, were recruited by community advertisements from the

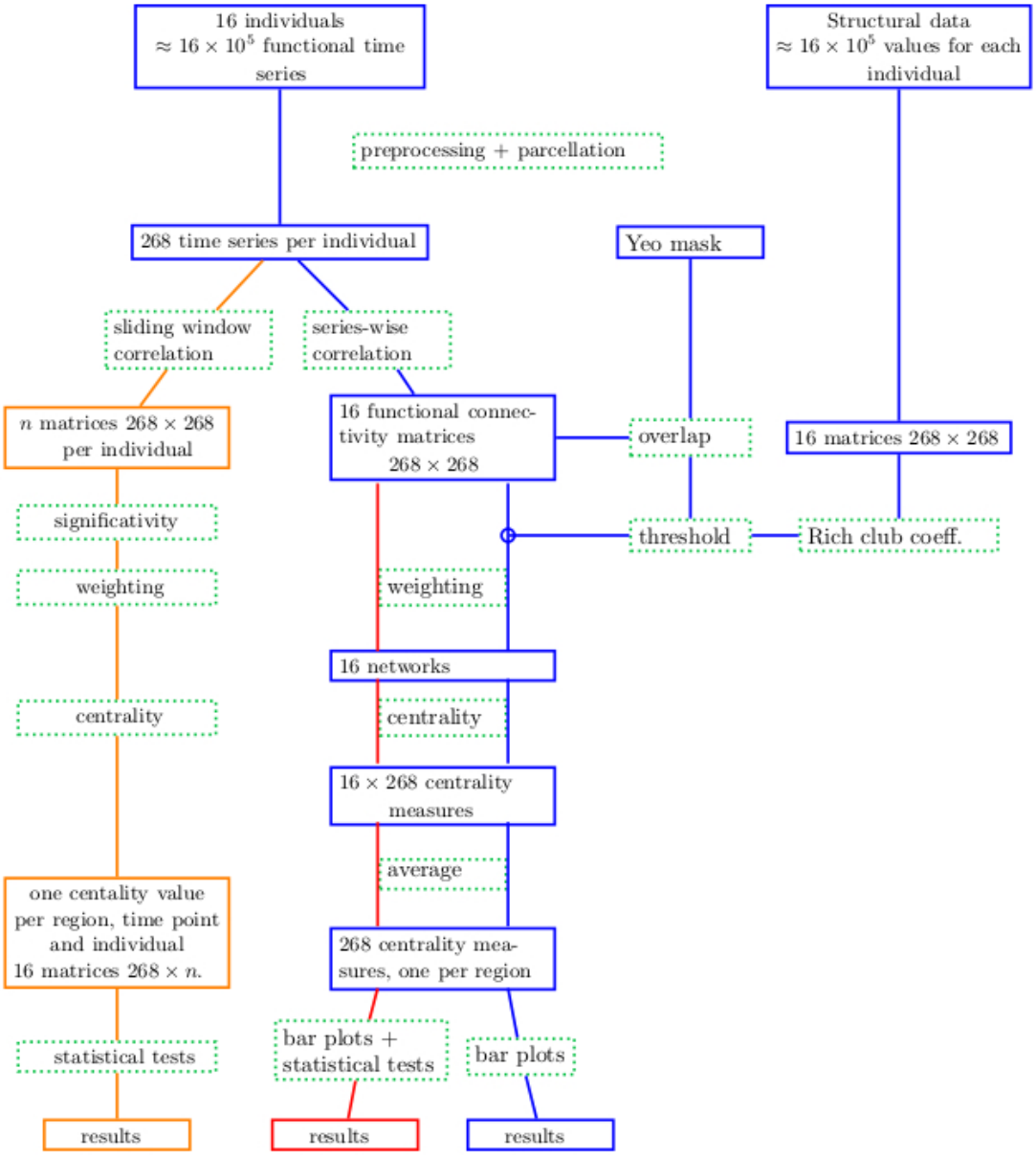

Figure 3.1: Block diagram of the utilised methods for the first dataset. Here centrality refers to all the analysed centrality measures. The orange workflow encompasses the dynamic behaviour of the network. On the right, the red line represents the workflow for the thresholded network, on the left the one for the unthresholded network. The red workflow has been applied also to the second dataset. On that dataset, after computing the centrality measures for each patients, the discriminant analysis has been performed.

Property	Dataset 1	Dataset 2
fMRI type	Echo-planar	Echo-planar
Repetition Time [s]	2	2.465
Echo Time [ms]	30	40
Voxel size [mm]	3x3x4	3.45x3.45x3
Volume size [voxels]	64x64x34	63x64x32
number of volumes	152	197 and 347

Table 3.1: Parameters used in the fMRI scans for the 2 different datasets.

Los Angeles area and completed extensive neuropsychogical testing, in addition to fMRI scanning. To be included individuals had to respect some designations of racial and ethnic minority groups, and hat to have completed at least 8 years of education. Modalities include T1-weighted and 64 direction DWI and BOLD contrast fMRI with a 3T Siemens MAGNETOM A Trio Tim. For the functional MRI the parameters in table 3.1 were used.

Given that this dataset consists of raw data, we had to perform all the preprocessing steps described in section 1.3.2. With the FSL toolbox we first normalised both the functional and the structural image to the standard MNI space (section 1.3.2). Then we did slice timing correction, realignment (that is head motion correction), coregistration and spatial smoothing. Indeed, structural T1 images were acquired for coregistration. Moreover we applied a bandpass filtering (0.01 Hz -0.08 Hz), in order to maintain the frequencies which are of more interest in resting state. We also obtained a DTI image, which contains the fibres connecting one voxel with another.

The second data set was acquired at the University Hospital of Liège and it was already used in previous studies [3, 9, 44]. Eighteen healthy right-handed volunteers participated in the study, which consists of the analysis of unconsciousness after Propofol infusion. This anaesthetic was infused through an intravenous catheter placed into a vein of the right hand or forearm. An arterial catheter was placed into the left radial artery. Throughout the study and the recovery period, electrocardiogram, blood pressure, pulse oxymetry (SpO2), and breathing frequency were continuously monitored. The level of consciousness was evaluated clinically throughout the study with the Ramsay scale [33]. This re-

sulted in four clinical states: normal wakefulness (W1), sedation (S1), unconsciousness (S2), and recovery of consciousness (W2). In the two conscious states the patient is able to quickly respond to verbal commands (Ramsay 2), in the sedation state the response to verbal command was clear but slow (Ramsay 3), and in unconsciousness there was no response to verbal command (Ramsay 5–6). In this case functional MRI acquisitions were taken with 3T Siemens MAGNETOM AG, and the corresponding parameters are again in table 3.1. While the first dataset consisted of raw, non-preprocessed data, this dataset had the preprocessing steps already performed; these include functional and structural images realignment, normalisation, smoothing and a bandpass filter (0.005 to 0.1 Hz).

3.2 Network construction

Network construction, as explained in section 2.5, consists of different steps, which basically serve to the definition of nodes and links. In principle we could assign one node to each voxel, but this is too computationally heavy. In fact at this stage we have a huge amount of data: the first datasets contains 131,072 voxels for each of the 152 time values and 16 patients, and the second contains 139,264 voxels, 197 (and 347 for six of the eighteen patients) time points, 18 individuals and 4 different states. This is indeed quite hard to deal with. Accordingly voxels are grouped into bigger regions, through a parcellation process (section 2.5). Grouping voxels together also increases the signal to noise ratio.

3.2.1 Parcellation

We grouped the voxels into specific macro-regions based on the Shen 268 regions parcellation (section 2.5). Basically, for each time point, we took the two files - the volume and the mask - to assign each voxel to a given region. Indeed the mask-file contains the 268 Shen functional parcellation. This step has been carried out with FSL for the first dataset and with SPM for the second. For the first dataset this has been done for the whole time series at once, given that the time series of each voxel were embedded within only one 4-D NIfTI file. For the second dataset, however we had separate volumes (analyze .img files) for each time point, therefore we had to perform the parcellation in a loop over the time points.

First we resliced the images in order for them to have the same number of voxels, to allow for their overlapping. Each voxel in the original image is assigned a label, that is the region it falls in. Afterwards all the time-courses of each regions (i.e. the values from each time point, for all the voxels in a given region) are averaged to get the region's time series.

Note that the use of a functional parcellation, rather than a structural one, results in a much lower standard deviation. In this way each node is characterised by a time series, and in the end we obtained a 268x152 matrix for each of the 16 individuals of the first dataset; in dataset 2 we obtained twelve 268x197 pattern matrices for twelve individuals and six 268x347 pattern matrices for the remaining six individuals. This is much better to deal with than a 131,072 x 152 matrix and a 139,264 x 347 matrix. Moreover, the average ensures that the noise is decreased, while the signal remains high due to the parcellation being functional-based. This parcellation process has been applied to the structural network, too. The only difference lies in the fact that for the structural network we do not have a property of a given voxel, rather we have the number of fibres among voxels, which results in the number of fibres across regions after parcellation.

3.2.2 Correlation and thresholding

While in the structural network links are represented by number of fibres, in the functional network two approaches have been considered for edges construction. First of all correlation between the time series of each pair of regions has been calculated. This is the first measure of how two different regions are connected to each other, and it is a common approach for evaluating functional connectivity in brain studies. A first branch point in the link building procedure is in the choice of the correlation window. For most analyses we computed a correlation coefficient for the entire time series, whereas to inspect the dynamics of the network we used the so called *sliding window* approach, which will be analysed later (section 3.2.3).

Apart from this distinction, in both cases a first problem arises, that is the network is complete. Often a threshold on the correlation value, to obtain an unweighted network, or to simply delete low correlations, is applied. Given that no ground truth exists on the threshold value to apply, we decided to choose the value which maximises the cluster

structure revealed by Yeo study described in section 1.2 [54]. In particular we used the summation over all clusters of the sum S of internal and external densities, as partition evaluator (section 2.4):

$$S = \sum_{i=1}^{8} \delta(C_i)_{int} + \delta(C_i)_{ext} \tag{3.1}$$

where i represents the cluster index. In order to see in which cluster each region falls, we have to overlap the 7 resting states (plus a subcortical cluster) mask by Yeo and colleagues (section 1.2) and the 268-regions Shen mask. We assign each of the 268 to one of the 8 clusters. This is not as straightforward as for the parcellation process itself, for reasons that are explained in section 3.3, where the issues become even more severe. Another way to assess the best threshold is evaluating the similarity between structural and functional networks. Given that the structural network is not connected, we did not use centrality as a comparison measure, rather we used the *rich club coefficient* (section 2.4). We performed the analyses both on the complete networks and on the thresholded ones.

One last modification has been carried out on network links. Since the correlation coefficient has values ranging from -1 to 1, while the weights of the edges must have non negative values, we have to remove negative values. Simplistic models just add 1 to each correlation value. However, since we want to give more importance to high correlations, we implemented chordal distance and exponential weighting. Denoting the pattern matrix with X, that is the matrix which has regions as rows and BOLD time series as columns, the adjacency matrix of the network is obtained through the steps

$$C_{ij} = corr(X) \tag{3.2}$$

$$S_{ij} = sin\left(\frac{arccos(C_{ij})}{2}\right) \tag{3.3}$$

$$A_{ij} = e^{-\frac{S_{ij}}{\sigma}} \tag{3.4}$$

The value of σ used in this case was $\sigma = 0.25$, which has utilised in other works [37].

3.2.3 The series-wise approach and the sliding window approach

In the previous section we mentioned that the correlation can be computed either for the entire time series at once, or for different windows. Such *sliding window* approach relies in computing the correlation coefficients on a smaller window which is shifted along the time series with fixed step. The goal of this approach is basically to see if the correlations we observe are dynamical, and therefore if the network has a detectable change in its structure over time. Two parameters have to be fixed, being window size and step.

When having a time series with n time points, a L points window and a s points step, the total number of windows, that is the total number of networks for each individual is $K = \left[\frac{n-L}{s}\right]$. Not all the values of these parameters are suitable; indeed, as for the step, a smaller value provides a more accurate estimate of the network dynamics, although the analysis becomes more computationally expensive. As for the window length, a rule of thumb has been suggested [28], that is the time window should not be smaller than $1/w_{min}$, where w_{min} is the minimum frequency present in the data, which corresponds to the lower limit of the applied bandpass filter. In fact they demonstrated that spurious fluctuations arise in part due to the mismatch between the window length and the high-pass filtering of the original series. Given that in the first dataset, which is the one where we applied the sliding window approach, we filtered out the data below 0.01 Hz, this is the lowest frequency in our time series. Therefore the minimum size for the window is 100 s, which corresponds to 50 time points, given that TR=2s. This means that the correlations arising from smaller windows are likely to be spurious. On the other hand, a big window has the drawback to average out the contributions of different time periods, detecting only a static behaviour. Although we have a rule of thumb to assess this behaviour, appropriate statistical tests have to be carried out.

Then we ask ourselves if the centrality values change significantly in the network. Nothing in fact assures that not detecting dynamical correlations implies not detecting dynamical centrality behaviours.

The test we used consists of defining a statistic based on the correlation measure, such as the variance of correlation or the fraction of windows where the average time series correlation, falls out of the time window confidence value. This statistics has to be later

compared to the values of the statistic coming from a null distribution. The way we built the null distributions, both for the sliding window approach and for the series-wise approach is explained in the next section.

3.3 Characterisation of centrality measures

In this section we describe all the methods we used to characterise the three different centrality measures. First of all, in order to compare the measures, we normalised them in a way that for each centrality c we have

$$\sum_{i=1}^{268} c_i^2 = 1 \tag{3.5}$$

where i is the region index. As previously mentioned, we analysed eigenvector, betweenness and, as for the class of k-spectral centralities, we computed both the 1-spectral and the 2-spectral (section 2.3). When using the series-wise design, we could average the measure over the 16 patients, whereas with the sliding window this was not possible, due to time points among patients being unrelated; as a result an averaging of correlations over patients in restricted time windows would cause variations in correlations to average out.

3.3.1 Null model of centrality values

In order to see if the values of each region were significantly higher or lower than we expected by chance, we had to compare our network to a null model, that is a network which behaves according to a null hypothesis. A simply random network does not seem to be suitable in this case, since it is not likely to preserve any of the features of the original network. Rather we exploit the time series, performing a randomisation on the time series itself. *Surrogate* data testing attempts to find the least interesting explanation that cannot be ruled out based on the data [43]These surrogate time series were obtained via Monte Carlo resampling techniques. In fact there is no ground truth which can help determining the true theoretical distribution of any network parameter..

The approach we used, *constrained* randomisation, avoids inferring model equations

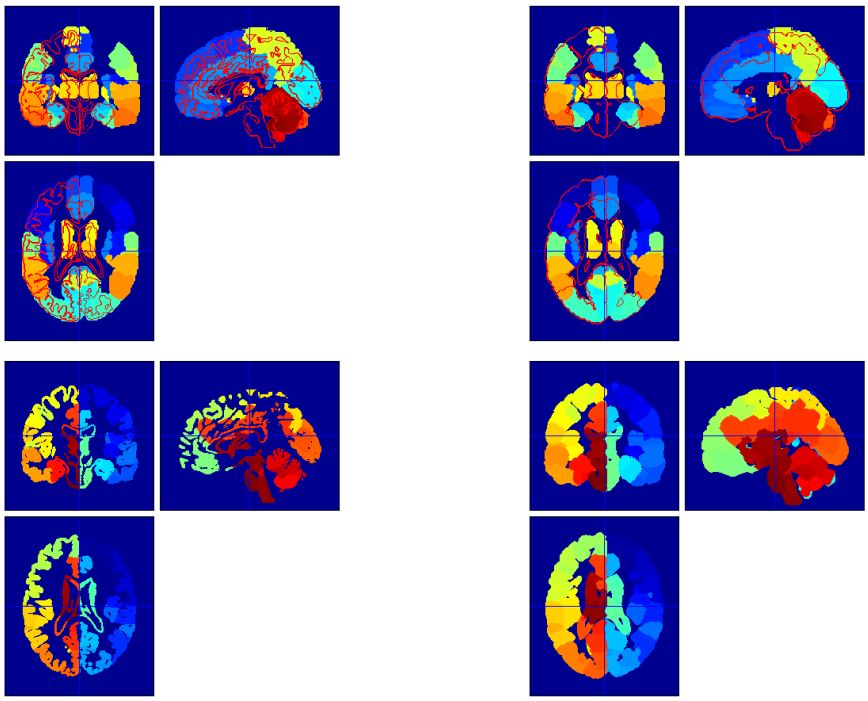

(a) before (b) after

Figure 3.2: Parcellation overlap before (3.2a) and after (3.2b) the dilation. The structural AAL map is on the top, whereas the functional on the bottom. Colors represent different regions. The red border on the top represents the functional map overlapped to the structural one.

by directly applying the desired structure on the data. The term constrained derives from the fact that surrogate data are constrained to have some properties which the original data have. The simplest example in this case is given by a trivial random shuffle of time series, that is the assigned value to a point in the new time series is randomly extracted from the values in the true time series, without replacement. As a result the independence between values within a given time series is tested. This trivial example, however, is not applied to our data, since we do not what to test for the independence within values in a time series, rather between different time series. We wanted to test if the centrality values of each regions are consistent, that is if they range between a fixed values interval.

A more suitable null model than a simple random shuffle - even though still quite simple - is a phase shuffle of the time series. Each region has its time series shifted by a random phase, resulting in a loss of timing among different series, but without disrupting the series temporal structure. This null model can provide an answer to the question: "*are the centrality values significantly high or low, compared to what we may expect in a reference network?*". For each region we computed 100 iterations of this phase shuffle, then we calculated the centrality values, resulting in a null distribution of 100 centrality values for each region and each individual.

Many times we are interested in knowing the correspondence between our node and an anatomical region, for example to compare our results with previously found hubs. Mapping two different parcellations to one another is not as straightforward as performing a parcellation from the original image. In fact we had to see where, in the anatomical parcellation, each voxel in one region for the functional parcellation falls. The first problem arises due to the fact that two masks may be non-consistent even after the coregistration. In our case the functional mask was smaller than the anatomical one, so we had to apply a three-steps dilation with a 3x3x3 cubic kernel. The 2 parcellations, the dilation and their overlap is shown in figure 3.2. Moroever the correspondence between the two parcellations is not exact, and the overlap bears ambiguities. For example, a region in the functional parcellation may correspond for 40% to region A in the anatomical parcellation, 30% to region B and 30% to region C. We therefore considered as "not assigned" regions having less than 40%[1] voxels assigned to the same region.

[1]This threshold is arbitrary

3.3.2 Testing presence of dynamical functional correlations

A common hypothesis made when testing for dynamical correlations in time series is that the underlying process is a stochastic process which is Gaussian, linear and stationary with constant coefficients. In time series analysis a *stochastic* process is simply defined as a collection of real valued variables $S = \{S(\omega, t); \omega \in \Omega, t \in T\}$, where time t is defined in a parametric space T and event ω is defined in the probability space Ω. A *time series* $x = x_1, ..., x_n$ is simply defined as the realisation of the stochastic process S; for each time point t_i we have $x_i = S(\omega, t_i)$. In principle the process can have a different probability distribution '$omega$ for each time t_i . In our model we just focus on Gaussian distributions, and the resulting process is Gaussian, too.

A *linear* process Z_t is defined by $Z_t = \sum_{j=0}^{\infty} \psi_j a_{t-j}$, that is it is a linear combination of the *white noise* processes a_{t-j}. A (wide-sense) *stationary* process is a process in which mean and variance function are finite and constant and covariance function only depends on the delay k, being independent of the particular time point t. Namely $cov(S_t, S_{t-k}) = E[(S_t - \mu)(S_{t-k} - \mu)] = \gamma_k$ [12].

Constrained realisations are created by requiring that the surrogate time series have the same Fourier amplitudes as the data [43]. Suppose we have two different time series $\{x(t_i)\}$ and $\{y(t_i)\}$, where $i = 1, 2, ..., N$ are the equally time points at which the signal was sampled, at regular intervals Δt. The process consists first of taking the (discrete) Fourier transforms of both the time series, yielding two transforms with exactly the same number of elements of the time-domain series: let us call the two transforms $X(f_i)$ and $Y(f_i)$, respectively, defined as

$$X(f) = F(x(t)) = \sum_{n=0}^{N-1} x_(t_n) e^{i2\pi n f \Delta t} \tag{3.6}$$

where F is the Fourier operator; analogously we obtain $Y(f)$. Then a random phase $\phi(f)$ is added to each frequency point f, and we obtain $\tilde{X}(f) = X(f)e^{i\phi(f)}$ and the same is obtained for $Y(f)$. Doing it for every frequency component f, results in a collection of

Fourier values $\tilde{X} = \{\tilde{X}(f)\}$, which is then transformed back to the time space

$$\tilde{x}(t) = F^{-1}(\{\tilde{X}(f)\}) = F^{-1}(\{X(f)e^{\phi(f)}\}) \tag{3.7}$$

This ensures that each frequency component, that is each cosine wave, is shifted with respect to the original signal, and therefore the components line up in a different way, forming a different signal. Beside preserving the autocorrelation, we also want the surrogate series to preserve the linear correlations *between* them, represented by the *cross-correlation* function, which is defined as

$$C_{xy}(k) = \frac{cov[x(t), y(t-k)]}{\sqrt{var(x)var(y)}} \tag{3.8}$$

Doing so alters neither the autocorrelation properties of one signal, nor the static correlations between the two signals. In fact, if the processes are stationary, the cross-correlation functions are the same, and so are the power spectra.

After having built the surrogate time series, we had to compute a statistic from the data and then compare it to the distribution of that statistic obtained from the null model. If the test rejects the null hypothesis, then, we can conclude that our correlations are non-stationary or non-linear. We performed 100 iterations of the null model, for each region pair. We then computed the correlation coefficient in every time window $\hat{\rho} = \{\hat{\rho_1}, ..., \hat{\rho_K}\}$, where K is the number of windows, yielding a correlation time series of K values. We used the variance η as our linear test statistic:

$$\eta^2 = \frac{1}{K-1}\sum_{i=1}^{K}(\hat{\rho}_i - \hat{\mu})^2 \tag{3.9}$$

where $\hat{\mu}$ is the estimated average of the new correlation value of the time series. Since the variance is a *linear* statistic, with this we just test for non-stationarity of the time series.

We then repeated this process for every pair of time series, which resulted in a quite computationally expensive approach. While being a time-demanding approach is certainly a drawback of this null model, its strong point lies in formulating a specific null hypothesis: the time series are the realisations of linear stationary white noise Gaussian processes.

3.3.3 Statistical rejection of the null hypotheses

When we performed the previously described statistical test we had to take into account that we are dealing with a high number of variables (the nodes), rather than just one. When calculating p-values the analysis is quite different from the unidimensional case. In fact as the number of variables increases, the probability that one would be rejected by chance, among the multiple null hypotheses, increases, too. As a result, we cannot just compare the p-value with a confidence value α and reject the null hypothesis for node j if $p_j < \alpha$, as this would increase the rate of false positives (type I errors). If we did so, denoting the number of nodes in the group, or *family* with J, the probability of getting a *false* rejection - the so called *false positive* - would be $p(\text{false}) = J \times p_i$.

What is usually done in this case is using a more stringent confidence threshold, in order to control the *Family-wise Error Rate* (FWER). Two different approaches can be employed to pursue this goal, depending on the strength of the control. Indeed we distinguish between *strong* and *weak* controls, Bonferroni Correction and False Discovery Rate (FDR) being the most representative implementations of the two aforementioned categories, respectively.

Bonferroni Correction simply consists of dividing the total confidence value, by the number of nodes for which we want to test the hypothesis. As a result the α value for a single node will be much smaller. We reject the null hypothesis for the j-th node if

$$p_j \leq \frac{\alpha}{J} \tag{3.10}$$

As can be inferred, the drawback of this correction is that a high number of nodes yields a too low confidence value, resulting in a too conservative test. This means that the test is quite likely to fail to reject the null hypothesis. We remark that strong FWER controls guarantee that the probability of even one false discovery is less than α.

FDR, on the contrary, only ensures that the *proportion* of false discoveries is less than a threshold α. In fact FDR is defined as the fraction of false discoveries, that is the number of rejections when the null hypothesis is actually true. Mathematically

$$FDR = \frac{V}{max\{1, V + S\}} \tag{3.11}$$

where V represents the number of false discoveries, whereas S is the number of true discoveries. The best-known procedure to control that the FDR is below a given threshold was developed by Benjamini and Hochberg and consists in the following steps. First one has to sort the p-values in ascending order. Afterwards the largest j for which

$$p_j \leq \frac{j\alpha}{J}. \tag{3.12}$$

Then, the first j null hypotheses are rejected. No rejection are made when no p_j is smaller than the fraction in equation 3.12.

3.4 Discriminating between different cases

In order to discriminate between two states - a conscious state versus an unconscious one - a classification is needed. For this purpose a classifier, that is a method which is able to distinguish data based on some features, has to employed. In our case the features used to discriminate between the two states are the centrality values of each region.

The design is the following. We have a pattern matrix whose n rows are the observations, and p columns are the centrality values of each region. We use a different centrality measure for each pattern matrix. Therefore, given that we have 18 patients and we use 2 different states, the number of observations is 36. The number of variables or features, then, is 268, yielding a 36x268 pattern matrix. There are several way of discriminating between two classes. The one used here is discriminant analysis, which can be either linear or quadratic.

3.4.1 Discriminant analysis

Discriminant analysis is a technique used for classification which assumes data in different classes are generated according to different Gaussian distributions, along each dimension. Therefore it consists of computing, in the p-dimensional feature space, the (vector) mean and standard deviation for each class, on data whose class is known.

The way the classifier assigns a data point to the corresponding region consists of minimising the sum of the conditional probabilities that the data belong to the other classes.

Given that we just have two classes, it results in the intuitive procedure of assigning a point to the class whose conditional probability is higher. Mathematically it reads

$$\hat{y} = \underset{k=1,2}{argmax} P(c_k|x) = \frac{P(x|c_k)P(c_k)}{P(x)} \tag{3.13}$$

where $\hat{y}$ is the expected class, $P(c_k|x)$ is the posterior probability of class c_k for observation x, $P(c_k)$ is the prior probability - based on the number of observation for class c_k over the total observations - and $P(x|c_k)$ is the multivariate normal density, namely

$$P(x|c_k) = (2\pi|\Sigma_k|)^{-1/2} exp\left(-\frac{1}{2}(x-\mu_k)^T {\Sigma_k}^{-1}(x-\mu_k)\right) \tag{3.14}$$

where $k = 1, 2$ is the index for the class, and μ_k and Σ_k are the mean and covariance matrix for class k, respectively.

When the covariance matrix is the same for the two classes we have a *linear* discriminant analysis. In this case a linear combination of the features is calculated and a hyper-plane cuts the 268-dimensional space in 2 parts, which are needed to *classify* the data. A data point falling into one side will then be assigned to one class, a data point falling into the other side is assigned to the other class. If the covariance matrices are different for the two classes, the discriminant is quadratic, therefore the classifying curve is a quadratic function, too. A common approach to simplify the computation, which we used in this analysis, is to take the diagonal covariance matrix, assuming independence of the features. This works quite well when an appropriate feature selection is operated.

The training-test design used is in this case is the Leave One Out Cross Validation (LOOCV). This has been chosen since the data points are not enough to solely divide the set into training and test. With this approach a loop is created, in whose iterations always a different point is left out. In our case the classifier was trained on the other 35 points and then tested on the one which is left out. This was repeated 36 times, until every time point was selected as the validation one. In the end the fraction of time the point has been assigned to the wrong class is counted and normalised on the total number of trials (36).

$$Err(\%) = \frac{\#\text{wrong classifications}}{\#\text{total classifications}} \tag{3.15}$$

This gave a true estimate of the error made by each measure. Among the three centrality measure, indeed, the one with the lowest error was considered the one which classifies better.

3.4.2 Feature extraction and feature selection

Although having a high number of features seems to increase the classification power, it is not always the case. A high number of features, in fact, may add some noise, because some regions may not be helpful at all in discriminating between conscious and unconscious states. Therefore we wanted to extract just the features which are useful in discriminating between a case and the other. Another reason why we needed this dimensionality reduction is a better visualisation of the results. Having just two features, for example, allows the visualisation in a 2-dimensional space.

Principal Component Analysis (PCA) serves to this goal: it combines the initial features to obtain new features, in a way that maximises the variance. The new features do not necessarily relate to some observable quantity; in our case we could not relate a feature to a region. Basically, the first component is the one with the highest variance, the second is the one with the second highest variance and so forth. All the principal components are orthogonal to one another. As a result it is a good way to quickly visually determine whether a measure can discriminate between two states.

What PCA mathematically does, is an orthogonal linear transformation, projecting the data onto a new (orthogonal) coordinate system, defined by the principal components. The projections of the data on those components are called principal component *scores*, and they are basically the values the data assume on the new axes. For an initial pattern matrix X we have a set of p-dimensional vectors, the principal components or *weights* $\vec{w_k} = (w_{1k}, w_{2k}, w_{pk})$, which map the old vectors $\vec{X_i} = (X_{i1}, X_{i2}, X_{ip})$ to the new scores vectors $\vec{t_i} = (t_{i1}, t_{i2}, ..., t_{ip})$, where $i = 1, ..., n$, and $k = 1, ..., p$ through the scalar product

$$t_{ik} = \vec{X_i} \cdot \vec{w_k} = \sum_{j=1}^{p} X_{ij} w_{jk} \tag{3.16}$$

The eigenvalues of the transformation determine what portion of the total variance that component is representing.

We were also interested in knowing what the regions which can discriminate better are, goal that cannot be achieved with PCA: in fact PCA combines the regions yielding components which do not have a one to one correspondence with physical regions. Therefore we used different approaches, based on the *selection* of features, rather than *extraction* of features.

- First of all we did a ranking of the best classifying single regions.
- Afterwards, we did the same ranking for the best classifying *pair* of regions.
- Moreover we utilised a feature selection algorithm, which chooses the best regions and the minimum number of regions which is necessary to minimise a criterion function.
- we also studied the behaviour of the discriminant power along with the number of best single components.

Using these feature extraction and feature selection techniques some problems arise in cross validation discriminant analysis. In fact, if we want to get the *true error* of the discriminant analysis, we cannot extract the features from the whole subset and then perform the discrimination, as this determines a bias in the testing phase [2]. The problem lies in using, for testing and validation, the same sample we used for feature extraction. We can neither do an internal cross-validation: the feature extraction or selection has to be carried out for each validation step, otherwise the error rate will be underestimated. What we did in order to overcome these issues is:

- When our goal is just to find the best features, without knowing the *true error* rate, we just minimised a criterion function, as explained above.
- When calculating the best *number* of components, we did a PCA at every step of cross validation. As a result there is no guarantee that the principal components we found are the same at each iteration, rather they are almost certainly different from one iteration to another. Even though this is a drawback, it does not affect the estimate of the best number of components to use [21].

- The best number of *regions* has not been done with a feature selection procedure, since we should loop on too many variables and the process would become too computationally expensive. We only obtained the best number of regions, without knowing the true error.

- Indeed the true error can be calculated from the entire set of features, as explained. The drawback, as already explained, is that using the entire set of feature might introduce some noise and decrease the discriminant power.

Therefore we calculated either the *true* error for the best *number* of components (in the case of PCA), without knowing what these components are, and the best pair of components, without knowing the true error rate. We point out that obtaining all the information together, that is the *true* error for a *given* pair of component, is not computable in this case. In fact this would require the division of the dataset into a training (on which we perform cross validation) and test sample, which unavoidably leads to a bias due to the small size of the sample.

Chapter 4

Results

We carried out several analyses, which emphasize the power of network theory in characterising brain functional connectivity.

First of all we tried to find a good threshold for network links, for which, as previously mentioned, there is no general prescription. We found that the value of correlation of 0.6, maximises the Yeo network structure according to an objective function depending on cluster density. It is interesting to note that this value also maximises the overlap between functional connectivity and structural connectivity. However we show that network thresholding increases the variability across patients, therefore we keep a complete network. Nevertheless, we applied a link transformation to emphasize high correlation compared to low ones. These results are discussed in sections 4.1.

In section 4.2 we compare the three different centrality measures, showing that spectral centrality and eigenvector centrality seem to be related and quite stable, whereas betweenness shows a different as well as more unstable behaviour.

In section 4.3 we look for significantly high or low values, comparing each value with its distribution under the null hypothesis. The null model we used seems to identify a lot of regions for eigenvector centrality, only a few (low) regions for spectral centrality and no regions for betweenness. Some differences are present when comparing regions among one another, with respect to the case of comparing each region to its null model.

Studying if centrality values change over time is the goal of section 4.4. Here we show that some centrality measures have time varying patterns, however only a few net-

work links show non-stationary behaviours when compared to a stationary time series null model.

In the last section (4.5), the most innovative result is presented. We used methods from supervised learning such as discriminant analysis and principal component analysis, to show that centrality measures can serve as features for discriminating between consciousness and unconsciousness states. We employed slightly different methods, which all gave consistent results.

4.1 Thresholding

As already pointed out in the previous chapters, the choice of link values is far from trivial. Therefore we studied the behaviour of network edges, in order to see whether a threshold is appropriate in this case and what transformations need to be made.

First of all, in figure 4.1 we show a histogram of correlation values. As can be seen there are many more positive correlations than negative correlations, which indicate the presence of underlying cooperative processes. In figure 4.2 the original correlation matrices averaged over the individuals for the non-thresholded network are reported. A clustered structure (fig. 4.2b) is highlighted when the regions are sorted according to the resting state networks identified by Yeo et al. [54], as explained in section 1.2.

We then analysed what threshold value best fits this cluster structure. We started from 0 and then proceeded adding fixed increments of 0.1 until we obtain the highest possible value which is 1. In figure 4.3 we can see that the best threshold value, which maximises the objective function (3.1) is 0.6. We obtained this value also comparing a structural and a functional network through the rich club coefficient described in section 2.4, as can be seen in figure 4.4. Note that with this value, the majority of correlations is removed. This is more visible for the thresholded network (figure 4.5).

The results indicate also that our network deviates to some extent from the Yeo reference clustering structure, in that many connections also among the sub-networks are present and the sub-networks are not distinguishable. This might be due in part to a non-exact assignment of Yeo networks when we overlapped the two parcellations. Nevertheless, considering a higher number of individuals could indeed provide with a more stable and clustered structure.

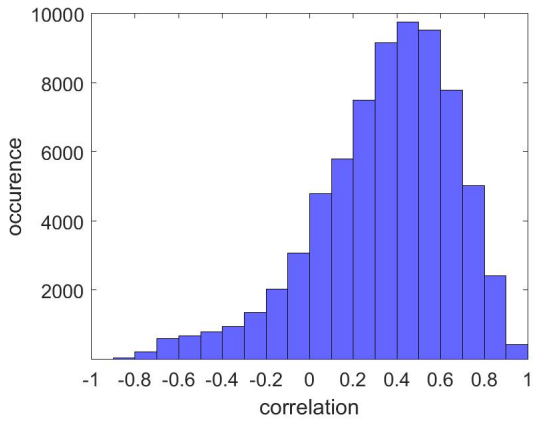

Figure 4.1: Histogram of the correlation values averaged over the sixteen individuals.

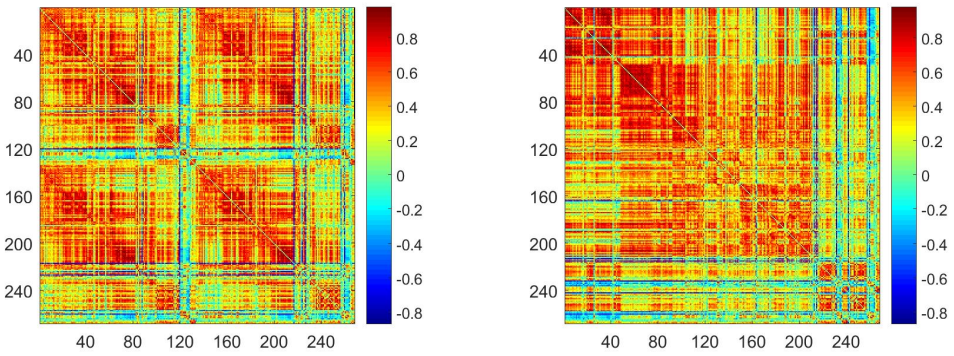

(a) (b)

Figure 4.2: Original correlation matrix (left) and correlation matrix sorted with the 8-sub-networks block structure (right).

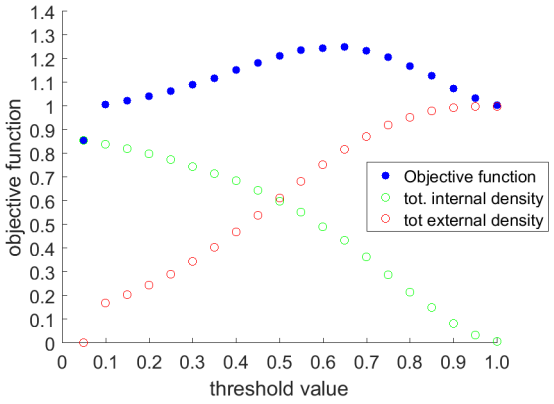

Figure 4.3: Objective function defined in 3.2. Red and green cricles represent the two different contributions - namely the goodness of partition inside and outside the blocks- to the total objective function

4.2 Comparison between centrality measures

In this section we study the relation among the different measures. As can be seen from figure 4.6, 1-spectral centrality is inversely related to eigenvector centrality, and the same is visible for 2-spectral centrality. As a consequence, hereafter we will use the inverse of spectral centrality for our analyses. Betweenness, on the other hand, seems to behave differently from the other measures. We carried out the same analysis for a thresholded network, with the threshold value found in the previous section; the values above the threshold are maintained, therefore the network is still weighted. The scatter plots for the thresholded network are shown in figure 4.7; in this case the relations seem to be much weaker. One feature that can be noted is the slightly inverse proportionality between spectral and betweenness (figures 4.7e, 4.7f).

Moreover, the stability behaviour of the centrality measures of each region averaged over the 16 individuals has been assessed. Here stability is evaluated as similarity of behaviour across individuals. Figures 4.8 and 4.9 show means and standard deviations of the centrality measures, for the original and the thresholded network, respectively. Indeed, the higher the standard deviation, the more unstable the measure. Referring to the original network, betweenness (figure 4.8b) seems to be much more unstable than all the other measures. This difference is lost in the thresholded network, where the other measures

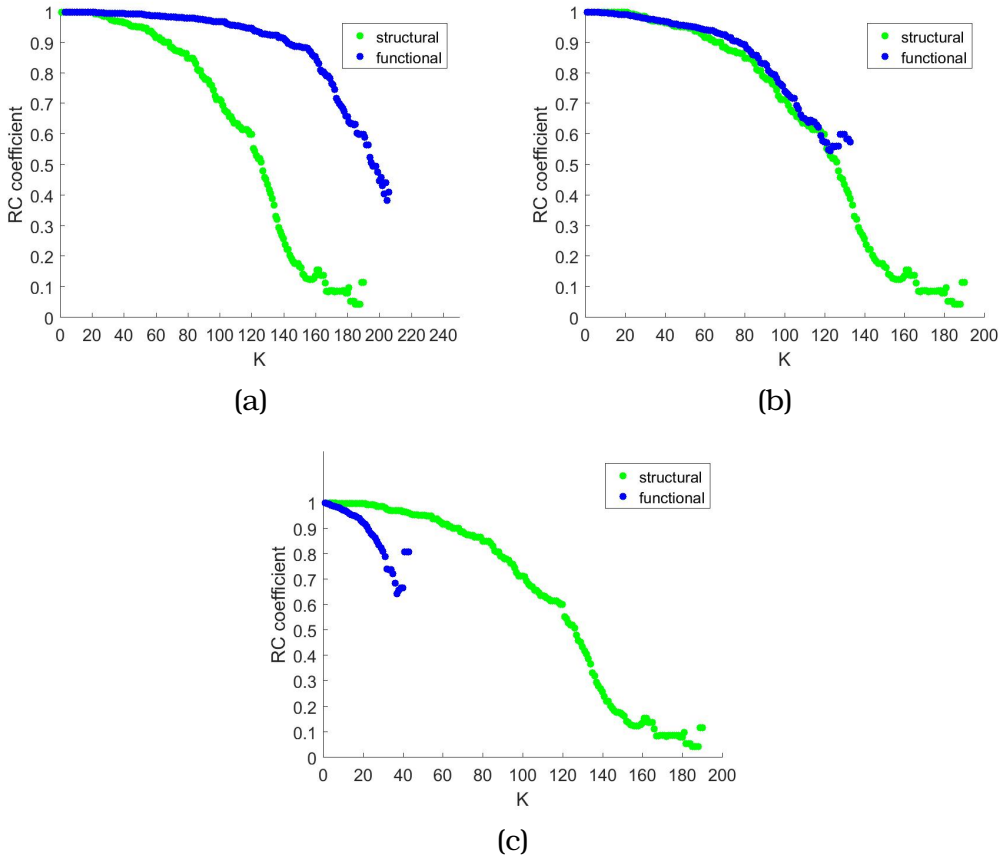

Figure 4.4: Rich Club Coefficient along degree K for three different threshold values: 0.4 (top left), 0.6 (top right), 0.8 (bottom).

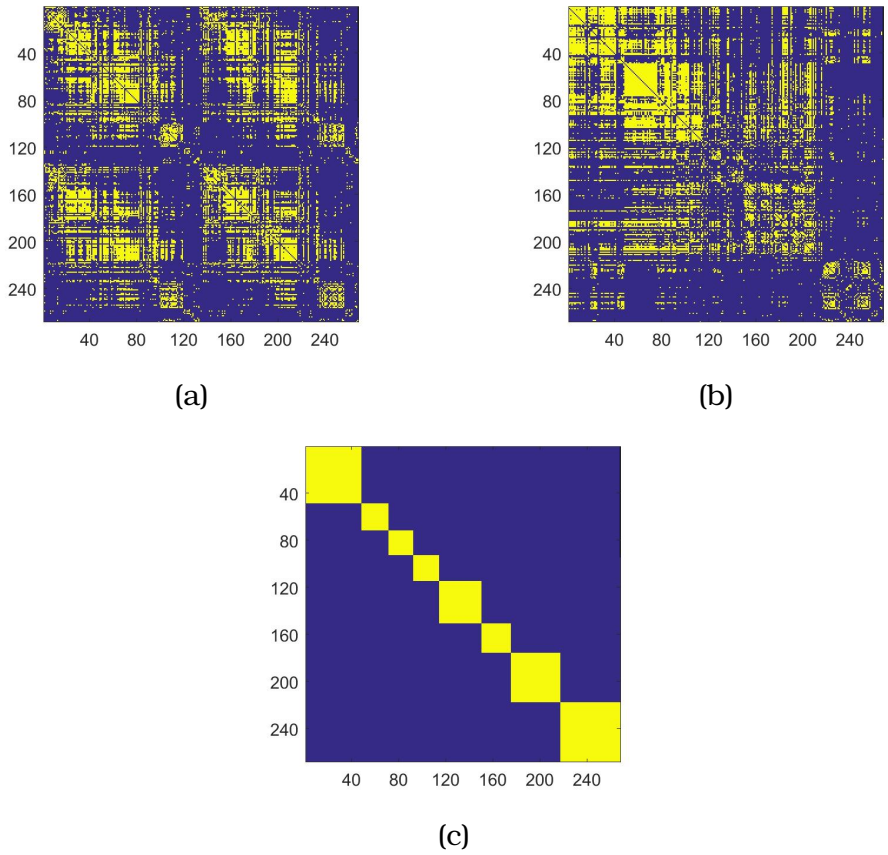

Figure 4.5: Original correlation matrix (top left) and correlation matrix sorted with the 8-sub-networks block structure (top right) after thresholding. The separate blocks structure is also reported (bottom).

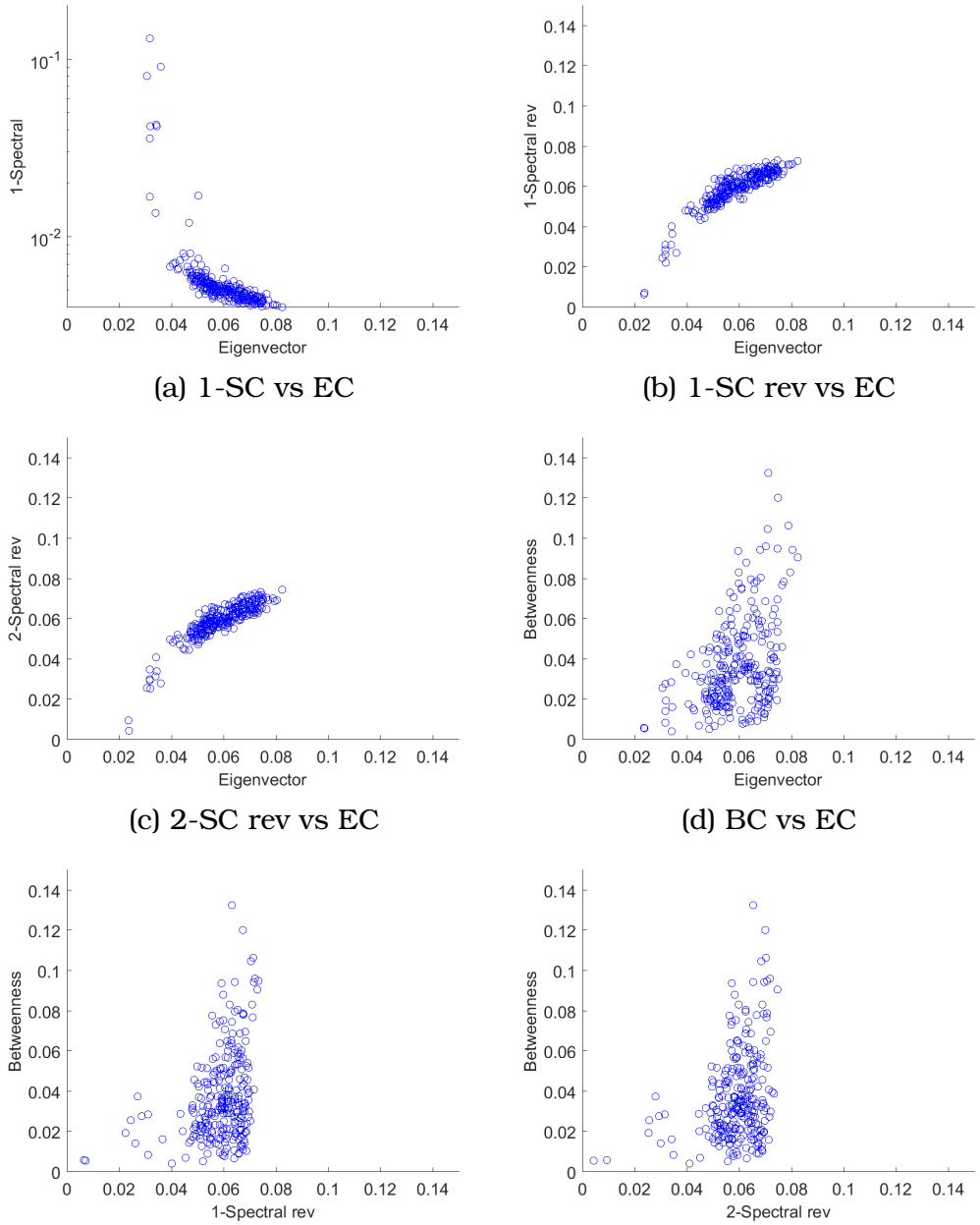

(a) 1-SC vs EC

(b) 1-SC rev vs EC

(c) 2-SC rev vs EC

(d) BC vs EC

(e) 1-SC rev vs BC

(f) 2-SC rev vs BC

Figure 4.6: Relations between the different centrality measures for the original network. The centrality values of each region have been averaged over the 16 patients. Note that spectral is reported on a logaritmic scale. Eigenvector and spectral are clearly related, whereas betweenness shows a different behaviour.

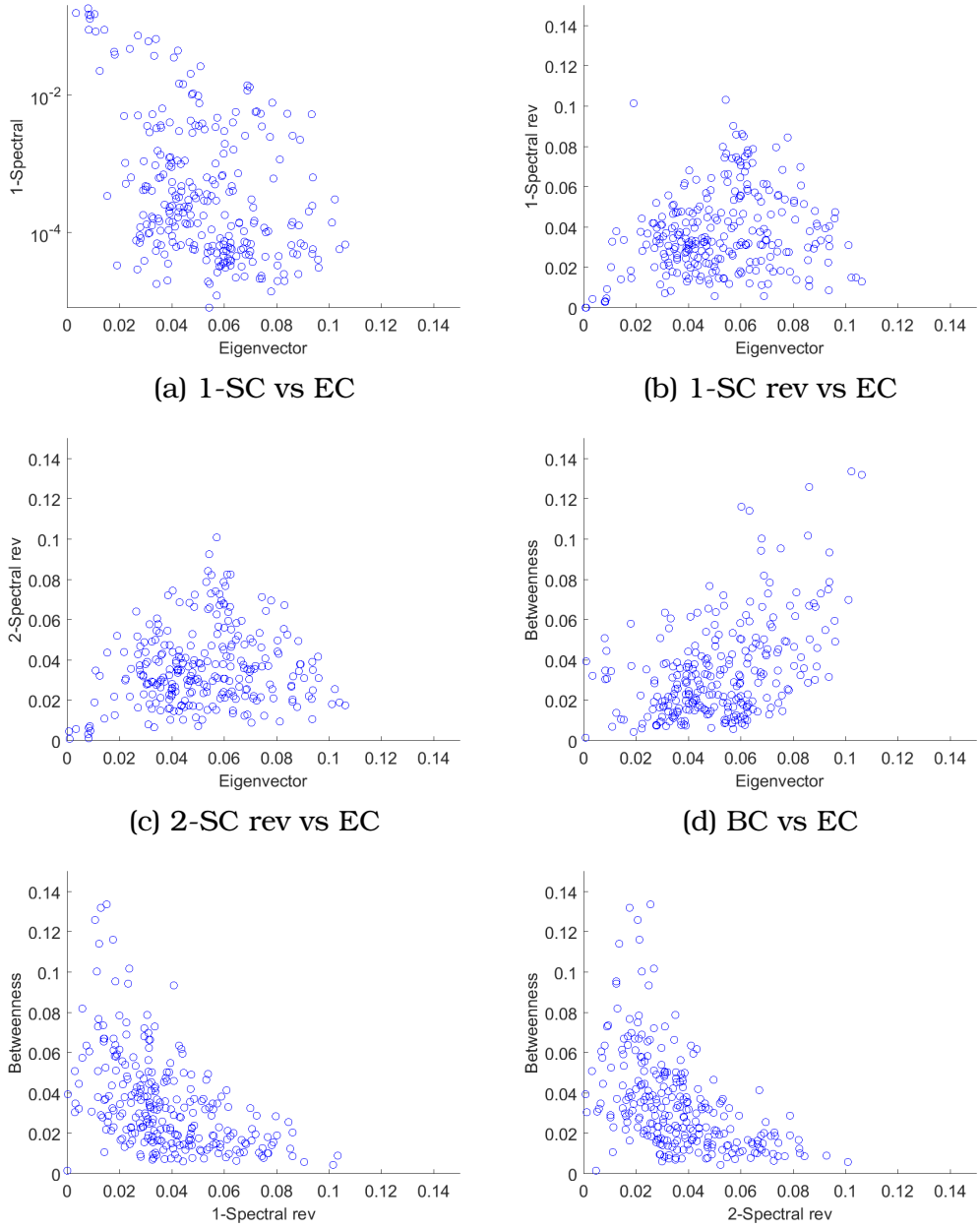

(a) 1-SC vs EC

(b) 1-SC rev vs EC

(c) 2-SC rev vs EC

(d) BC vs EC

(e) 1-SC rev vs BC

(f) 2-SC rev vs BC

Figure 4.7: Relations between the different centrality measures for the thresholded network. The centrality values of each region have been averaged over the 16 patients. Note also that spectral is reported on a logaritmic scale. The proportionality between spectral and eigenvector seems to decrease compared to the unthresholded network, whereas the one between spectral and betweenness seems to increase compared to the unthresholded network.

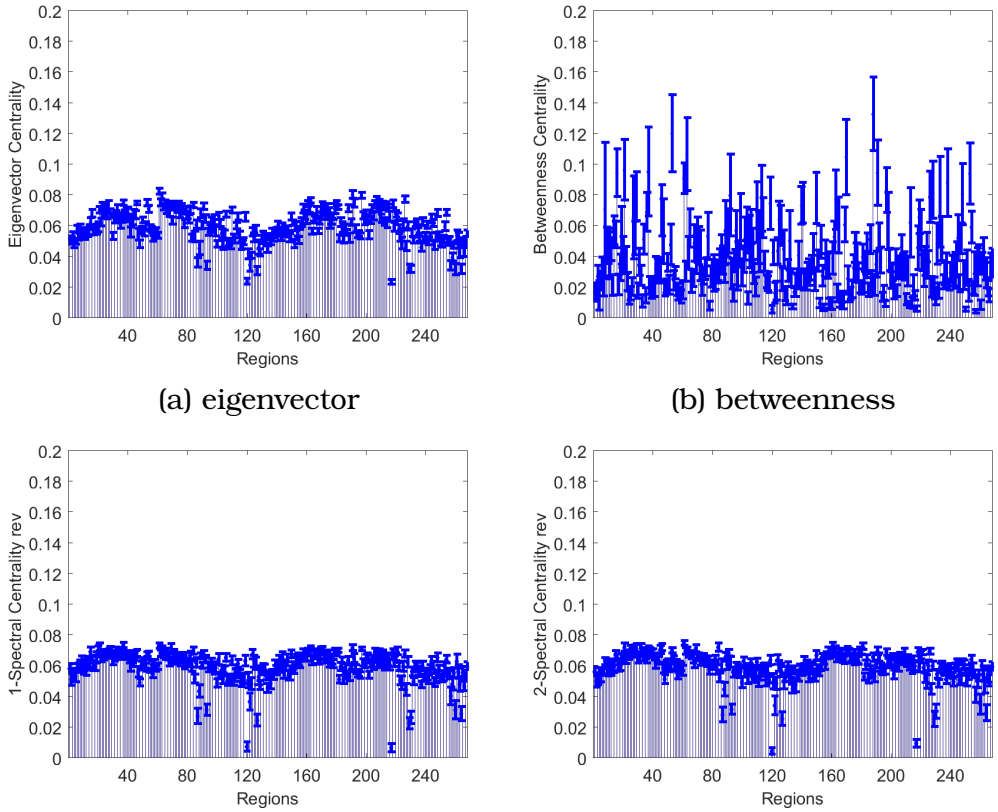

(a) eigenvector (b) betweenness

(c) reversed 1-spectral (d) reversed 2-spectral

Figure 4.8: Behaviour of the three centrality measures as a function of brain regions averaged over the 16 individuals for the original network. Eigenvector (4.8a), betweenness (4.8b), 1-spectral (4.8c) and 2-spectral (4.8d). Errorbars represent standard deviations.

seem to be quite unstable, too. Given that the original networks provide stabler results, we will use them in the following analyses, discarding the thresholded networks.

4.3 Regions with significant centrality

We analysed if the values are statistically significant compared to the null model described in section 3.3, (figure 4.10), and, if so, what the regions presenting such unusual values

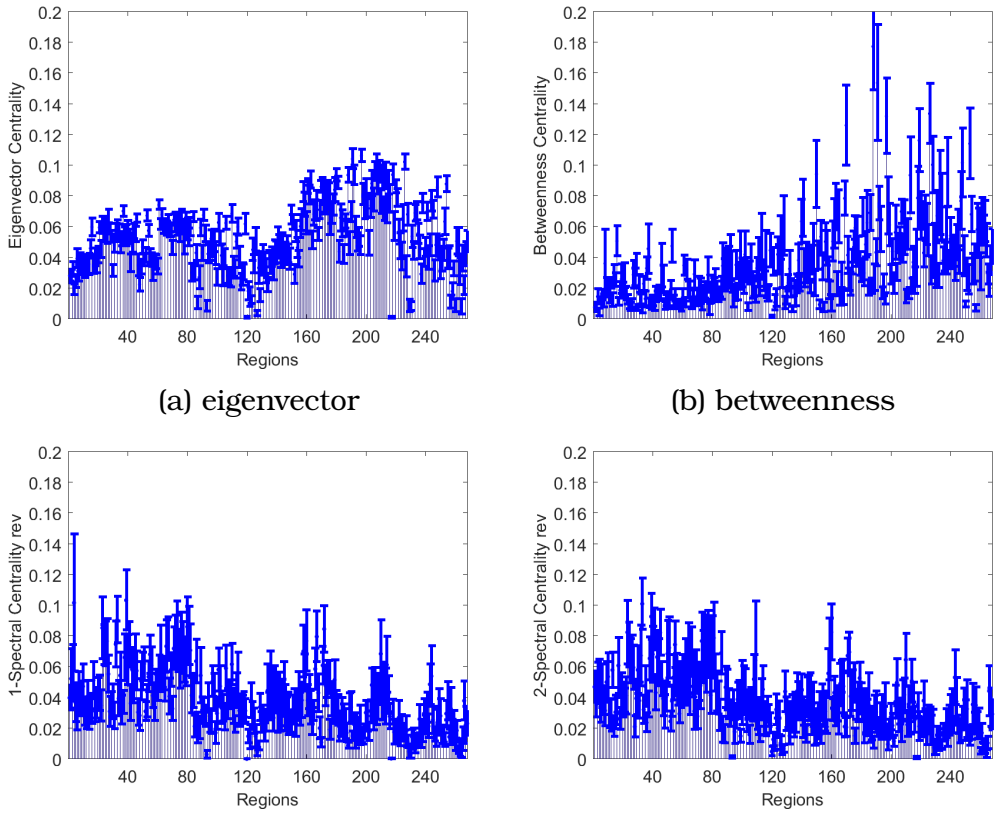

(a) eigenvector (b) betweenness

(c) reversed 1-spectral (d) reversed 2-spectral

Figure 4.9: Behaviour of the three centrality measuresas a function of brain regions averaged over the 16 individuals for the thresholded network. Eigenvector (4.8a), betweenness (4.9b), 1-spectral (4.9c) and 2-spectral (4.9d). Errorbars represent standard deviations.

are. We used a confidence level of 0.05, and we applied a FDR (section 3.3.3). As can be seen from figures 4.10, only eigenvector gave significantly high (88) and low (125) values. Among the high values the relative majority (41%) belongs to the limbic system, Yeo region 5. Others belong to visual, ventral attention and default. Among the low values 49% belong to the ventral attention, and other involve somatomotor, visual and dorsal attention. 1-Spectral only gave 2 significantly low values, being region 120 and 217, both belonging to Yeo ventral attention network, in accordance with eigenvector. This result indicates that eigenvector behaves differently from spectral, with respect to the applied null model. The latter showed almost no difference between the data and the null model, whereas the former did. This is due to the eigenvector variability in the null model, being particularly low, as can be seen in figure 4.10d. Regions 120 and 217 do not have a correspondence on the AAL atlas, rather they belong to other subcortical areas, as confirmed by the overlap with the 8-networks Yeo structure. 2-spectral gave similar results to 1-spectral, but it only found region 120 as significant.

4.4 Time varying behaviour

To analyse the time varying behaviour of the network we calculated the variance of correlations on 20, 50 and 100 time points windows for each patient, and then we averaged the results. A 50 points time window was the best according to previous studies [27] given the rule of thumb $T_{min} = 1/w_{min}$, explained in section 3.3, and the experimental conditions (section 3.3). This results in 21 correlation matrices per region. The behaviour of variance for two pair of sample regions is shown in figure 4.12.

Using the 50 points window, however, only 0.8% of correlations, obtained by a one-tailed FDR p-value with a 0.05 confidence interval, proved to have non-stationary behaviours. A 20 points window proved to slightly increase this fraction, when compared to the null model. In this case 1.5% of the correlation values resulted to be significant. This is in contrast with the aforementioned rule of thumb. A 100 points window, on the other hand, only proved to yield 0.5% significant correlation values. However changing the step size, that is the amount of points with which we shift the window, may result in a decreased difference between small and big time windows significant values.

We applied this null model in one sample patient also to calculate the variance of

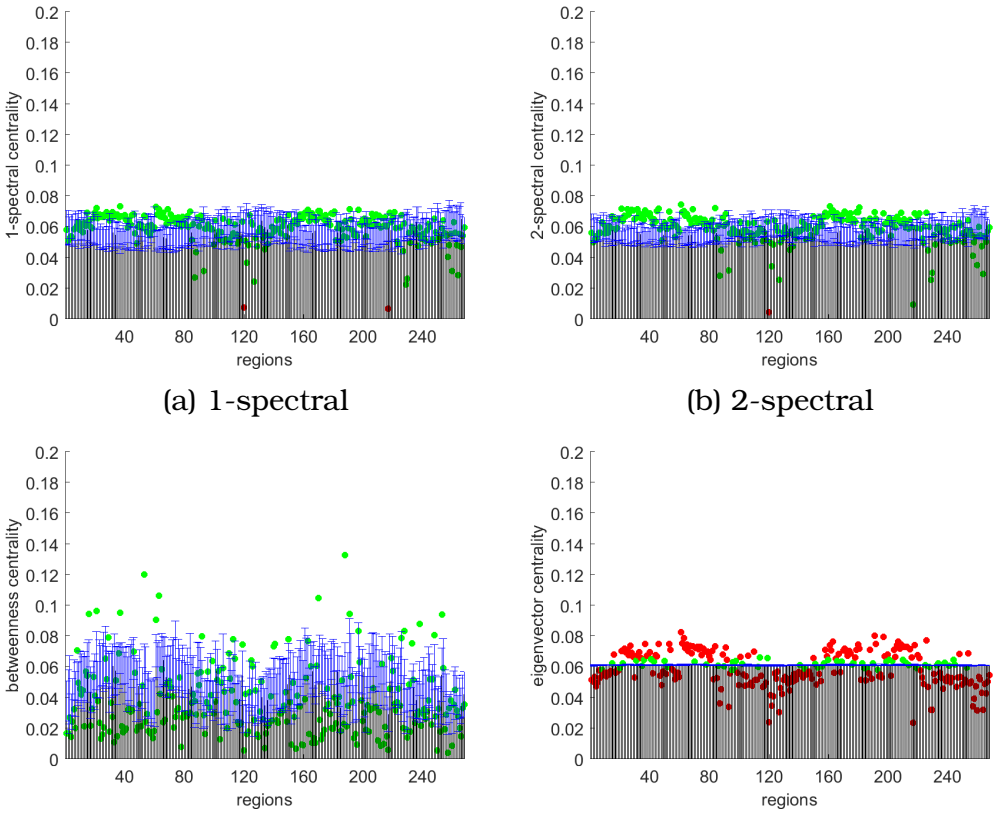

(a) 1-spectral

(b) 2-spectral

(c) betweenness

(d) eigenvector

Figure 4.10: Bar plots of the null model of each centrality measure, with the corresponding data values (scatter plot). Significant data values according to a 0.05 confidence threshold with a FDR are represented with red dots, other values are in green.

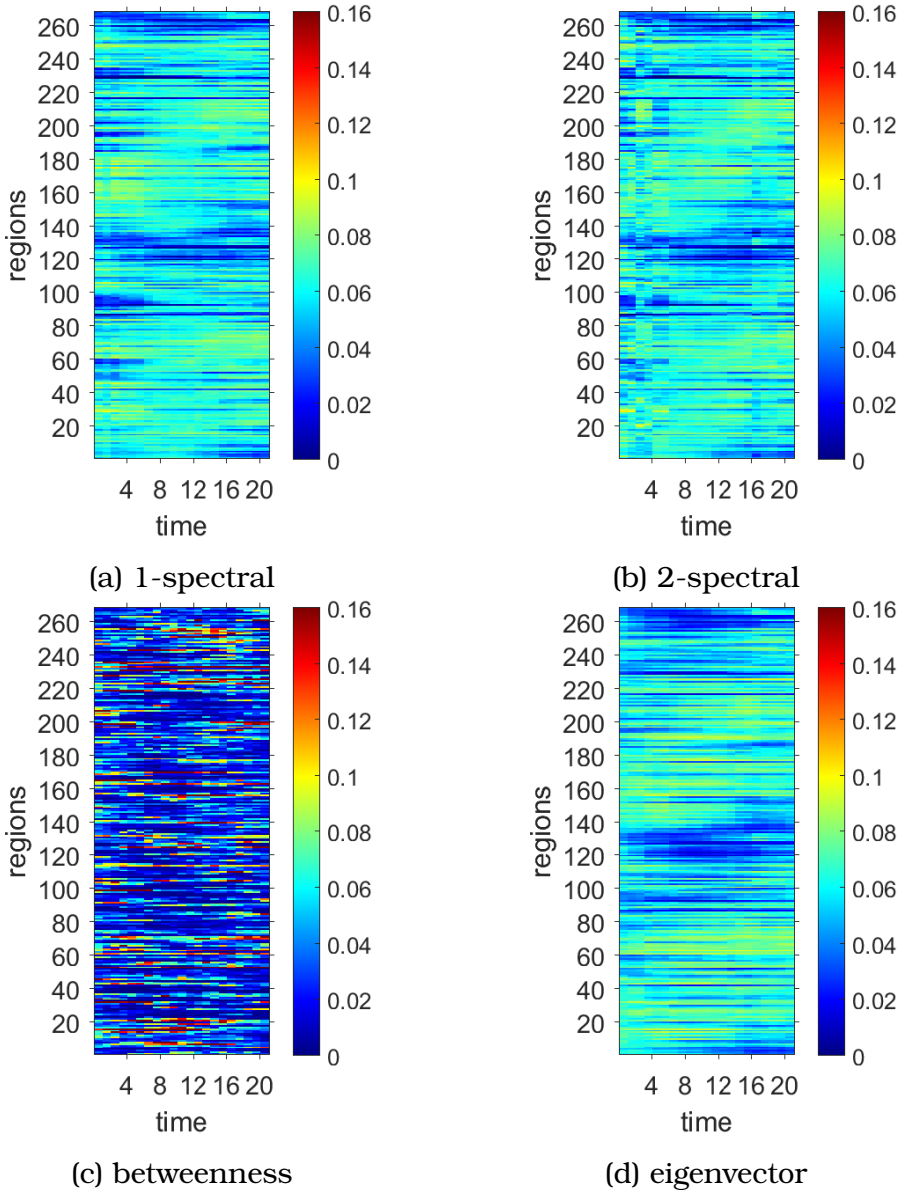

(a) 1-spectral

(b) 2-spectral

(c) betweenness

(d) eigenvector

Figure 4.11: Time varying behaviour of centrality measures for one individual. A time window of 50 points and a step of 5 points have been used. Colours indicate higher or lower values of centrality.

centrality values. The results, among the 268 centrality values, gave no significant values for the two spectral measures, whereas they provide 37 significant values for betweenness and 267 for eigenvector. According to this, the variations observed for spectral are not significant, whereas they are significant for betweenness and for eigenvector. However, as in the case of static correlations, spectral and eigenvector have quite similar behaviours in real data, whereas their behaviours completely differ in the null model. Again, the reason lies in the variability of eigenvector in the null model being extremely low. The reason why this happens, however, still needs to be investigated. Moreover, even though this model has already been used to test variations in *correlation* values [1], it has never been utilised for testing variations of *centrality* values, and therefore more analyses have to inspect the applicability of the model in this context.

4.5 Differences between resting states

We analysed the behaviour of the different centrality measures in the second dataset, as we did in the first dataset. The average centralities plot for the 4 cases are reported in figures 4.13, 4.14, 4.15, 4.16, for 1-spectral and 2-spectral centrality, betweenness centrality and eigenvector centrality, respectively. As can be seen, betweenness centrality is the most variable across individuals, whereas eigenvector is the least variable. From these plots, only small differences among the four resting states are visible and patterns are difficult to detect at a first sight. In the next subsections more detailed analyses to find differences among these resting states are performed.

First, we performed a LDA accounting for all the 268, in order to obtain a true error rate in the discrimination. Second, we used a PCA to see if it is possible to discriminate using only a few components. Afterwards a general feature selection has been performed, the best pair of discriminating region has been identified, and the behaviour of the error rate for different number of features has been analysed.

[1] Whether this model is appropriate or not, is still a debated matter.

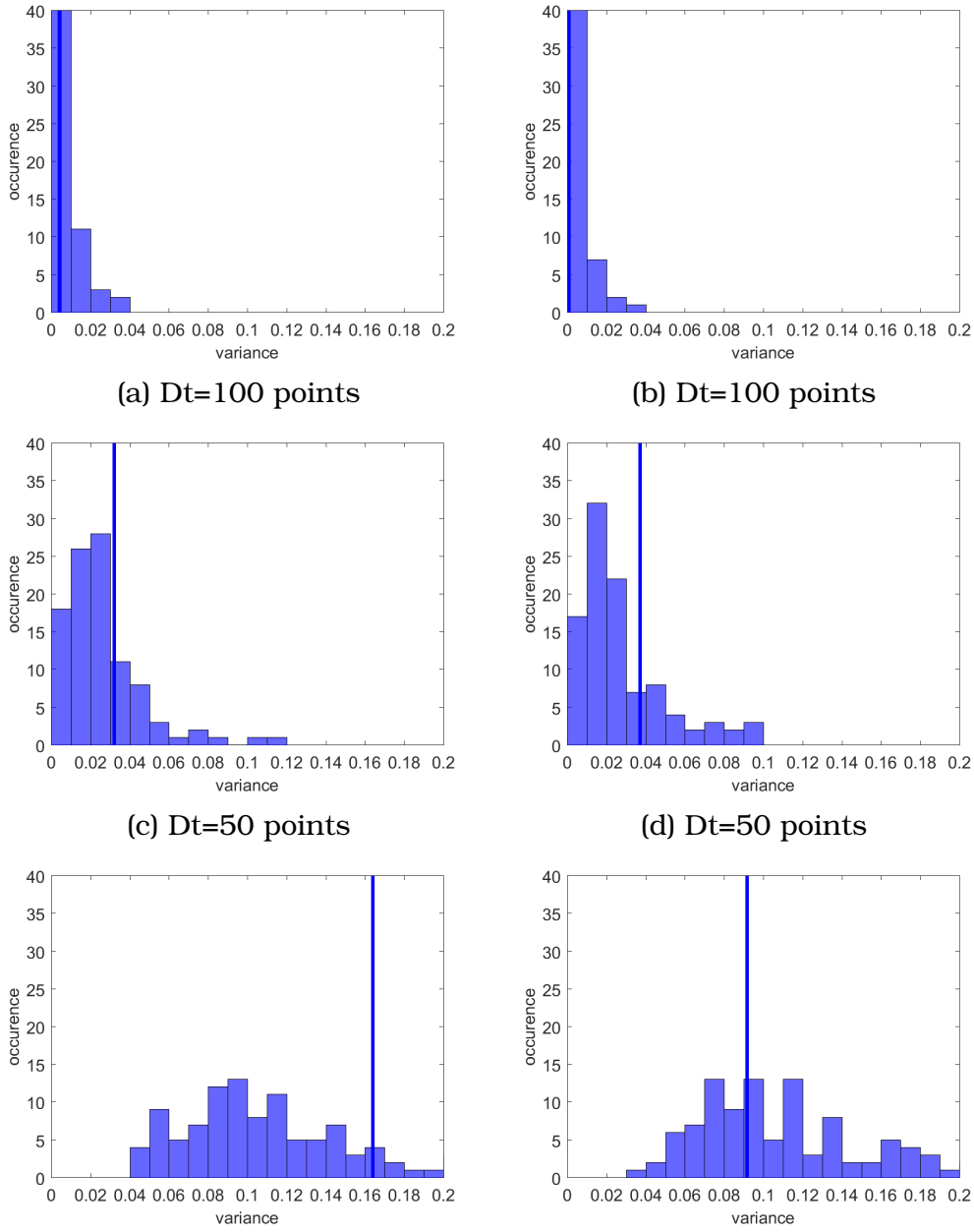

(a) Dt=100 points

(b) Dt=100 points

(c) Dt=50 points

(d) Dt=50 points

(e) Dt=20 points

(f) Dt=20 points

Figure 4.12: Variances of correlation values between two pair of sample regions. Three different values of time window are used: 100 points (top), 50 points (middle), 20 points (bottom). Bars represent the null model, whereas the vertical line is the value calculated from the data. The same axes values have been used in all the three different cases to allow for a comparison among them.

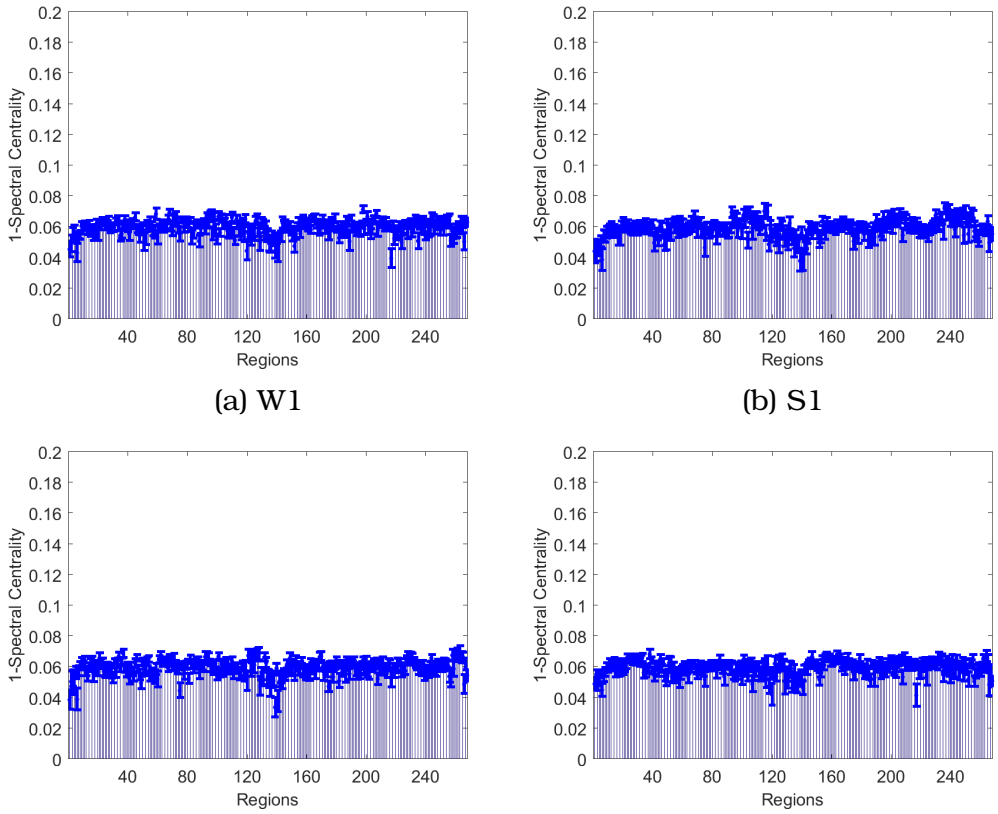

(a) W1 (b) S1

(c) S2 (d) W2

Figure 4.13: Behaviour of reversed spectral centrality as a function of brain regions averaged over the 16 individuals. Errorbars represent standard deviations.

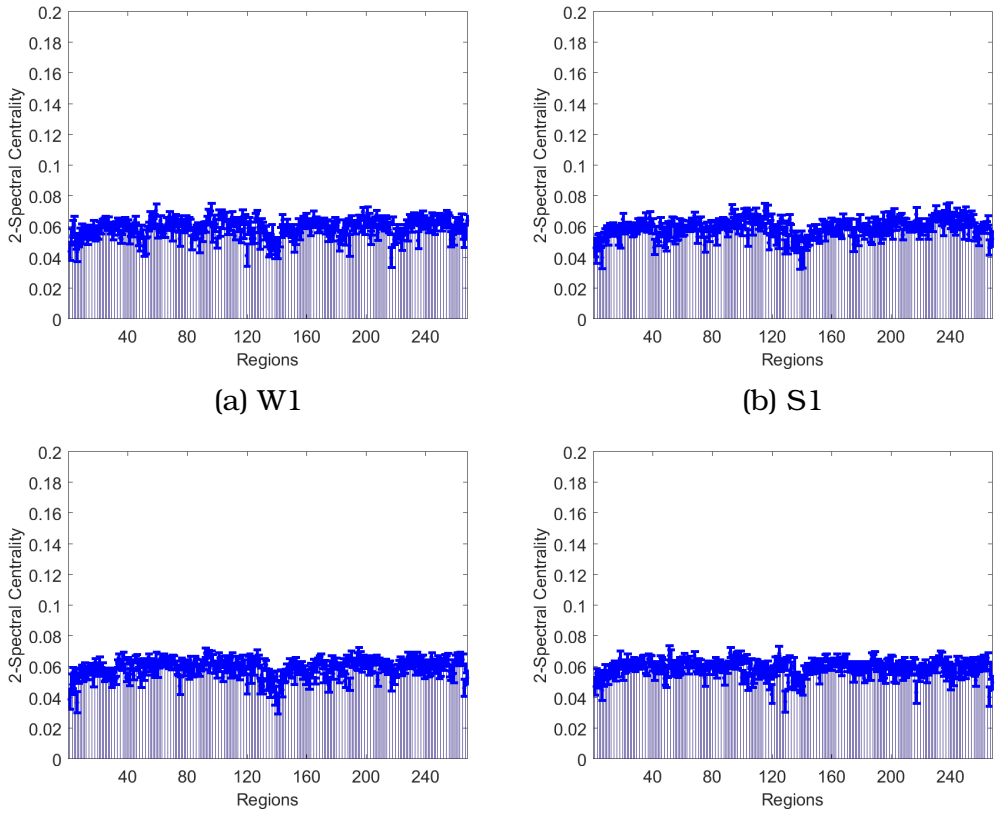

(a) W1 (b) S1

(c) S2 (d) W2

Figure 4.14: Behaviour of reversed spectral centrality as a function of brain regions averaged over the 16 individuals. Errorbars represent standard deviations.

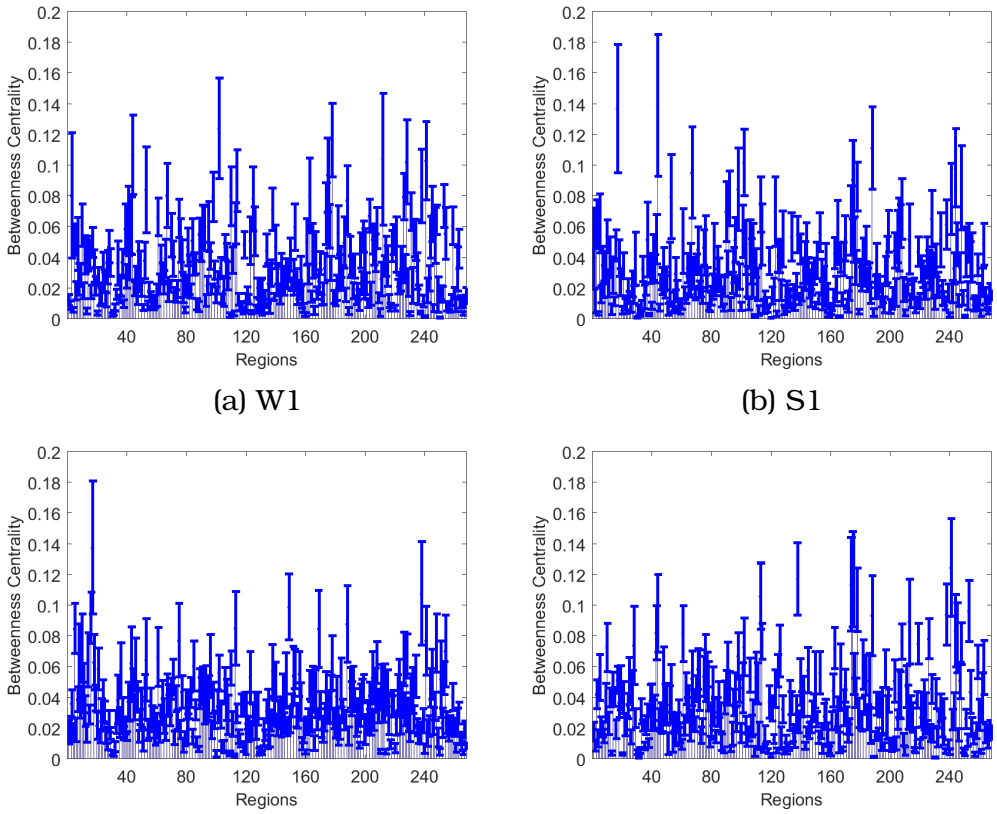

(a) W1 (b) S1

(c) S2 (d) W2

Figure 4.15: Behaviour of betweenness centrality as a function of brain regions averaged over the 16 individuals. Errorbars represent standard deviations.

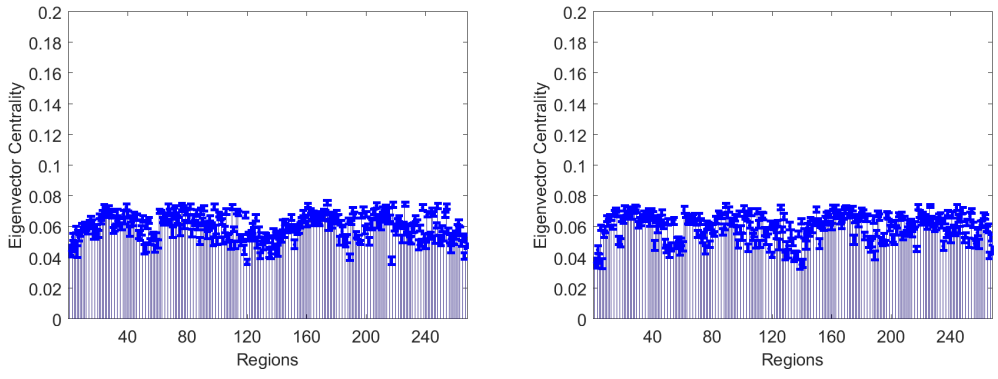

(a) W1

(b) S1

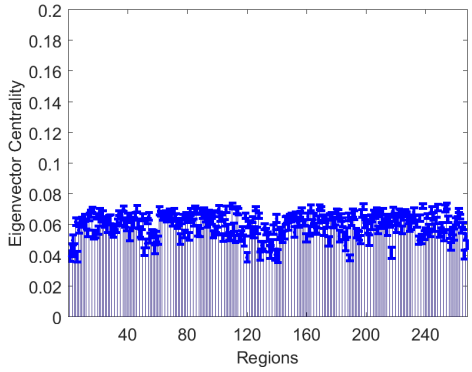

(c) S2

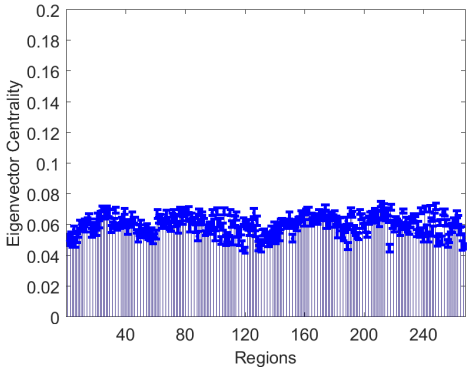

(d) W2

Figure 4.16: Behaviour of eigenvector centrality as a function of brain regions averaged over the 16 individuals. Errorbars represent standard deviations.

measure	W1 vs S2	W1 vs W2
1-spectral	0.44	0.39
1-spectral (norm)	0.36	0.50
2-spectral	0.17	0.44
betweenness	0.28	0.69
eigenvector	0.19	0.56

Table 4.1: (True) error rates for the discrimination between W1 and S2 (second column) and between W1 and W2 (third column). Among the spectral centralities, the choice of the second smallest eigenvalue (2-spectral) leads o a better discrimination than the case of Fiedler number (1-spectral). A normalised laplacian, does not seem to change the discriminant power of spectral centrality.

4.5.1 All features LDA

We first performed a LDA accounting for all the 268 features. In this way we obtained the true error rates for the discrimination between resting states W1 and S2 (one conscious, one unconscious), and between resting states W1 and W2 (two conscious states, serving as control case). The results are reported in table 4.1. The best performances are given by eigenvector, 2-spectral centrality and betweenness, while 1-spectral shows even a slightly better discrimination rate in the control than in the other. In particular eigenvector and 2-spectral have a true error rate below 20%. Here we tried to use the normalised laplacian, instead of the usual laplacian, however this did not increase the discriminant power of 1-spectral, as visible in table 4.1.

In this case we also used a diagonal quadratic classifier. However, the linear classifier discriminated better. This is due to the fact that a diagonal classifier is good only if the features have high degree of independence, which is not the case. Furthermore, we could not even use a full quadratic classifier since the covariance matrices of some classes were singular.

4.5.2 PCA

We first show a bar plot of the (normalised) eigenvalues in order to see how well PCA can discriminate. As explained in the method section, this accounts for how much of the data variability each component is able to extract. Looking at figures 4.17 and 4.18 one can see that there is a number of low components having consistent values, usually resulting in data structures, which are difficult to discriminate.

The xy plots of the 2 components that seemed to best discriminate, among the first five, are shown in figure 4.19 for the conscious-unconscious case and in figure 4.20 for the control case. As in the previous subsection, it can be seen that eigenvector and betweenness performed better than 1-spectral. 2-spectral and 1-spectral with normalised laplacian represent a little improvement, even though choosing only two components does not provide a good discrimination power. This can be also due to an intrinsic pitfall of PCA, namely it is not certain that the first components can discriminate well, especially if the variability among intraclass observations is high.

Therefore, feature selection algorithms provide more accurate information in this sense, as we will show.

4.5.3 Feature selection

First of all we did a ranking of the regions which alone performed better in discriminating among states. The discrimination is evaluated by a diagonal quadratic classifier, with a leave one out cross validation. The results are reported in tables 4.4, 4.3 and 4.2. Associating each region to the corresponding Yeo network (chapter 1) might be useful if one wants to infer the processes involved in different states. Here it becomes evident how the overlap between parcellations is a delicate processing step, given that different choices in the assignment of ambiguous regions can lead to a misinterpretation of the results. We report here the Yeo networks associated to the numeric labels (figure 4.6).

Eigenvector seems to find pair of regions belonging to somatomotor and dorsal attention cortices. Among the four highest regions three are found in the somatomotor cluster, and perform with a biased error of 13.9 (31 correct classifications out of 36) and 19.4 (29 correct classifications) .Moreover the discrimination between W1 and W2 is more difficult: each of the best two regions correctly classifies only 26 out of 36 points. These

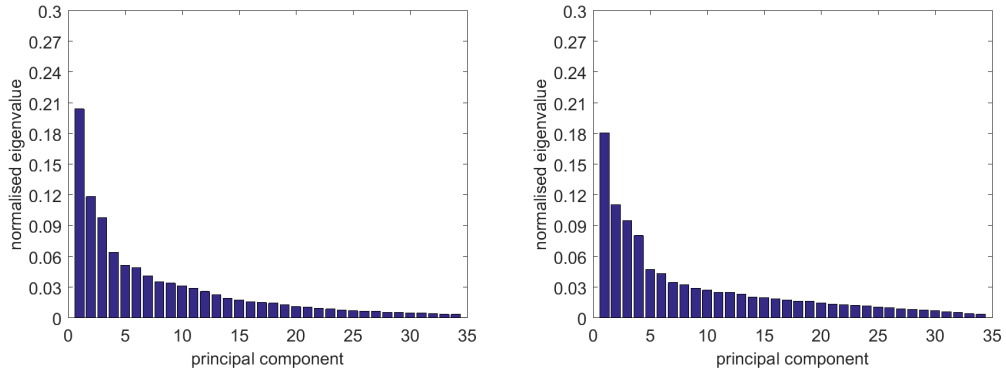

(a) 1-spectral

(b) 1-spectral norm

(c) 2-spectral

(d) betweenness

(e) eigenvector

Figure 4.17: Normalised eigenvalues of PCA in case W1 against S2. 1-spectral (4.17a), 1-spectral with normalised laplacian (4.17b), 2-spectral (4.17c), betweenness (4.17d), eigenvector (4.17e). The normalised eigenvalue indicates how much variability the measure is able to take into account.

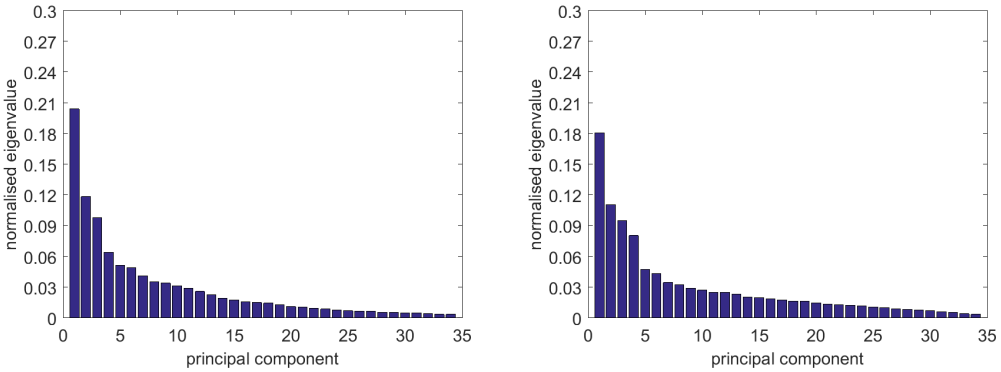

(a) 1-spectral

(b) 1-spectral norm

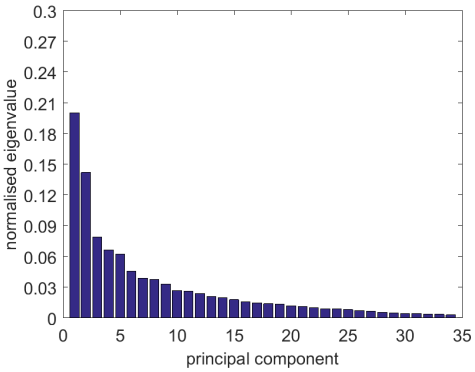

(c) 2-spectral

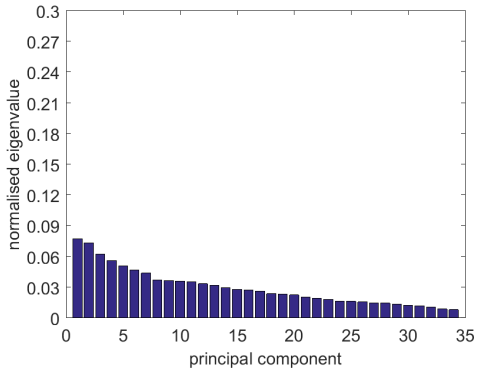

(d) betweenness

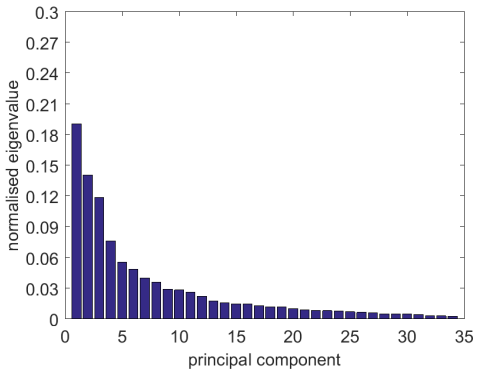

(e) eigenvector

Figure 4.18: Normalised eigenvalues of PCA in case W1 against W2. 1-spectral (4.18a), 1-spectral with normalised laplacian (4.18b), 2-spectral (4.18c), betweenness (4.18d), eigenvector (4.18e). The normalised eigenvalue indicates how much variability the measure is able to take into account.

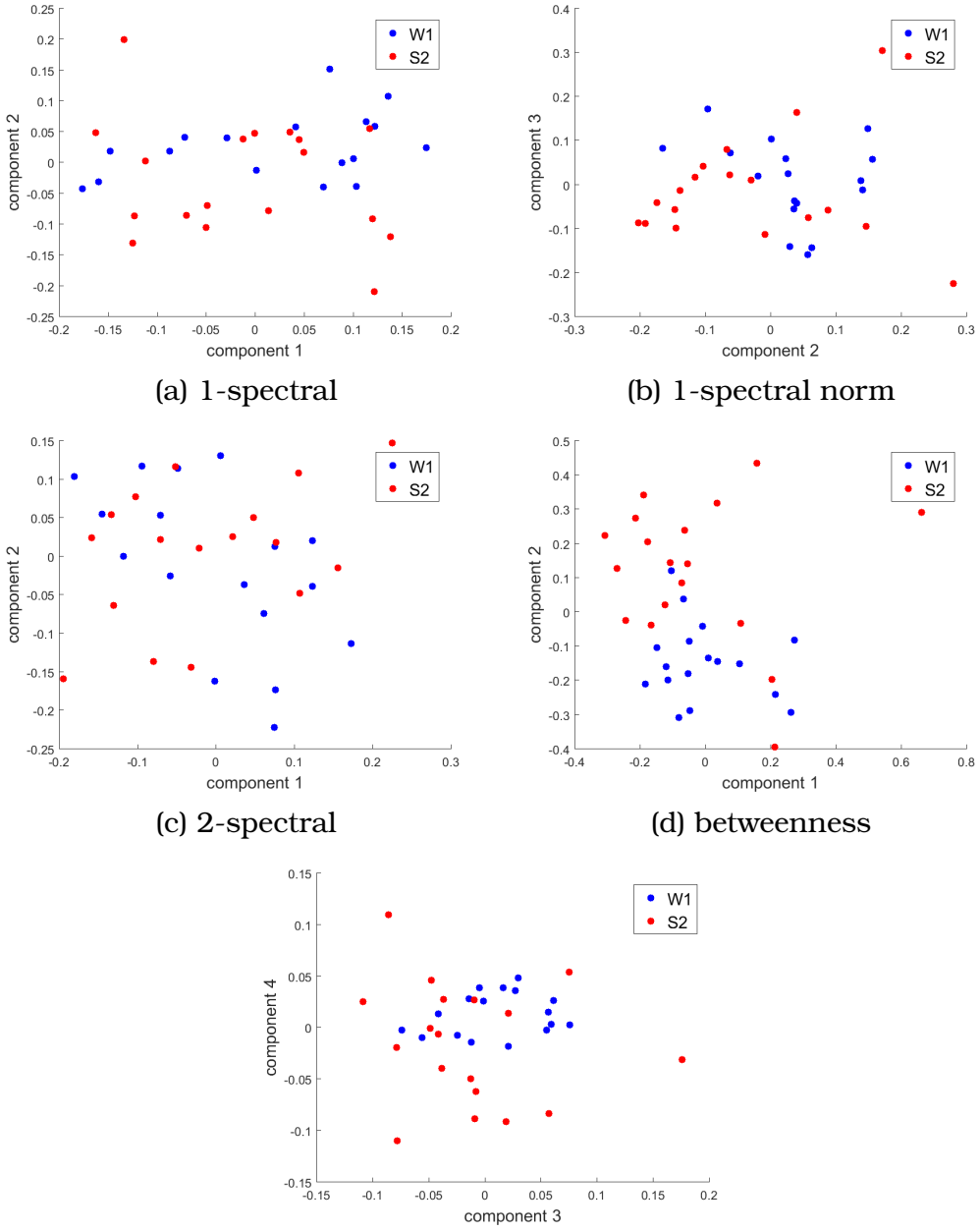

(a) 1-spectral

(b) 1-spectral norm

(c) 2-spectral

(d) betweenness

(e) eigenvector

Figure 4.19: Plots of W1 and S2 with the 2 components that better discriminate between these 2 states. To discriminate we used a diagonal quadratic classifier.

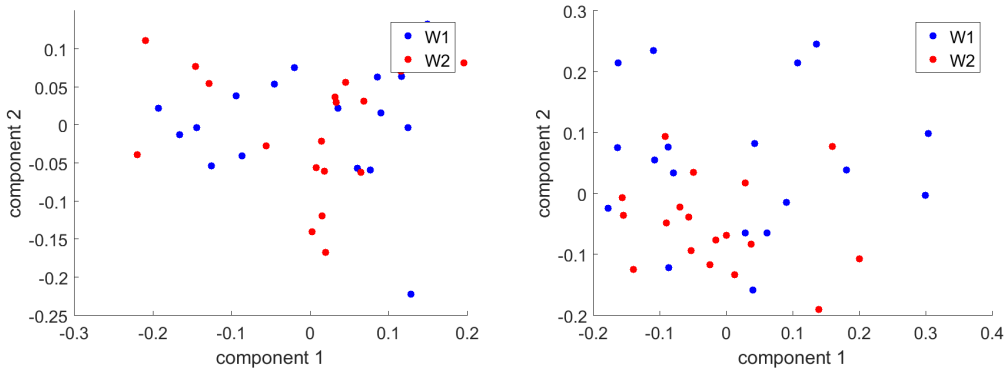

(a) 1-spectral

(b) 1-spectral norm

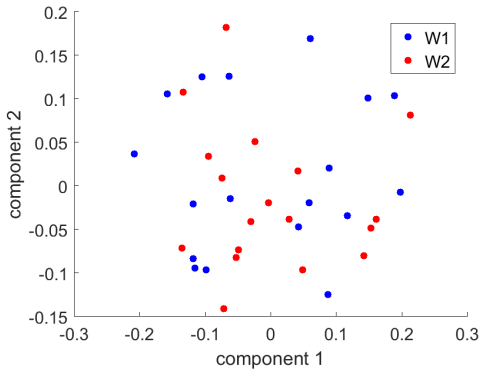

(c) 2-spectral

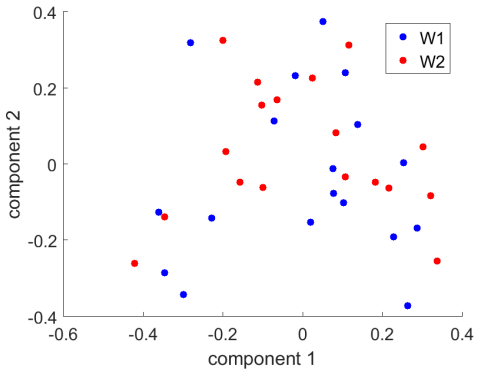

(d) betweenness

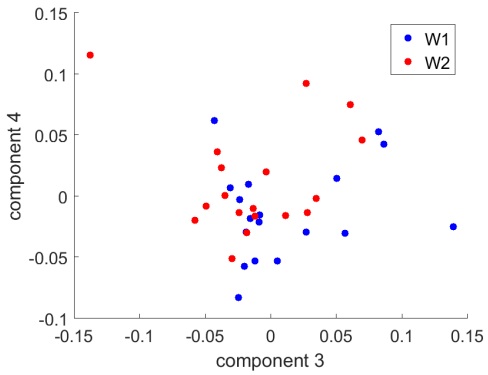

(e) eigenvector

Figure 4.20: Plots of W1 and W2 with the 2 PCA components that seem to discriminate best between the 2 resting states. Again, we used a diagonal quadratic classifier in the discriminant analysis.

W1-S2			W1-W2		
region	network	err [%]	region	network	err [%]
35	4	28	156	7	19
194	5	28	52	5	28
46	4	31	18	5	31
94	8	31	51	5	31
144	4	31			
228	5	31			

Table 4.2: Ranking of regions which best discriminate between two resting states using 2-spectral centrality. The discrimination between a conscious state and an unconscious state is reported on the left, whereas the one between the two conscious states is on the right.

W1-S2			W1-W2		
region	network	err [%]	region	network	err [%]
16	7	22	57	5	33
73	1	28	231	8	33
117	8	28	255	8	33
124	8	31	266	8	33
143	6	31			
214	1	31			

Table 4.3: Ranking of regions which best discriminate between two resting states using betweenness centrality. The discrimination between a conscious state and an unconscious state is reported on the left, whereas the one between the two conscious states is on the right.

regions belong to the ventral attention and default network. Other regions belong to somatomotor network or cerebellar and subcortical regions. Betweenness centrality seems to have a lower discrimination power, and spectral seems to discriminate better between W1 and W2 than between W1 and S2. Spectral centrality best regions mostly belong to the limbic network, even with a peak in the default network, whereas betweenness shows mostly subcortical regions.

W1-S2			W1-W2		
region	network	err [%]	region	network	err [%]
174	2	14	91	4	28
31	3	19	145	7	28
39	2	19	51	5	31
172	2	19	62	2	31
19	6	25	95	1	31
83	7	25	263	8	31
			266	8	31

Table 4.4: Ranking of regions which best discriminate between two resting states using eigenvector centrality. The discrimination between a conscious state and an unconscious state is reported on the left, whereas the one between the two conscious states is on the right.

Afterwards, we calculated the best features that minimised a criterion, which is again the error rate when performing a diagonal quadratic discriminant analysis, but without constraints on the number of components. This has been done in order to obtain both the minimum number of components which minimises the criterion and also what these components are. Again we point out that the error rate is biased, because the feature selection is performed on the same samples on which the criterion is computed.

4.5.4 Best number of components

The evolution of error rate along with the number of regions has been calculated. We just used the first best discriminating n regions for each iteration. Accordingly the error rate is biased, since the ranking of features was computed on the entire observables. Nevertheless we can see the differences between the discrimination among the conscious and unconscious states and the one between the two conscious states. The first case has a much lower error rate, providing further indications that the centrality measures are able to discriminate between unconscious and conscious states to some extent (figure 4.21).

Furthermore we calculated the best number of principal components. As explained in the methods section, the feature extraction process was performed at each step of the cross

	eigenvector				betweenness				2-spectral			
	WS	Yeo	WW	Yeo	WS	Yeo	WW	Yeo	WS	Yeo	WW	Yeo
regions	174	2	59	5	15	4	1	5	14	6	19	6
	248	8	62	2	16	7	47	6	35	4	106	8
			91	4	62	2	57	5	64	7	156	7
			110	8			199	6	159	2		
			245	8								
err. rate	0.11		0.14		0.14		0.19		0.17		0.11	

Table 4.5: Features minimising a diagonal quadratic criterion. Regions are represented as well as their corresponding Yeo network. The criterion function corresponds to the biased error rate.

Number	Yeo network
1	Visual
2	Somatomotor
3	Ventral attention
4	Dorsal attention
5	Limbic
6	Frontoparietal
7	Default
8	Subcortical

Table 4.6: Yeo networks labels

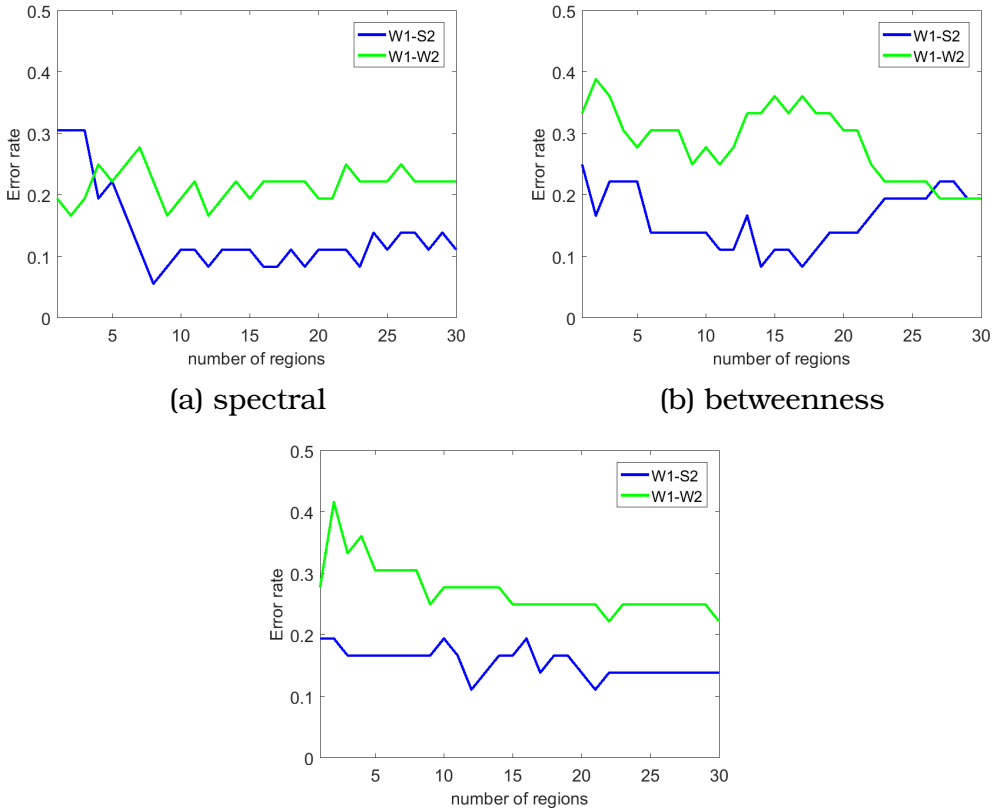

(a) spectral

(b) betweenness

(c) eigenvector

Figure 4.21: Behaviour of (biased) error rate along variable number of best components.

validation. As a result the components are different at each iteration. The advantage is that with this approach we found the *true* error. The results are shown in figure 4.22. As can be seen, in this case betweenness seems to be the measure with the highest difference between the two designs (W1-S2, versus W1-W2), whereas 2-spectral seemed the one with the lowest difference.

4.5.5 Best pair of regions

In this section we report a discriminant analysis aimed to find the best pair of regions in discriminating between states. We show the plot of the best pair which discriminates

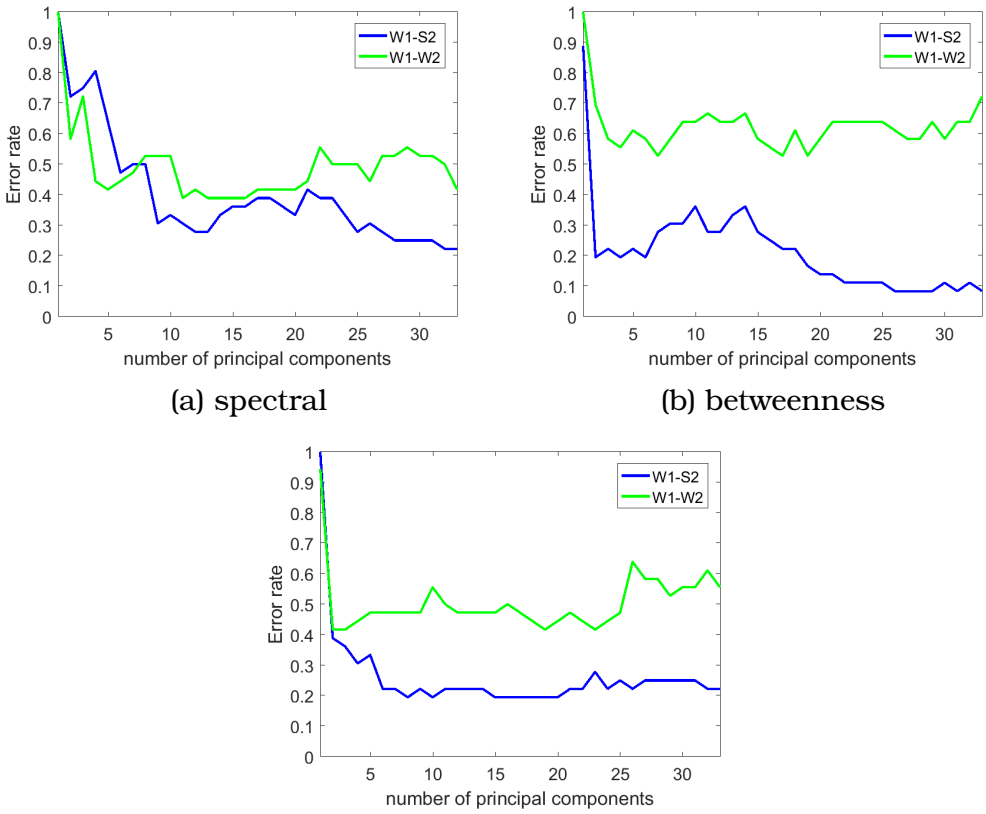

(a) spectral

(b) betweenness

(c) eigenvector

Figure 4.22: Behaviour of *true* error rate along variable number of best principal components. The principal components change, since they are a linear combination of original regions.

Measure	Eigenvector	Betweenness	Spectral
Error W1-S2 [%]	11	17	14
Error W1-W2 [%]	19	19	14

Table 4.7: Features minimising a diagonal quadratic criterion. Regions are represented as well as their corresponding Yeo network. The criterion function corresponds to the biased error rate.

between $W1$ and $S2$, and the corresponding two features to discriminate between $W1$ and $W2$. As a comparison, we also plot the best pair of regions discriminating $W1$ and $W2$ and the corresponding pair discriminating between $W1$ and $S2$. As for eigenvector, we can see from figure 4.24, that the 2 best features of W1-S2 discriminate well W1 from S2 (fig. 4.24a), and do not discriminate well W1 from W2 (fig. 4.24b). On the other hand the two features that best discriminate S2 from W1 (figure 4.24d) do not perform so well, and, anyway do not seem to perform much better than in discriminating W2 and W1 (figure 4.24c). This is a powerful result, in that provides strong evidence that the discrimination between the conscious and unconscious states is not simply due to chance. This behaviour is different for betweenness and for spectral, where we cannot conclude that the discrimination is better in one case, than in the other (figures 4.25, 4.23).

At this stage one last thing to answer to is whether or not spectral and eigenvector have the same pair of regions as best discriminant features, since they showed similar behaviours in the previous sections. We analysed the first 10, 20, 50 and 100 pairs for each measures and try to find how many regions were in common (at least one region per pair). These values were compared to values we will expect when randomly choosing 10, 20, 50, 100 regions among the 268, for the two centrality measures, to see if the number of regions in common is significant. In figure 4.26 the histograms of the number of pair for which one region is found which is in common between the two centrality measures, is shown. As can be seen, in none of the four cases the number of common regions is significantly high. This indicates that even though the behaviours of spectral and eigenvector is quite similar, differences are present. In particular the regions which discriminate well between consciousness states are different. We can conclude that the two centrality measures encode different information.

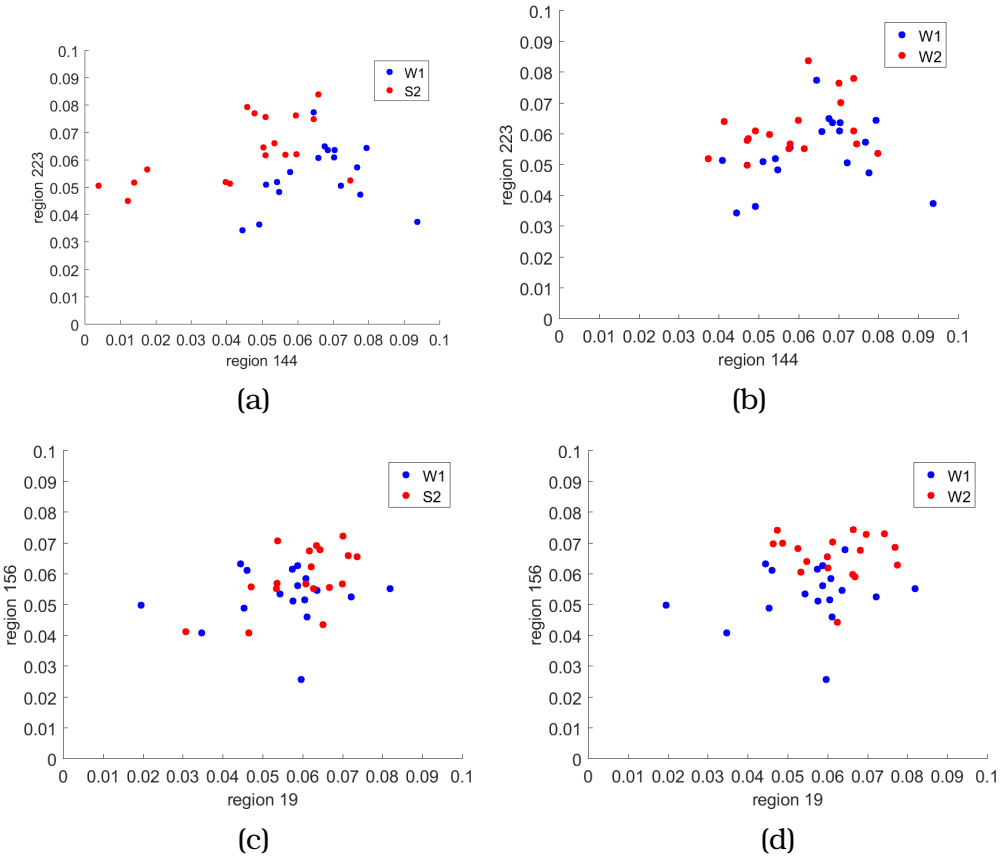

Figure 4.23: Best 2 regions for 2-spectral. On the top the axes are the two regions which best discriminate between W1 and S2 (left); the results are shown for the case W1-S2 and the control case W1-W2 (right). On the bottom the axes are the two regions which best discriminate between W1 and W2; the results are shown for the case W1-W2 (right) and the control case W1-S2 (left).

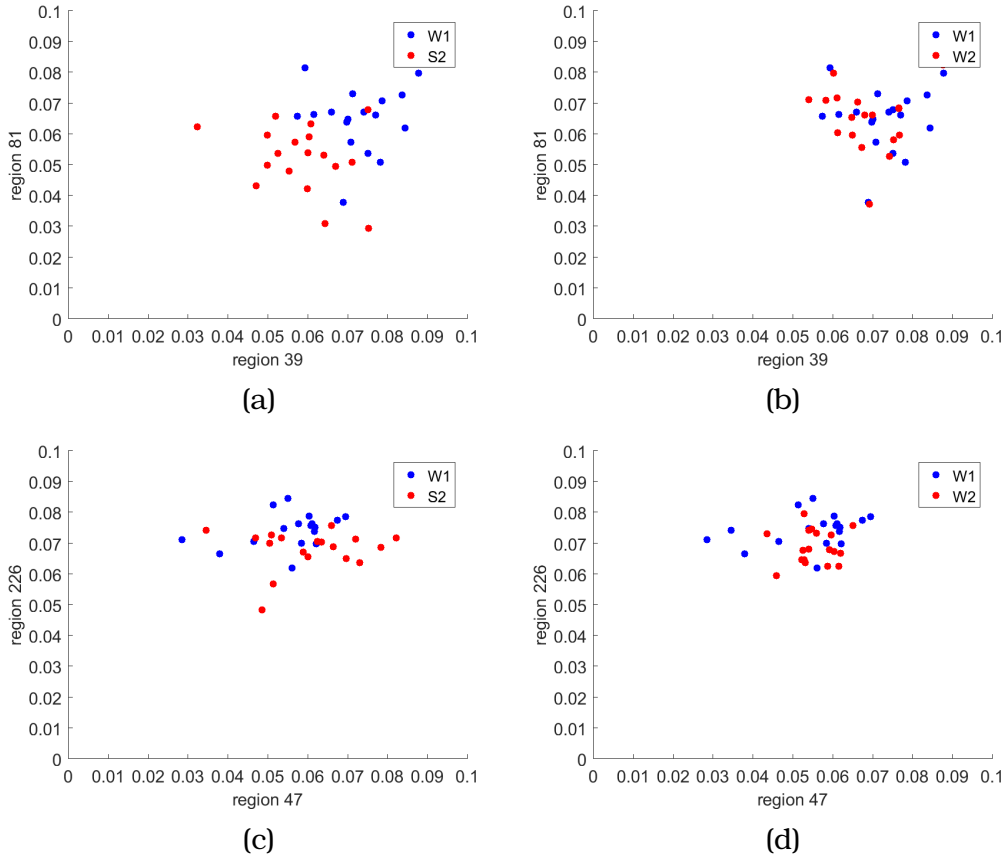

Figure 4.24: Best 2 regions for eigenvector. On the top the axes are the two regions which best discriminate between W1 and S2 (left); the results are shown for the case W1-S2 and the control case W1-W2 (right). On the bottom the axes are the two regions which best discriminate between W1 and W2; the results are shown for the case W1-W2 (right) and the control case W1-S2 (left).

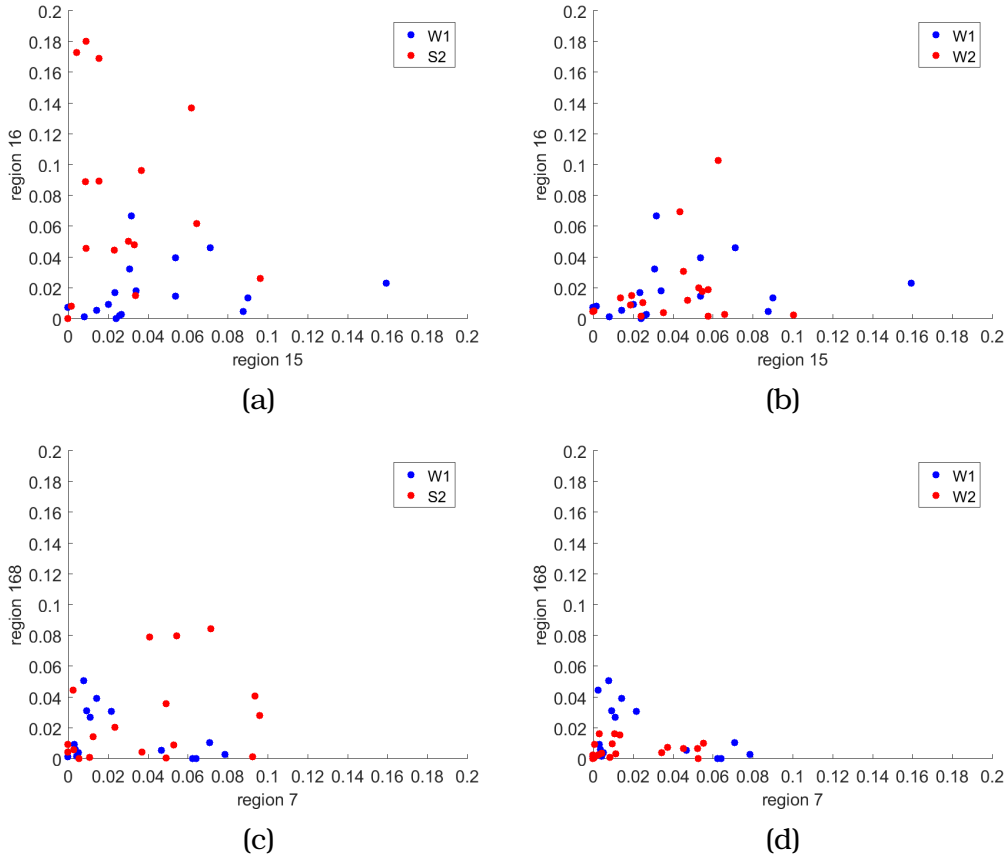

Figure 4.25: Best 2 regions for betweenness. On the top the axes are the two regions which best discriminate between W1 and S2 (left); the results are shown for the case W1-S2 and the control case W1-W2 (right). On the bottom the axes are the two regions which best discriminate between W1 and W2; the results are shown for the case W1-W2 (right) and the control case W1-S2 (left).

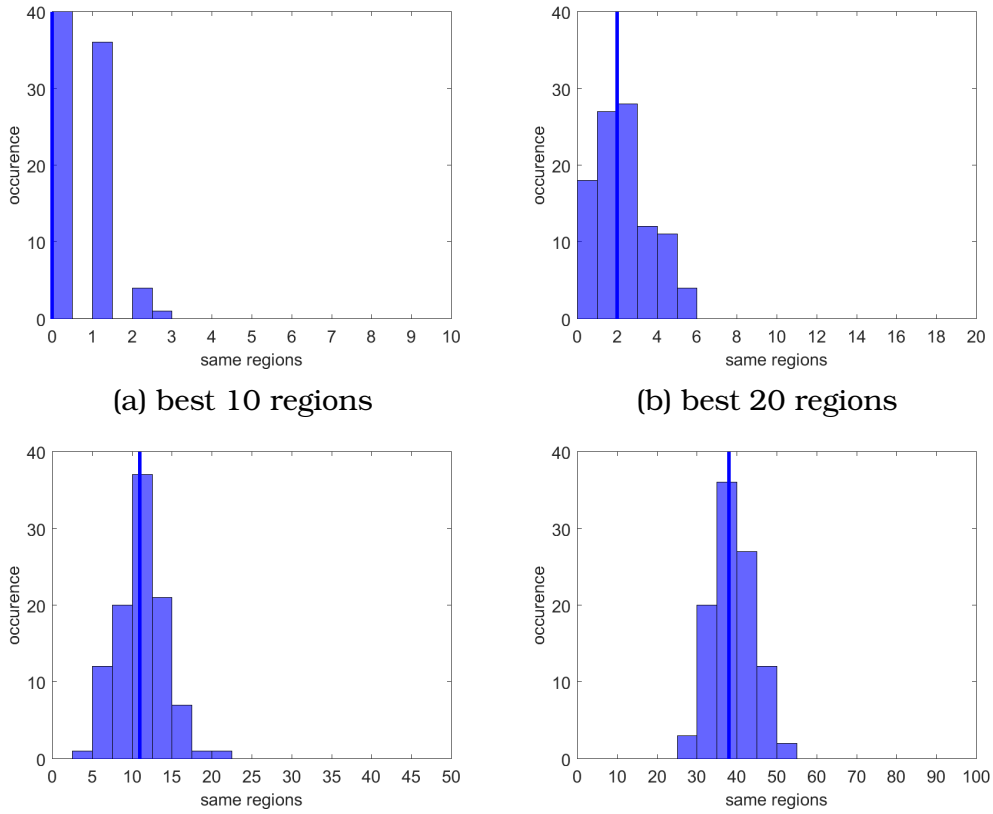

(a) best 10 regions

(b) best 20 regions

(c) best 50 regions

(d) best 100 regions

Figure 4.26: Histograms of the discriminating regions which are in common between eigenvector and 2-spectral. We analysed the first 10, 20, 50 and 100 regions respectively.

Conclusions

n this thesis we analysed two brain resting state fMRI datasets, through the tools of network theory. The resting state of brain functioning is not only important for itself, but it is useful as it can shed light on brain functional organisation. The employment of network theory arises naturally from the structure of data: from the time series of brain regions, correlation values are calculated, which constitute the basis of network links. This work puts particular focus onto three different centrality measures, two of which are well known, eigenvector and betweenness, whereas the remaining, spectral, was only recently introduced.

We used the first dataset, which is publicly available on the OpenfMRI website, to characterise network properties and centrality stability. We demonstrated that eigenvector centrality and the spectral centralities are stabler than betweenness centrality, that is they show less variability across individuals. We also utilised a thresholded version of the network, which minimises a criterion function dependent on partition density; moreover the utilised threshold proved to minimise the differences between structural and functional networks. However we showed that the use of this thresholded network decreases the stability of the utilised centrality measures.

In order to assess whether some regions show significant values we employed a null model, obtained from surrogate time series. The results, validated with a false discovery rate and a confidence level of 0.05, indicated that betweenness shows no significance, spectral shows only a few regions which are *below* the average value for null model, and eigenvector shows several values which are either above or below the null model value, proving to be the stablest, but also rising questions on the applicability of the null model. Furthermore we investigated the indications of time variability of the functional network, through a validation employing a more complex null model, which tests for non-stationarity of

the time series. Although some correlation proved to be dynamical, the total number of dynamical correlations is considerably low.

With the second dataset, encompassing individuals in different levels of consciousness, we investigated the discriminant power of the three centrality measures between these states. We used a fully consciousness state against a deep unconsciousness state, and, as a control case, two different conscious states. The discriminant power is evaluated with a diagonal quadratic discriminant analysis, both accounting for all the features and with previously selected features. Eigenvector seems to perform best, even though to assess this analyses with more individuals are needed. An interesting feature, compared to the analyses of the first dataset is that while eigenvector and spectral showed similar behaviours, the regions which better discriminate between two states are different. This may indicate that the two measures encode different information, and thus one of them can be more appropriate in one type of analysis than the other and vice versa.

We point out that this study is, at least to our knowledge, unique in its experimental design, in that it is the first to employ network measures in consciousness studies in healthy brains. Previous studies on consciousness, in fact, either did not use network theory, or they referred to injured brain, where the experimental conditions are less subtle.

From this work it is clear how much have still to be done in order to reach unequivocal procedures to analyse brain functional connectivity, accounting for all the issues that may arise, mainly coming from the many computationally expensive and difficult processing steps. The overall results, however, showed the great contribution that network theory can provide in studying brain connections.

Bibliography

[1] R. Albert and A.-L. Barabási. Statistical mechanics of complex networks. *Reviews of modern physics*, 74(1):47, 2002.

[2] C. Ambroise and G. J. McLachlan. Selection bias in gene extraction on the basis of microarray gene-expression data. *Proceedings of the national academy of sciences*, 99(10):6562–6566, 2002.

[3] E. Amico, F. Gomez, C. Di Perri, A. Vanhaudenhuyse, D. Lesenfants, P. Boveroux, V. Bonhomme, J.-F. Brichant, D. Marinazzo, and S. Laureys. Posterior cingulate cortex-related co-activation patterns: a resting state fmri study in propofol-induced loss of consciousness. *PloS one*, 9(6):e100012, 2014.

[4] J. Ashburner, G. Barnes, C.-C. Chen, J. Daunizeau, G. Flandin, K. Friston, V. Glauche, R. Henson, C. Hutton, S. Kiebel, et al. Statistical parametric mapping. 1994.

[5] F. G. Ashby. *Statistical analysis of fMRI data*. MIT press, 2011.

[6] C. F. Beckmann, M. DeLuca, J. T. Devlin, and S. M. Smith. Investigations into resting-state connectivity using independent component analysis. *Philosophical Transactions of the Royal Society of London B: Biological Sciences*, 360(1457):1001–1013, 2005.

[7] B. Biswal, F. Zerrin Yetkin, V. M. Haughton, and J. S. Hyde. Functional connectivity in the motor cortex of resting human brain using echo-planar mri. *Magnetic resonance in medicine*, 34(4):537–541, 1995.

[8] S. P. Borgatti. Centrality and network flow. *Social networks*, 27(1):55–71, 2005.

[9] P. Boveroux, A. Vanhaudenhuyse, M.-A. Bruno, Q. Noirhomme, S. Lauwick, A. Luxen, C. Degueldre, A. Plenevaux, C. Schnakers, C. Phillips, et al. Breakdown of within-and between-network resting state functional magnetic resonance imaging connectivity during propofol-induced loss of consciousness. *The Journal of the American Society of Anesthesiologists*, 113(5):1038–1053, 2010.

[10] E. Bullmore and O. Sporns. Complex brain networks: graph theoretical analysis of structural and functional systems. *Nature Reviews Neuroscience*, 10(3):186–198, 2009.

[11] C. Chang and G. H. Glover. Time–frequency dynamics of resting-state brain connectivity measured with fmri. *Neuroimage*, 50(1):81–98, 2010.

[12] E. B. Dagum. *Analisi delle serie storiche: modellistica, previsione e scomposizione*. Springer Science & Business Media, 2001.

[13] J. Damoiseaux, S. Rombouts, F. Barkhof, P. Scheltens, C. Stam, S. M. Smith, and C. Beckmann. Consistent resting-state networks across healthy subjects. *Proceedings of the national academy of sciences*, 103(37):13848–13853, 2006.

[14] J. S. Damoiseaux and M. D. Greicius. Greater than the sum of its parts: a review of studies combining structural connectivity and resting-state functional connectivity. *Brain Structure and Function*, 213(6):525–533, 2009.

[15] M. De Luca, C. Beckmann, N. De Stefano, P. Matthews, and S. M. Smith. fmri resting state networks define distinct modes of long-distance interactions in the human brain. *Neuroimage*, 29(4):1359–1367, 2006.

[16] I. Diez, P. Bonifazi, I. Escudero, B. Mateos, M. A. Muñoz, S. Stramaglia, and J. M. Cortes. A novel brain partition highlights the modular skeleton shared by structure and function. *Scientific reports*, 5, 2015.

[17] A. C. Evans, D. L. Collins, S. Mills, E. Brown, R. Kelly, and T. M. Peters. 3d statistical neuroanatomical models from 305 mri volumes. In *Nuclear Science Sym-*

posium and Medical Imaging Conference, 1993., 1993 IEEE Conference Record., pages 1813–1817. IEEE, 1993.

[18] S. Fortunato. Community detection in graphs. *Physics reports*, 486(3):75–174, 2010.

[19] L. C. Freeman, D. Roeder, and R. R. Mulholland. Centrality in social networks: Ii. experimental results. *Social networks*, 2(2):119–141, 1979.

[20] G. H. Golub and C. F. Van Loan. Matrix computations. johns hopkins studies in the mathematical sciences, 1996.

[21] I. Guyon, J. Weston, S. Barnhill, and V. Vapnik. Gene selection for cancer classification using support vector machines. *Machine learning*, 46(1-3):389–422, 2002.

[22] E. C. Hansen, D. Battaglia, A. Spiegler, G. Deco, and V. K. Jirsa. Functional connectivity dynamics: modeling the switching behavior of the resting state. *Neuroimage*, 105:525–535, 2015.

[23] R. Hindriks, M. Adhikari, Y. Murayama, M. Ganzetti, D. Mantini, N. Logothetis, and G. Deco. Can sliding-window correlations reveal dynamic functional connectivity in resting-state fmri? *NeuroImage*, 2015.

[24] R. M. Hutchison, T. Womelsdorf, J. S. Gati, S. Everling, and R. S. Menon. Resting-state networks show dynamic functional connectivity in awake humans and anesthetized macaques. *Human brain mapping*, 34(9):2154–2177, 2013.

[25] M. Jenkinson, C. F. Beckmann, T. E. Behrens, M. W. Woolrich, and S. M. Smith. Fsl. *Neuroimage*, 62(2):782–790, 2012.

[26] K. E. Joyce, P. J. Laurienti, J. H. Burdette, and S. Hayasaka. A new measure of centrality for brain networks. *PLoS One*, 5(8):e12200, 2010.

[27] N. Leonardi, J. Richiardi, M. Gschwind, S. Simioni, J.-M. Annoni, M. Schluep, P. Vuilleumier, and D. Van De Ville. Principal components of functional connectivity: a new approach to study dynamic brain connectivity during rest. *NeuroImage*, 83:937–950, 2013.

[28] N. Leonardi and D. Van De Ville. On spurious and real fluctuations of dynamic functional connectivity during rest. *Neuroimage*, 104:430–436, 2015.

[29] M. A. Lindquist, Y. Xu, M. B. Nebel, and B. S. Caffo. Evaluating dynamic bivariate correlations in resting-state fmri: A comparison study and a new approach. *Neuroimage*, 101:531–546, 2014.

[30] X. Liu and J. H. Duyn. Time-varying functional network information extracted from brief instances of spontaneous brain activity. *Proceedings of the National Academy of Sciences*, 110(11):4392–4397, 2013.

[31] N. K. Logothetis. What we can do and what we cannot do with fmri. *Nature*, 453(7197):869–878, 2008.

[32] G. Lohmann, D. S. Margulies, A. Horstmann, B. Pleger, J. Lepsien, D. Goldhahn, H. Schloegl, M. Stumvoll, A. Villringer, and R. Turner. Eigenvector centrality mapping for analyzing connectivity patterns in fmri data of the human brain. *PloS one*, 5(4):e10232, 2010.

[33] R. MacLaren, J. M. Plamondon, K. B. Ramsay, G. M. Rocker, W. D. Patrick, and R. I. Hall. A prospective evaluation of empiric versus protocol-based sedation and analgesia. *Pharmacotherapy: The Journal of Human Pharmacology and Drug Therapy*, 20(6):662–672, 2000.

[34] G. Menichetti, D. Remondini, P. Panzarasa, R. J. Mondragón, and G. Bianconi. Weighted multiplex networks. *PloS one*, 9(6):e97857, 2014.

[35] S. Milgram. The small world problem. *Psychology today*, 2(1):60–67, 1967.

[36] M. E. Newman. The structure and function of complex networks. *SIAM review*, 45(2):167–256, 2003.

[37] S. D. Pauls and D. Remondini. Measures of centrality based on the spectrum of the laplacian. *Physical Review E*, 85(6):066127, 2012.

[38] J. D. Power, B. L. Schlaggar, C. N. Lessov-Schlaggar, and S. E. Petersen. Evidence for hubs in human functional brain networks. *Neuron*, 79(4):798–813, 2013.

[39] D. Purves, G. Augustine, D. Fitzpatrick, W. Hall, A. LaMantia, and L. White. Neuroscience, 5th edn, 2011.

[40] M. E. Raichle and A. Z. Snyder. A default mode of brain function: a brief history of an evolving idea. *Neuroimage*, 37(4):1083–1090, 2007.

[41] M. Rubinov and O. Sporns. Complex network measures of brain connectivity: uses and interpretations. *Neuroimage*, 52(3):1059–1069, 2010.

[42] R. Salvador, J. Suckling, C. Schwarzbauer, and E. Bullmore. Undirected graphs of frequency-dependent functional connectivity in whole brain networks. *Philosophical Transactions of the Royal Society of London B: Biological Sciences*, 360(1457):937–946, 2005.

[43] T. Schreiber and A. Schmitz. Surrogate time series. *Physica D: Nonlinear Phenomena*, 142(3):346–382, 2000.

[44] J. Schrouff, V. Perlbarg, M. Boly, G. Marrelec, P. Boveroux, A. Vanhaudenhuyse, M.-A. Bruno, S. Laureys, C. Phillips, M. Pélégrini-Issac, et al. Brain functional integration decreases during propofol-induced loss of consciousness. *Neuroimage*, 57(1):198–205, 2011.

[45] X. Shen, F. Tokoglu, X. Papademetris, and R. T. Constable. Groupwise whole-brain parcellation from resting-state fmri data for network node identification. *Neuroimage*, 82:403–415, 2013.

[46] O. Sporns. Brain connectivity. *Scholarpedia*, 2(10):4695, 2007.

[47] G. Sugihara, R. May, H. Ye, C.-h. Hsieh, E. Deyle, M. Fogarty, and S. Munch. Detecting causality in complex ecosystems. *science*, 338(6106):496–500, 2012.

[48] E. Tagliazucchi, F. Von Wegner, A. Morzelewski, V. Brodbeck, and H. Laufs. Dynamic bold functional connectivity in humans and its electrophysiological correlates. *Front Hum Neurosci*, 6(339.10):3389, 2012.

[49] J. Talairach and P. Tournoux. Co-planar stereotaxic atlas of the human brain. 3-dimensional proportional system: an approach to cerebral imaging. 1988.

[50] Q. K. Telesford, S. L. Simpson, J. H. Burdette, S. Hayasaka, and P. J. Laurienti. The brain as a complex system: using network science as a tool for understanding the brain. *Brain Connectivity*, 1(4):295–308, 2011.

[51] M. P. van den Heuvel, R. C. Mandl, C. J. Stam, R. S. Kahn, and H. E. H. Pol. Aberrant frontal and temporal complex network structure in schizophrenia: a graph theoretical analysis. *The Journal of Neuroscience*, 30(47):15915–15926, 2010.

[52] M. P. Van Den Heuvel and H. E. H. Pol. Exploring the brain network: a review on resting-state fmri functional connectivity. *European Neuropsychopharmacology*, 20(8):519–534, 2010.

[53] M. P. van den Heuvel, C. J. Stam, M. Boersma, and H. H. Pol. Small-world and scale-free organization of voxel-based resting-state functional connectivity in the human brain. *Neuroimage*, 43(3):528–539, 2008.

[54] B. T. Yeo, F. M. Krienen, J. Sepulcre, M. R. Sabuncu, D. Lashkari, M. Hollinshead, J. L. Roffman, J. W. Smoller, L. Zöllei, J. R. Polimeni, et al. The organization of the human cerebral cortex estimated by intrinsic functional connectivity. *Journal of neurophysiology*, 106(3):1125–1165, 2011.

[55] A. Zalesky, A. Fornito, and E. Bullmore. On the use of correlation as a measure of network connectivity. *Neuroimage*, 60(4):2096–2106, 2012.

Acknowledgements

This work was possible thanks to my supervisor, professor Daniel Remondini and thanks to Daniele Marinazzo, who allowed me to spend three months at the department of data analysis, at Ghent University. I would like to thank all professor Marinazzo's group, for having helped me throughout my stay, especially Almu, who always encouraged me.

Un ringraziamento particolare va ad Alice e a mia sorella Giulia, per la pazienza e tutto l'aiuto che mi hanno dato nella fase di scrittura della tesi.
Inoltre devo senza dubbio ringraziare tutta la mia famiglia e i parenti per il supporto, anche e soprattutto economico, che ho ricevuto.

E ancora...

Grazie a Matteo, che mi ha dovuto sopportare in questo ultimo mese.

Grazie al gruppo PeapAll e ai Bugs, per l'accoglienza e per tutti gli eventi a cui abbiamo partecipato insieme.

Thanks to all the people I met during these years, in Bologna, Adelaide and Ghent.
Thanks to all my friends because, even though some of them spread out all over the world, they are still close to me.